



Statistical Mechanics of Fluctuating Membranes

by

P. Pieruschka

MSc, University of Canterbury, New Zealand (1990)

A thesis submitted for the degree of Doctor of Philosophy of the
Australian National University



September 1994



Statistical Mechanics of Fluctuating Membranes

F. Partridge

Ph.D. Thesis, University of Cambridge, New Zealand (1981)

A thesis submitted for the degree of Doctor of Philosophy of the

Australian National University



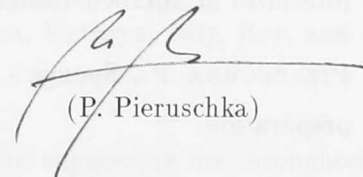
September 1981

Preface

This thesis is the result of research conducted at the Department of Applied Mathematics, Research School of Physical Sciences and Engineering, Australian National University, between January 1991 and September 1994. Two periods, June 1992 - December 1992 and October 1993 - January 1994, were spent at the Department of Materials and Interfaces, Weizmann Institute of Science (Rehovot, Israel).

The content of this thesis represents work done in individual collaboration with, and under the supervision of, Stjepan Marčelja, Samuel Safran and Barry Ninham.

The work presented here is my own, unless explicitly stated to the contrary. None of the work reported here has been submitted to any other institution of learning for any degree.



(P. Pieruschka)

Refereed Publications

1. PIERUSCHKA P., MARČELJA S., *J. Phys. France II* **2** (1992) 235.
2. PIERUSCHKA P., SAFRAN S. A., *Europhys. Lett.* **22** (1993) 625.
3. PIERUSCHKA P., MARČELJA S., *Langmuir* **10** (1994) 345.
4. PIERUSCHKA P., MARČELJA S., TEUBNER M., *J. Phys. France II* **4** (1994) 763.
5. PIERUSCHKA P., SAFRAN S. A., *J. Phys. Cond. Matter* **6** (1994) A357.

Publications Submitted or in Preparation

1. PIERUSCHKA P., SAFRAN S. A., Random Interface Model of Sponge and Vesicle Phases, submitted to *Europhys. Lett.*
2. MARČELJA S., PIERUSCHKA P., SAFRAN S. A., Comment on 'Fluctuating Interfaces in Microemulsions and Sponge Phases', submitted to *Phys. Rev. E*.
3. PIERUSCHKA P., Sponge - Lamellar Instability in Amphiphilic Systems, in preparation.

Acknowledgements

I am indebted to my supervisor Stjepan Marčelja for generously sharing his innovative ideas and physical insights which inspired much of the work presented in this thesis. My thanks also to my co-supervisor Sam Safran whose enthusiasm and patience in introducing me to the statistical mechanics of colloidal systems were very helpful. Thanks also for his efforts in organizing my stays in Israel. I am also grateful to my advisor Barry Ninham for scientific and administrative support.

I also acknowledge all the researcher who shared their expertise with me: D. Andelman, I. S. Barnes, M. Cates, P. Chandra, S. H. Chen, S. Edwards, D. Gazeau, W. Helfrich, J. S. Huang, S. T. Hyde, E. Kaler, M. A. Knackstedt, R. Menes, P. Nelson, J. Percus, P. Pincus, G. Porte, S. Ramaswamy, A. P. Roberts, D. Roux, M. Schick, R. Strey, M. Teubner, T. Zemb. In particular, my thanks to M. Teubner for discussing [37], M. Teubner and one of the referees for critical comments on item 4 on the previous page, T. Zemb, R. Strey and G. Porte for providing experimental data and T. Zemb for his hospitality in Paris.

Thanks also to my fellow students Aharon, Becky, Erica, Kathryn, Nily, Roy, and Tony for putting up with me.

Finally, my deepest thanks to my parents and Ling-Li for supporting me throughout.

Abstract

Two of the most successful models of fluctuating amphiphilic systems are the effective interface and the Ginzburg - Landau models. The former have a clear energetic basis (the bending Hamiltonian), offer an elegant approach to the structural patterns of fluctuating membranes and nearly effortlessly explain phenomena related to scale-invariance properties. However, because the partition function of the bending Hamiltonian is unknown consistent thermodynamic treatment has so far been limited to smectic lamellar systems in the low temperature limit. Ginzburg - Landau models on the other hand are purely phenomenological but have revealed some fundamental mechanisms which can explain the bulk and film structure factors of sponge phases.

We develop a coherent structural and thermodynamic description of fluctuating membranes which combines patterns of field theory with the simplicity of the bending Hamiltonian. The model relies on the Feynman - Hellman variational theorem which is used to determine an optimal Gaussian ensemble of random interfaces at given concentrations and bending moduli. Thus the structure factors and the free energy density are consistently determined in terms of observable parameters.

The approach is most easily applied to the well-known smectic lamellar systems studied by Helfrich. We show that variational theory can with relative ease unify many known low temperature results and is also able to deal rigorously with the full non-linear bending Hamiltonian and relevant physical constraints beyond the low temperature limit. The results show that considerable deviations from low temperature theory can be expected in systems with low bending stiffness and concentration.

Full non-linear treatment of the bending Hamiltonian and physical constraints is even more powerful in the most extreme example of fluctuating membranes, the sponge phase. A variational random interface model yields a successful and unified approach to bulk and film structure factors and thermodynamics of sponge phases. The steric repulsion force in sponges is calculated, the symmetric - asymmetric transition is considered and the microemulsion phase diagram is drawn. All results are given in terms of concentrations and bending moduli with no adjustable parameters. The relationship to bulk Ginzburg - Landau models is clarified by determining their phenomenological parameters.

In experiment, dilute lamellar phases are often found adjacent to the sponge phase. The relative stability of these two phases has experienced hardly any attempts of consistent theoretical treatment. Consistent extension of the random interface approach to nematic lamellar phases results in the expected first order transition and allows us to estimate the relative stability of these two phases with respect to amphiphile concentration, bending and saddle-splay moduli.

Finally, we treat the 'exact' bending Hamiltonian problem by a \vec{k} -space Monte Carlo simulation which allows us to study truly continuous, self-avoiding, curvature-elastic systems on large scales. The method is used to assess the accuracy of the random interface model of sponges and to support our analytical results for the sponge - lamellar instability. We also use the simulation to gain insight into the effect of the saddle-splay modulus on topological and structural properties in amphiphilic phases.

Contents

CHAPTER 1 Introduction	1
1.1 Experimental Facts and Theoretical Concepts	1
1.2 Models of Fluctuating Interfaces	10
1.3 Free Energy of Gaussian Random Interfaces	15
CHAPTER 2 Variational Theory of Smectic Lamellar Phases	19
2.1 Introduction	19
2.2 Variational Theory	22
2.2.1 Renormalization of the Bending Constant	25
2.2.2 Structure Factor and Free Energy	26
2.2.3 Helfrich Limit and Crumpling Corrections	28
2.2.4 Numerical Results: Free Energy, Structure Factor, Swelling, Renormalization	30
2.3 Conclusions	32
2.A Appendix	34
CHAPTER 3 Random Interface Model of Sponge Phases	37
3.1 Introduction	37
3.2 Structure and Thermodynamics	40
3.2.1 Structural Properties	41
3.2.2 Phase Transitions	64
3.2.3 Relation to Coarse Grained and Ginzburg - Landau Theories	74
3.3 Discussion and Outlook	76
3.A Appendix	79
CHAPTER 4 Sponge - Lamellar Instability	87
4.1 Introduction	87

4.2 Nematic Lamellar Phase	89
4.2.1 Statistical Averages	91
4.2.2 Structure Factor	92
4.3 Stability of the Sponge Phase	97
4.4 Smectic Lamellar Phase	102
4.5 Conclusion	103
4.A Appendix	104
CHAPTER 5 Monte Carlo Simulation of Curvature - Elastic Interfaces	107
5.1 Introduction	107
5.2 Methods	108
5.2.1 Simulation of Continuous, Self-Avoiding Surfaces	108
5.2.2 Analysis of Bulk and Film Structure Factors	111
5.2.3 Topology, Curvature	113
5.3 Application to Disordered Surfactant Interfaces	113
5.4 Summary and Outlook	125
5.A Appendix	127

Introduction

Surfactants in solution consist of simple constituents, for example, water and soap (surfactant) and yet bear extraordinarily complex phase diagrams, special interfacial behaviour and exotic structural properties [1]. In recent years it has become clear that despite the rich variety of experimental phenomena many features of amphiphilic systems have universal character independent of the details of solute and solvent. This intriguing connection of simplicity and complexity continues to pose a challenge to scientists and engineers. Despite much theoretical effort over the past years a model which can reflect the underlying simplicity and at the same time capture at least some of the richness of structure and phase behaviour – in a way comparable to experimental results – remains an extraordinarily difficult problem.

In the introductory section we will give a brief review of the experimental and theoretical state of the art of surfactant science. The remaining sections in this chapter will provide some preliminary studies and fundamental concepts which form the basis and motivate the work presented in the remaining chapters.

1.1 Experimental Facts and Theoretical Concepts

Surfactants are substances which consist of linear, amphiphilic ($\alpha\mu\phi\iota\ \phi\iota\lambda\omega = \textit{loving both}$) molecules characterized by two subunits, a polar head group and a hydrocarbon tail. When dissolved the surfactant molecules tend to orient themselves so that the head

group is in contact with a high dielectric medium (*e.g.* water) and the tail resides in a low dielectric medium (*e.g.* oil). Typical examples of surfactants in solution are ternary mixtures of water, oil and surfactant or binary systems which are composed of water *or* oil and surfactant. In ternary systems the amphiphile adjusts to the surrounding medium by self-assembling into monomolecular films (monolayers) which separate the oil from the water parts so that the polar heads point in the direction of water and the tails towards the oil. In binary systems the tails (heads) can only be shielded from unfavorable contact with water (oil) by facing each other. This leads to the arrangement of the molecules as a bilayer where the tails lie on the inside and the head groups on the outside or vice versa depending on whether the surrounding medium is water or oil. The tendency to build up spontaneously interfaces is dominant for a very large range of system parameters. Only at very high temperature or surfactant dilution can the entropy of a molecular dispersion supersede the energetic tendency of the surfactant to self-assemble and lead to phase separation between water and oil, or formation of a dilute dispersion in binary systems.

Unique interfacial and structural properties are associated with the formation of interfacial films¹. Self-assembly at oil - water interfaces, for example, causes a strong reduction in the interfacial tension making surfactants ideal for use as detergents or in oil recovery. Similarly, unique microstructures can be exploited technologically *e.g.* droplet or bicontinuous film geometries can serve as microscopic containers for drug delivery or as microscopically fine sieves for ultra-filters, respectively [2]. The development of these applications would of course be helped, if we could provide a better understanding of the physical mechanisms which drive amphiphilic systems [3].

Interfacial shapes depend on a large number of parameters such as temperature, salinity, alcohol content, surfactant concentration *etc.* Yet, in experiment the occurrence of certain structures is often strongly correlated to the surfactant concentration and typically develops from ordered phases at high surfactant concentration to isotropic phases at high dilution. Typical representatives of ordered phase are cubic or hexagonal phases. These structures show genuine long range order and are essentially insensitive to thermal fluctuations. At lower surfactant concentration thermal fluctuations start to dominate and destroy long range order. Typical phases in this regime are smectic and nematic lamellar phases which consist of stacked sheets of undulating layers or a recently identified strongly hyperbolic sponge-like phase. We show in fig. (1-1) a representative phase

¹ *cf.* [1, 2] for a more complete collection of examples.

diagram of a ternary mixture of water, oil and surfactant which shows a lamellar phase at high surfactant concentration and a sponge-like phase at low surfactant concentration

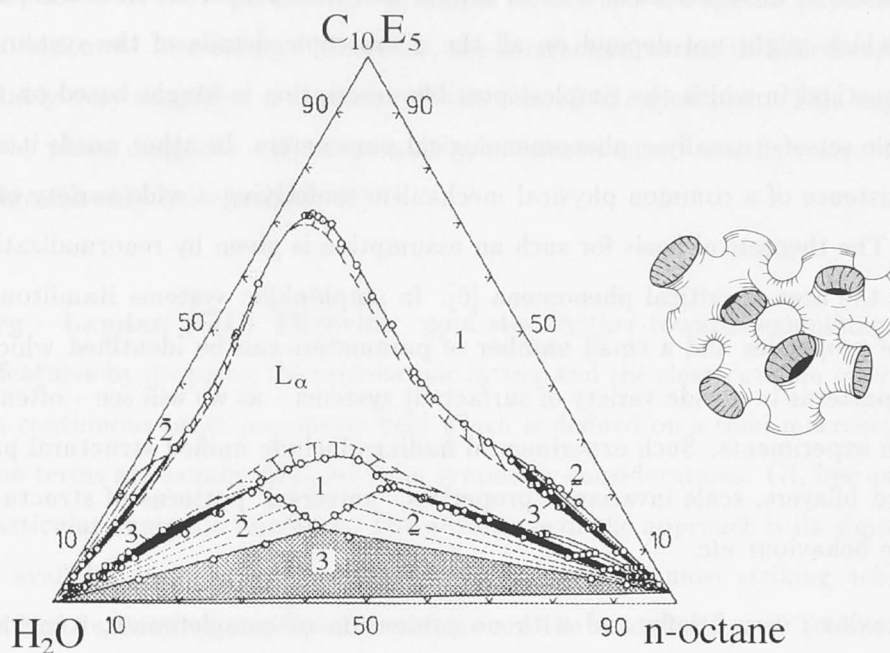


Figure 1-1: Gibbs triangle of the ternary system $H_2O - n - octane - C_{10}E_5$. The symbol 1 denotes the one-phase microemulsion. 2 and 3 symbolize multiphase regions where the microemulsion coexists with oil or/and water rich phases. At higher surfactant concentration the lamellar phase L_α prevails (from [4]). (inset) Schematic image of a sponge-like microemulsion phase, denoted 1 in the phase diagram (from [5]).

Fluctuating membranes pose a particular challenge to statistical mechanics as crossover structures between entropically dominated fluids and energetically driven, ordered systems. Their structure can therefore in general neither be described the way done in simple fluids, by means of a correlation length ξ only, nor by merely measuring the structural length scale k_0 (Bragg peak) as in crystalline phases². We expect therefore that both k_0 and ξ should form the necessary (but not sufficient) core of a structural description of fluctuating amphiphilic systems. Similarly, any approach to the phase transitions which occur in these systems must include both the energy and entropy of a complex ensemble of fluctuating amphiphilic films.

The various theories which have attempted to overcome the formidable problem of describing structure and thermodynamics of fluctuating systems can be essentially distinguished as traditional and modern statistical physics approaches. In a traditional approach one

²These phases are thus mesomorphic in the most literal sense.

would try to include as many of the fine details and interactions which govern a particular system as possible in order to achieve a maximum of realistic modelling. Modern statistical mechanics on the other hand tries to extract universal properties from a set of physical systems which might not depend on all the microscopic details of the systems. It is a minimal method in which the simplest possible description is sought based on the smallest possible set of – usually – phenomenological parameters. In other words it speculates on the existence of a common physical mechanism underlying a wide variety of different systems. The theoretical basis for such an assumption is given by renormalization group theory in the area of critical phenomena [6]. In amphiphilic systems Hamiltonians with invariance properties and a small number of parameters can be identified which predict common patterns in a wide variety of surfactant systems – as we will see – often in agreement with experiments. Such experimental findings include unified structural patterns of mono- and bilayers, scale invariance properties, ‘universal’ patterns of structure factors and phase behaviour *etc.*

We will review, very briefly and with no pretension of completeness, some major approaches to the physics of fluctuating amphiphilic systems; emphasis will be laid on the models which are to some extent connected to the concepts used in this thesis.

Microscopic Models can be of lattice or continuous type [7]. Lattice descriptions are often based on Ising Hamiltonians of spin - $\frac{1}{2}$ or spin - 1 type with more or less complex interaction terms [8, 7] (*cf.* also introduction to Chapter 3). These models, however, do not take the molecular geometry of the constituents into account and are therefore not overly realistic. Improvements in this direction were made by Larson [9] who incorporated details of the surfactant tail length into the lattice description and Smit *et al.* [3] whose model is similar to Larson’s but defined in a continuum (based on molecular dynamics simulations).

One merit of this class of models is that they can describe surfactants which are appreciably soluble (short chain surfactants) in the bulk so that properties of simple solutions can be important. They can also address a number of fundamental issues, such as the process of self-assembly and the dependence of phase behaviour on details of the molecular structure. Moreover, phase diagrams comparable to experiment are readily obtained, and interfacial tensions can be calculated.

The major disadvantage of microscopic models is that they cannot take long range inter-

actions into account which are implied by the occurrence of self-assembled films which can extend over many hundreds or thousands of Ångstroms, *e.g.* [10]. Such 'good' complex fluids, however, show (in contrast to simple fluids) just the special physical patterns which we find most interesting. Moreover, the interaction terms in microscopic models are inevitably very simplified and can hardly be related to experiment. This might be the reason, why phase diagrams – if comparable to measured ones – usually resemble realistic phase diagrams only quite roughly [1].

Ginzburg - Landau (GL) Theories go a step further towards examining universal physical features by dropping the microscopic lattice and the clear-cut spin interactions in favor of a continuous order parameter field which is defined on a semi-macroscopic scale. Interaction terms are usually deduced from symmetry considerations. GL free energy thus has no particular energetic reference. The advantage of the approach is its simplicity and a readily available body of solution techniques. Among its most striking achievements in the field of fluctuating amphiphilic systems are the contribution of Teubner & Strey on the bulk structure of microemulsions [11], and the results of Roux *et al.* on the film structure factor and the symmetric / asymmetric (S/A) transition in L_3 sponge phases [12]. The main shortcoming of GL theories is their lack of underlying energetics so that, for example, interface properties (*cf.* Membrane Models) are not taken into account. This also leads to a tendency to employ a number of phenomenological parameters which exceeds the number naturally expected in certain problems [13]. Phase diagrams as functions of these parameters can usually not be compared to experimental data, and structure factors are due to the semi-macroscopic nature of the field only defined at long wave lengths. Nevertheless, GL theories can give useful information about general tendencies in amphiphilic systems and their role in the understanding of fundamental structural patterns in microemulsion and L_3 sponge phases and the S/A transition has been pioneering [11, 12].

Membrane Models should apply in the idealized case when the tendency to spontaneous self-assembly is so strong that nearly all the surfactant molecules form interfaces and only little surfactant remains dissolved in the bulk. The interfacial free energy achieves a minimum when the interface is saturated [14, 15]

$$\sigma = \left. \frac{\partial f_0}{\partial \Sigma} \right|_{\Sigma=\Sigma_0} \approx 0 \quad (1.1)$$

i.e. a surfactant concentration has been reached where the area per surfactant molecule, Σ , does not change any longer but remains at the optimum value Σ_0 . Upon further addition of surfactant more interface is built up and the area per surfactant molecule stays unchanged.

If we accept this premise the process of self-assembly is taken as a starting point, and all physical phenomena should be derived from the statistical mechanics of the surfactant film. Description of small-scale micellar solutions is then by definition beyond the scope of these models³ while large-scale interfacial structures should be well described. The interfacial film can be mathematically modelled by a fictitious, two dimensional effective interface embedded in three dimensional space. The position of the interface is usually defined at the centre of the bilayers or at the surfactant head positions of monolayers. All details of the local interactions between surfactant molecules – such as chain - chain and headgroup interactions, bulk - chain interactions and head - tail couplings – have been dropped by postulating an effective interface. They should re-appear in form of phenomenological parameters which couple to the deformation modes of the interface. Physically relevant modes can be represented by operators invariant under coordinate transformations. They can be written as a series, where the first, simplest term is a surface tension term σ , followed by the lowest order invariants of the curvature tensor⁴ of the interface. These invariants are just the mean curvature $H = 1/2(c_1 + c_2)$ and Gaussian curvature $K = c_1 c_2$ of the interface where c_1, c_2 are the local principal curvatures. Since our discussion is based on the assumption of negligible interfacial tension, $\sigma \approx 0$, the lowest order Hamiltonian which was first given by Canham and Helfrich [16] reads

$$\mathcal{H} = \int_S \left[2\kappa (H - H_0)^2 + \bar{\kappa}K \right] dS \quad (1.2)$$

where S denotes the total interfacial area of the system and $\kappa, \bar{\kappa}$ (in units of $k_B T$) couple the mean and Gaussian curvature terms to the energy. H_0 is the spontaneous curvature of the interface which quantifies the tendency of the film to bend towards the water or oil part of the bulk fluid. It is only important in ternary systems. Even in these systems careful adjustment of the temperature or salinity can usually eliminate the spontaneous curvature term. Throughout most of the thesis we will therefore operate with $H_0 = 0$. Although the interfacial term can be omitted from the Hamiltonian we have to make sure that only surface configurations with constant head group area per surfactant molecule

³We will encounter this basic weakness again later in the thesis.

⁴For a concise introduction *cf.* [2].

Σ_0 are allowed. Hence we have to impose a constraint on the interfacial area per molecule or

$$\frac{S}{V} = \text{const} \quad (1.3)$$

where S is the total surface area of the interface and V is the sample volume. We can also take excluded volume effects implicitly into account – which, as we will soon see, appear to play an important role in fluctuating membrane systems – by further restricting the ensemble to configurations which are self-avoiding⁵. The bending Hamiltonian together with the constraints on surface area and self-avoidance will play a central role in our discussion of fluctuating amphiphilic phases.

Of course, the above formulation neglects direct interactions such as electrostatic and van der Waals which might well play an important role for the detailed behaviour of amphiphilic phases. Inclusion of these interactions, however, leaves our basic objective of creating a simple theory which can account for a rich variety of phenomena related to self-assembled amphiphilic systems. We therefore prefer to refrain in the context of this thesis from discussing direct interactions. This minimalistic approach finds indeed also overwhelming experimental motivation. The above-mentioned ‘universal’ patterns of surfactant behaviour indicate that many microscopic details can be lumped together into a few effective parameters which govern the system:

Firstly, we note that the Helfrich Hamiltonian is less phenomenological than it might appear. Surfactant concentration is a well defined experimental quantity and numerous techniques have been devised to measure the bending constant κ [18] or derive it from microscopic models [19]. Even the demanding task of measuring the saddle-splay modulus $\bar{\kappa}$ has been tackled with some success [20]. Thus, the parameters which characterize the Hamiltonian can be closely related to experiment so that the results of a theory based on eqns. (1.2,1.3) stand a good chance to be comparable to experiment. Accordingly, some of the most striking successes in explaining fluctuating amphiphilic structures are based on effective interface theory.

A straightforward yet non-trivial consequence of the formulation eqns. (1.2,1.3) is that the effective interface formalism does not distinguish between mono- and bilayers (this distinction is a problem in microscopic or GL models). Hence we expect that the structural properties of ternary and binary amphiphilic systems should at suitable surfactant

⁵It is interesting that systems of self-avoiding random surfaces are also of concern for the random surface formulation of gauge theory [17].

concentrations be identical. This has been confirmed experimentally [21]. Membrane theory thus represents a unified theory of both mono- and bilayer systems.

Another simple and at the same time very elegant consequence of the form of the Hamiltonian eqn. (1.2) is the notion of scaling in amphiphilic systems which was established by Porte in 1989 [22]. Scaling is in general a functional relationship of the form of a power law, $x = y^\gamma$. In thermodynamics the most important example of scaling relationships are the power law divergences of many physical quantities around the critical point. In amphiphilic systems scaling is a consequence of the invariance of the Hamiltonian under dilation transformations [22]. This can be easily cast into the language of well-known transformation theory [22]: The scale factor of the transformation is given by the dilation factor λ . When the transformation is applied to the Hamiltonian eqn. (1.2) we see that $(c'_1, c'_2) = \lambda^{-1}(c_1, c_2)$ and $dS' = \lambda^2 dS$ and therefore

$$\mathcal{H}' = \mathcal{H}$$

Hence the partition functions, $\mathcal{Z}'(\mathcal{H}') = \mathcal{Z}(\mathcal{H})$, and the total free energies, $\mathcal{F}'(\mathcal{H}') = \mathcal{F}(\mathcal{H})$, are unchanged. However, the free energy density *i.e.* the free energy *per volume*, the inverse structural length scale k_0 and the correlation length ξ (which were introduced above) have to obey $f' = \lambda^{-3}f$, $k'_0 = \lambda^{-1}k_0$, $\xi' = \lambda\xi$, respectively [23]. In experiment, dilation is approximately the same as dilution *i.e.* changes in the surfactant concentration $\lambda = \phi_s/\phi'_s$, so that – if we introduce a reference state – the free energy density is expected to scale like

$$f \sim \phi_s^3$$

while the inverse structural and correlation lengths scale like

$$k_0 \sim \phi_s, \quad \xi \sim \phi_s^{-1} \quad (1.4)$$

Indeed many experiments on lamellar and sponge-like phases, *e.g.* [5, 24], indicate that the peak and width of the scattering structure factor (which correspond just to the above mentioned inverse structural length and inverse correlation length) obey eqn. (1.4). This holds for smectic lamellar phases where the peak position is often clearly visible as a sharp quasi-Bragg peak at k_0 which is observed to scale as we expect, $k_0 \sim \phi_s$. Scattering measurements also clearly confirm the conjecture eqn. (1.4) *e.g.* for semi-rigid AOT sponge phases as shown in fig. (1-2). The free energy is not directly measurable, but there is indirect indication that the scaling $f \sim \phi_s^3$ holds. Considering the parameters in the

Hamiltonian, eqn. (1.2), we can further specify [25]

$$f = b(\kappa, \bar{\kappa}, \phi) \phi_s^3 \quad (1.5)$$

where ϕ is the volume fraction of, say, water in ternary systems, or the amount of bulk fluid on the, say, 'inside' the bilayer in binary systems. The free energy scaling – although not identified as such at the time of its discovery – has in fact been established under the notion of the Helfrich's steric repulsion force in multilamellar systems long ago [26]

$$f \sim \kappa^{-1} d^{-3} \quad (1.6)$$

and belongs to one of the milestones in the study of complex fluids. It is a low temperature result ($\kappa^{-1} \rightarrow 0$) in which the layer spacing d^{-1} is proportional to the surfactant concentration (*cf.* Chapter 2).

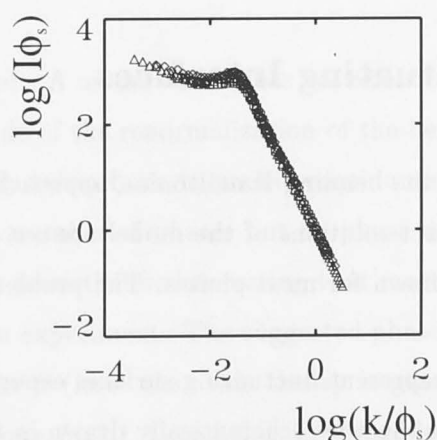


Figure 1-2: *Scaling in amphiphilic sponge phases: scattering structure factors of AOT/brine L_3 sponge phases at three different dilutions $\phi_s = 0.0432, 0.0653, 0.0869$ symbolized by \diamond, \triangle and \square , respectively. All curves approximately collapse when plotted in reduced units $I\phi_s$ over k/ϕ_s (data courtesy of G. Porte).*

Despite the elegant and concise formulation of the flexible interface model and although it can reproduce nearly effortlessly some of the universal features of amphiphilic systems, its main shortcoming is that – unlike microscopic or GL models – there is not even an approximate theory available to solve the partition function or to estimate the free energy. It comes as no surprise that eqn. (1.6) – a low temperature approximation neglecting topological effects ($\bar{\kappa} = 0$) – stands since 1978 without any major improvements and with no comparable successes for other surfactant phases. Furthermore, it is obvious that scaling relationships of the type discussed above cannot be the whole truth. Eqn. (1.5) is

strictly monotonic, so that once κ , $\bar{\kappa}$ and ϕ are determined the macroscopic phase with the smallest coefficient $b(\kappa, \bar{\kappa}, \phi)$ is predicted to be stable at all surfactant concentrations [22, 25, 27] in contrast to experiment. Thus, although scaling considerations are of fundamental interest, they are insufficient to discuss phase transition induced by changes in surfactant concentration. Corrections to scaling are needed.

Scaling (and the departure from it) in amphiphilic systems beyond Helfrich's low temperature discussion of smectic lamellar systems, its detailed structural and thermodynamic implications in the framework of a unified, consistent theory roughly describe the challenge in the membrane description of surfactant solutions. This thesis will provide both approximate analytic and numerical methods mainly for nematic, smectic, sponge and dilute vesicle phases. We will start our discussion by reviewing briefly previous theoretical efforts.

1.2 Models of Fluctuating Interfaces

Having firmly established that the bending Hamiltonian approach is sensible and promising we had to concede that exact solutions of the model are out of reach, and that even approximate solutions are unknown for most phases. The problem has two major roots

- (a) it is not obvious how to represent fluctuating surfaces especially if they are of very complex topology as the ones schematically drawn in fig. (1-1).
- (b) even if one succeeds in finding a mathematical formulation of these interfaces there is yet no way of calculating their free energy. In particular, calculation of the entropy of random surfaces is a problem not yet surpassed.

Strategies to overcome these problems have been devised by several authors.

Coarse Grained Models One major attempt has been based on the spatial discretization of random surfaces [28, 29, 30]. Best results were achieved by a coarse grained lattice approach due to Andelman, Cates, Roux and Safran (henceforth called ACRS model) [31], where real space is subdivided into cubes with lattice constant $d = 6a\phi_s^{-1}\phi(1-\phi)$ (a is the film thickness). Different film configurations could then be achieved by randomly assigning water or oil occupation to the cubes and defining interfaces at the plaquettes

(with rounded corners) which delineate water and oil domains. The bending energy could be evaluated using the well-known curvature of spherical objects. The entropy was taken as the random mixing entropy of the bulk domains. Another crucial ingredient was the thermal softening of the bending constant κ of a continuous flat interface due to undulations around its average position (in detail discussed in Chapter 2). The main virtue of this model was that it could present phase diagrams (including sponge and lamellar phases) which could be compared to experimental phase diagrams. Golubović & Lubensky later refined this approach (adding Helfrich interaction and discussing the various phases more consistently) without changing the lattice structure [32].

Perhaps the most important results of this work were the prediction of a symmetric - asymmetric transition and the calculation of L_3 sponge phase and microemulsion phase diagrams [31, 32].

Huse & Leibler Model A model which does not refer to discretization but argues semi-quantitatively on grounds of the renormalization of the bending constant and other well-known arguments mostly taken from harmonic continuum elasticity of flat and spherical membranes suggested a number of phases but no phase diagram which could be related to experiment [33]. It is nevertheless interesting that most of the postulated phases were later indeed identified in experiment. The suggested phase sequence for ascending values of the interfacial tension σ (note that this theory is grandcanonical in contrast to the canonical formulation eqns. (1.2,1.3) and thus in principle not a solution to the problem we are discussing) is

smectic lamellar - nematic lamellar - random isotropic - tense bicontinuous - dilute droplets

Most of these names are self-explaining, except possibly 'random isotropic' and 'tense bicontinuous' which are now better known under the names 'symmetric' and 'asymmetric sponge'. While this work initiated fruitful new developments related to the postulation of new phases, its formal basis was still far away from a quantitative continuum model of topologically complex, fluctuating interfaces.

Cahn & Berk Model An important step towards a genuine continuum theory of interfaces was done by Berk in 1986 [34] (based on work by Cahn [35]) who was the first to realize that the morphology of excursion sets of random fields [36] resembles freeze-

fracture microscopic images of microemulsion sponge phases and that these level sets could give a consistent description of both film and bulk scattering structure factors. If $s(\vec{r})$ denotes a scalar random field in three dimensions with $-\infty < s(\vec{r}) < \infty$ one can consistently identify *both bulk partitions and interfaces* by the prescription

$$s(\vec{r}) \begin{cases} > \alpha & \text{water} \\ = \alpha & \text{interface} \\ < \alpha & \text{oil} \end{cases} \quad (1.7)$$

drawn schematically in fig. (1-3).

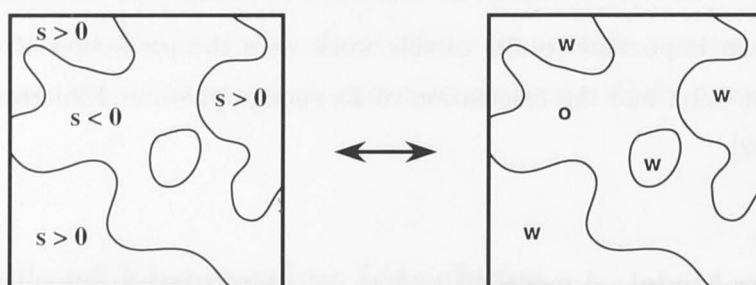


Figure 1-3: Sketch depicting the zero level cut ($\alpha = 0$) delineating areas of the random field which are smaller or greater than zero which are assigned to e.g. water (w) and oil (o).

The original representation of the random field used by Berk is

$$s(\vec{r}) = \sqrt{\frac{2}{N}} \sum_{i=1}^N \cos(\vec{k}_i \vec{r} + \phi) \quad (1.8)$$

where the ϕ are uniformly distributed and the \vec{k}_i have a spectral distribution $\nu(\vec{k})$. This representation disguises the fact that eqn. (1.8) constitutes a random field of Gaussian type. It was Teubner [37] who realized this by calculating moments of eqn. (1.8). Instead of working with the more common definition where the amplitudes have Gaussian distribution (*cf.* next subsection) eqn. (1.8) fixes the amplitudes and uses a non-Gaussian distribution of the wave vectors, $\nu(\vec{k})$. While this is very convenient for fitting algorithms and numerical simulations (Chapter 5), it is not convenient for analytical purposes. Initial work on these structures concentrated therefore on finding a distribution of \vec{k} which appeared best for purposes of fitting scattering data. Various distributions were used by Teubner (sixth order inverse polynomial, [37]) and Chen *et al.* (Schultz distribution, *e.g.* [24]) which fitted bulk spectra very well.

While the Cahn - Berk model is useful for data fitting it somewhat lacks a physical basis.

It would be interesting to see whether one can (a) relate the spectral distribution to physical parameters and thus go beyond its use as an adjustable fit parameter and (b) perform consistent fits to both film and bulk structure factors as a more stringent test of the structural properties of the model.

In accordance with our basic considerations one can try to base the model on the two length scales $d_0 = 2\pi k_0^{-1}$ and ξ which denote the average domain size of the microemulsion and the correlation length quantifying the short range order present in microemulsions, respectively. A natural representation of a Gaussian process is then given by superposing localized wave packets [38] each characterized by k_0 and ξ

$$s(\vec{r}; \xi, k_0) \sim \sum_{i=1}^N u(|\vec{r} - \vec{r}_i|; \xi) \cos[\vec{k}_i \cdot (\vec{r} - \vec{r}_i)], \quad \text{with } \vec{k}_i = k_0 \cdot \vec{e}_i \quad (1.9)$$

where $u(r)$ is an envelope function with characteristic decay length ξ . The directions of \vec{k}_i and the positions \vec{r}_i of the local wave packets are uniformly distributed. For an envelope *e.g.* of Yukawa type

$$u(\vec{r}) = r^{-1} \left[e^{-r/\xi} - e^{-r/r_m} \right] \cos \vec{k}_0 \cdot \vec{r} \quad (1.10)$$

where r_m is a molecular cut-off (layer thickness) necessary to avoid the singularity the two-point correlation function is then

$$g(r) = \langle s(\vec{0}) s(\vec{r}) \rangle_0 \sim \left[e^{-r/\xi} + O(a^{-1}) \right] \frac{\sin k_0 r}{k_0 r}$$

with $a = \xi/r_m \gg 1$ so that after isotropic Fourier transform we find

$$\nu(k) \sim \left[\xi^{-2} + (k - k_0)^2 \right]^{-1} \left[\xi^{-2} + (k + k_0)^2 \right]^{-1} + O(a^{-1})$$

Note that in leading order $\nu(k) \sim [k^4 - bk^2 + c]^{-1}$ which is well-known from a purely phenomenological GL theory due to Teubner & Strey [11] and which was successfully applied to fit bulk scattering from microemulsions (but not film scattering which cannot be described in a unified way in GL theories, [11]). Having deduced (not *a priori* fixed) $\nu(k)$ from the natural representation eqn. (1.9) of random interfaces we can proceed now in predicting the film and bulk scattering. A quick way of doing this is by straightforwardly modelling the contrasted experimental scattering samples. In film samples the scattering length density of the surfactant film is contrasted against a background of solvent by deuteration. Bulk samples are prepared by contrasting the oil and water parts. Contrast- ing creates to a good approximation regions of homogeneous scattering length densities which are mathematically well described as Heaviside step functions. The contrast profile

– when going from the water side via the interface to the oil side – is then described by a succession of steps [39]. If β_1, β_2, \dots denote the level sets around the interface at which discontinuous, stepwise changes in the scattering length density occur the according correlation function $\Gamma^{\beta_1\beta_2\dots}(r)$ can be described by a bivariate Gaussian integral over a product of linear combinations of the appropriate Heaviside step functions. For the case of two phase contrasts the step function $\Theta_{\beta_1\beta_2}$ is sufficient, where $\Theta_{\beta_1\beta_2} = 1$ for $\beta_1 \leq x \leq \beta_2$ and zero otherwise so that

$$\Gamma^{\beta_1\beta_2}(r) = \int_{-\infty}^{+\infty} \int_{-\infty}^{+\infty} \frac{1}{2\pi\sqrt{1-g^2(r)}} e^{-\frac{x^2+y^2-2g(r)xy}{2(1-g^2(r))}} \Theta_{\beta_1\beta_2}(x) \Theta_{\beta_1\beta_2}(y) dx dy$$

After normalization, essentially $\gamma^{\beta_1\beta_2}(r) \sim \Gamma^{\beta_1\beta_2}(r) - \phi_s^2$, and the usual Fourier transform [40]

$$I(k) = 4\pi \langle \eta^2 \rangle \int_0^\infty \gamma(r) r^2 j_0(kr) dr \quad (1.11)$$

where $\gamma(r) = \gamma^\alpha(r)$ (i.e. $\beta_1 \rightarrow \alpha, \beta_2 \rightarrow \infty$) for bulk scattering and $\gamma(r) = \gamma^{\alpha-\epsilon, \alpha+\epsilon}(r)$ for film scattering (where ϵ corresponds to twice the film thickness) a consistent description of both film and bulk scattering from symmetric random bicontinuous phases is achieved.

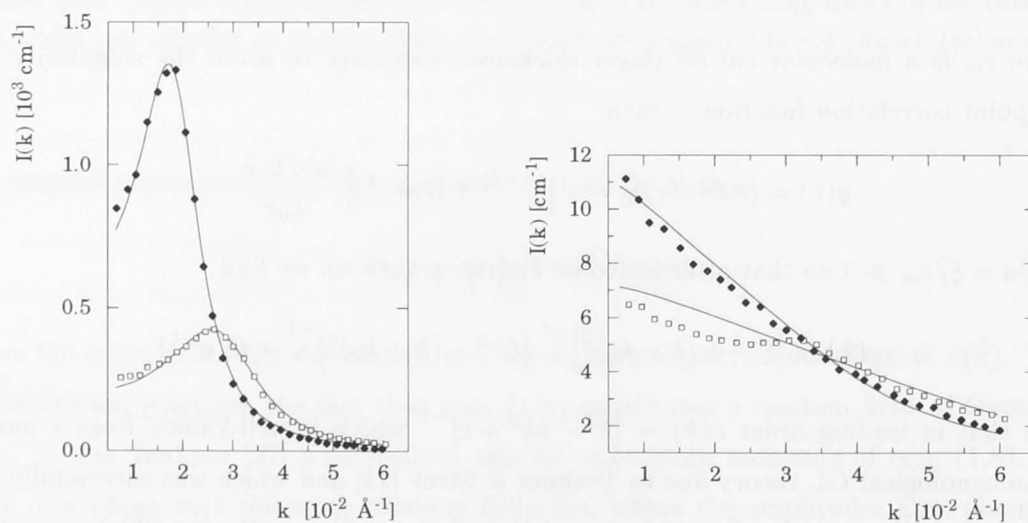


Figure 1-4: (left) SANS bulk intensity for a 7 (\diamond) and a 10 (\square) weight% SDS microemulsion systems. The experimental data are taken from [39]. Lines are fits to the data. Fit parameters: for 7% SDS: $\xi = 133 \text{ \AA}$, $k_0 = 1.87 \cdot 10^{-2} \text{ \AA}^{-1}$. for 10% SDS: $\xi = 87 \text{ \AA}$, $k_0 = 2.822 \cdot 10^{-2} \text{ \AA}^{-1}$. For both systems the cut-off values were $r_m = 10 \text{ \AA}$ and $r_c = 55 \text{ \AA}$ (cf. Chapter 3 for the definition of r_c) while $\langle \eta^2 \rangle$ had the experimental value of $3.32 \cdot 10^{21} \text{ cm}^{-4}$. The surfactant volume fractions were $\phi_s(7\% \text{ SDS}) = 5.5\%$ and $\phi_s(10\% \text{ SDS}) = 7.5\%$. (right) SANS film intensity for the same systems with the same fit parameters (with the exception of $\langle \eta^2 \rangle = 2.79 \cdot 10^{21} \text{ cm}^{-4}$).

Auvray *et al.* have published suitable pairs of bulk and film scattering data [39], fig. (1-

4). Values for $\langle \eta^2 \rangle$ (essentially the scattering length densities) and other experimental parameters needed for fitting were taken from [39]. The volume fraction of the surfactant was estimated by the weight densities and molecular weights for SDS heads and tails [39]⁶. Fig. (1-4) gives the results and fit parameters for the cases of SDS weight fractions of 7% and 10% respectively (the relative experimental error for weight fractions is about 5% [39]). Taking into account that the model is only varying the two natural scales ξ and k_0 , and that no adjustment of ξ and k_0 was performed when fitting the film scattering, the agreement with the experimental data is very good (in the case of 10% SDS film scattering the hump pattern of the scattering curve is not reproduced; however, this hump is most likely an artefact due to a slight contrast mismatch of the bulk partitions [39]).

We can conclude this section by noting that a consistent structural description of film and bulk in sponge-like microemulsions based on Gaussian random interfaces characterized by two natural parameters k_0 and ξ has been tested and compares well with experimental data. This encourages a more rigorous treatment of the random interface approach. In particular, although our treatment is more fundamental than previously used fitting procedures, the theory is still only a geometric one without reference to thermodynamics. In the next section we will therefore bridge the gap between structure and thermodynamics by means of a variational approximation.

1.3 Free Energy of Gaussian Random Interfaces

A consistent discussion of the structure and thermodynamics of Gaussian random interfaces has to go beyond the mere use of Gaussian interfaces for structural modelling and scattering data fitting. The free energy density of an ensemble of fluctuating, random Gaussian interfaces has to be calculated so that not only thermodynamic phenomena (*e.g.* phase transitions) can be studied but also consistent determination of the interfacial structure becomes possible by minimization of the free energy density and not by fits to scattering data.

We start with a representation of Gaussian random fields as an expansion in a function

⁶Refer for details about the fitting procedure to [42]. For the development of our model ideas these details are not relevant.

space

$$s(\vec{r}) = \sum_m \eta_m \phi_m(\vec{r}) \quad (1.12)$$

with $\eta_m = [\int \phi_m^*(\vec{r}) s(\vec{r})] [\int \phi_m^*(\vec{r}) \phi_m(\vec{r})]^{-1}$. Here we will mostly use standard Fourier representation [41]

$$s(\vec{r}) = \sum_{\vec{k}} s(\vec{k}) e^{i\vec{k}\vec{r}} \quad (1.13)$$

where the amplitudes $s(\vec{k})$ are assumed uncorrelated and distributed according to a Gaussian distribution [41]

$$p[s(\vec{k})] = \frac{1}{\sqrt{2\pi\nu(\vec{k})}} \exp\left[-\frac{|s(\vec{k})|^2}{2\nu(\vec{k})}\right] \quad (1.14)$$

with zero mean and fluctuation $\nu(\vec{k}) \sim \langle |u(\vec{k})|^2 \rangle_0$ where the subscript $_0$ denotes henceforth a Gaussian ensemble average. The amplitudes obey the usual symmetry relations [6] $\Re[s(\vec{k})] = \Re[s(-\vec{k})]$ and $\Im[s(\vec{k})] = -\Im[s(-\vec{k})]$ which make sure that $s(\vec{r})$ is real.

Assume now that there is a well-defined prescription for defining an interface by means of the Gaussian field. This can, for example, be two dimensional Monge gauge (Chapter 2) or a three dimensional implicit representation (Section 1.2, Chapters 3 and 4). In any way, by defining an interface ensemble the Hamiltonian eqn. (1.2) is well-defined. Then we can apply the Feynman - Hellman theorem [43] to establish an upper bound F to the free energy \mathcal{F} of the bending Hamiltonian \mathcal{H} by using a model ensemble characterized by a model Hamiltonian \mathcal{H}_0 . This can be derived from

$$\begin{aligned} \mathcal{Z} &= \int \mathcal{D}s e^{-\mathcal{H}} \approx \int \mathcal{D}s e^{-\mathcal{H}_0} [1 - (\mathcal{H} - \mathcal{H}_0)] \\ &= \mathcal{Z}_0 - \int \mathcal{D}s e^{-\mathcal{H}_0} (\mathcal{H} - \mathcal{H}_0) = \mathcal{Z}_0 [1 - \langle \mathcal{H} - \mathcal{H}_0 \rangle_0] \end{aligned}$$

where we have in the last step absorbed the normalization factor \mathcal{Z}_0^{-1} into the definition of the average. Now,

$$\begin{aligned} \mathcal{F} = -\log \mathcal{Z} &= -\log \mathcal{Z}_0 - \log [1 - \langle \mathcal{H} - \mathcal{H}_0 \rangle_0] \\ &\approx \mathcal{F}_0 + \langle \mathcal{H} - \mathcal{H}_0 \rangle_0 \end{aligned}$$

which is just the Feynman - Hellman theorem. A more detailed derivation including higher order terms can be found *e.g.* in [43, 2]. In our discussion the model Hamiltonian is always Gaussian, eqn. (1.14), so that

$$\mathcal{H}_0 = \frac{1}{2} \sum_{\vec{k}} \nu(\vec{k})^{-1} s(\vec{k}) s(-\vec{k})$$

and

$$\begin{aligned}\mathcal{Z}_0 &= \int \mathcal{D}s \exp[-\mathcal{H}_0] = \int \mathcal{D}s \exp\left[-\frac{1}{2} \sum_{\vec{k}} \nu(\vec{k})^{-1} |s(\vec{k})|^2\right] \\ &= \prod_{\vec{k}} \int ds(\vec{k}) \exp\left[-\frac{|s(\vec{k})|^2}{2\nu(\vec{k})}\right]\end{aligned}$$

and $\langle \mathcal{H}_0 \rangle_0$ is a constant [2] which will not be further considered. Now remembering that real and imaginary parts of $s(\vec{k})$ are independent degrees of freedom so that $|s(\vec{k})|^2 = \Re[s(\vec{k})]^2 + \Im[s(\vec{k})]^2$, the Gaussian double integral can be performed and

$$\mathcal{F}_0 = -\log \mathcal{Z}_0 = -\frac{1}{2} \sum_{\vec{k}} \log \nu(\vec{k})$$

so that finally (in units of $k_B T$)

$$F = -\frac{1}{2} \sum_{\vec{k}} \log \nu(\vec{k}) + \langle \mathcal{H} \rangle_0 \quad (1.15)$$

which is valid in both two and three dimensions. We have also derived eqn. (1.15) independently (apart from an irrelevant additive constant) in a purely information theoretical context in [42] without reference to thermodynamics (details of the derivation are in [42, 44]). There we found that the Gaussian term is of entropic origin and we will therefore sometimes refer to this term as an entropy term.

Evaluation of the remaining term $\langle \mathcal{H} \rangle_0$ is less simple. It is carried out for the twodimensional case in Chapter 2 and is given in three dimensions by (for the case of bulk symmetry)

$$\begin{aligned}\langle \mathcal{H} \rangle_0 &= \left\langle \int_S dS [2\kappa(H - H_0)^2 + \bar{\kappa}K] \right\rangle_0 \\ &= \int_V dV \left[2\kappa \left\langle \delta(s) \frac{dS}{dV} H^2 \right\rangle_0 + \bar{\kappa} \left\langle \delta(s) \frac{dS}{dV} K \right\rangle_0 \right] \\ &= 2\kappa V \left\langle \delta(s) \frac{dS}{dV} H^2 \right\rangle_0 + \bar{\kappa} V \left\langle \delta(s) \frac{dS}{dV} K \right\rangle_0\end{aligned} \quad (1.16)$$

where we chose $H_0 = 0$ because interfaces described by $s(\vec{r}) = 0$ have (*cf.* following Chapters) zero curvature. We have also used the fact that $s(\vec{r})$ is translationally invariant and the Dirac delta function makes sure that evaluation of the curvature energy is restricted to the interface. The ensemble averages $\left\langle \delta(s) \frac{dS}{dV} H \right\rangle_0$ and $\left\langle \delta(s) \frac{dS}{dV} K \right\rangle_0$ contain in general zeroth, first and second derivatives – associated with the curvatures H and K – of the

random variable $s(\vec{r})$. The ensemble average $\langle \mathcal{H} \rangle_0$ was first calculated in the seminal paper [37] by Teubner who used the fact that the joint distribution of the Gaussian random process $s(\vec{r})$ and its derivatives is a multivariate Gaussian distribution [37, 41, 45]

$$p = \frac{1}{\sqrt{(2\pi)^n |A|}} \exp \left[-\frac{1}{2} \vec{x} A^{-1} \vec{x}^T \right] \quad (1.17)$$

where \vec{x} contains the whole set of n random variables comprising s and its first and second derivatives, and where the matrix elements of the correlation matrix A contain all possible auto- and cross correlations between the random variables. Although practical evaluation of eqn. (1.17) and $\langle \mathcal{H} \rangle_0$ can be quite complicated (Chapters 2 - 4) it is also clear that because our calculation is Gaussian and only depends on $\nu(\vec{k})$ the final result for $\langle \mathcal{H} \rangle_0$ can again only be a function of $\nu(\vec{k})$. Similarly, the constraint eqn. (1.3) (in three dimensions) can be calculated as

$$\left\langle \frac{S}{V} \right\rangle_0 = \left\langle \delta(s) \frac{dS}{dV} \right\rangle_0 \quad (1.18)$$

which usually only involves a reduced correlation matrix containing elements up to the first derivatives. The last constraint which has to be implemented to complete the theoretical formulation is self-avoidance. This will be discussed more appropriately in the respective Chapters. Eqns. (1.16,1.18) thus establish the basis for a systematic approximation to the thermodynamics of eqns. (1.2,1.3).

The next step is to find the best possible approximation within this scheme. We have pointed out that all constituents of eqn. (1.15) only depend on $\nu(\vec{k})$. Hence finding the optimal solution can be done by functionally minimizing the free energy density $f = F/V$ with respect to the only available parameter, the structure factor $\nu(\vec{k})$

$$\frac{\partial f[\nu(\vec{k})]}{\partial \nu(\vec{k})} = 0 \quad (1.19)$$

By functionally minimizing with respect to $\nu(\vec{k})$ we pick the *best possible Gaussian theory* whose free energy density $f[\nu(\vec{k})]$ comes closest to the free energy density F/V of the real ensemble of fluctuating interfaces. At the same time, by determining variationally $\nu(\vec{k})$ we have also *consistently determined the structure* of the interface ensemble. $\nu(\vec{k})$ determines the film and/or bulk structure factor depending on the detailed formulation of the theory.

Variational Theory of Smectic Lamellar Phases

In the preceding chapter we established a variational method which will allow us to formulate approximate solutions to the structure and thermodynamics of systems governed by the bending Hamiltonian. Smectic lamellar phases are probably the most studied among fluctuating amphiphilic phases and are therefore an ideal starting point of our investigation before proceeding to more complex systems.

2.1 Introduction

Lamellar film geometries are commonly observed in both binary and ternary amphiphilic systems, where the bulk material is separated by regularly stacked sheets of surfactant film with a characteristic average layer spacing d . The inverse spacing $k_0 = 2\pi/d$ can often be measured in scattering experiments by the position of a quasi-Bragg peak [46, 47]. A peak of this type indicates systems with long range order in the orientation of the films – *i.e.* all the films are essentially parallel – but only quasi long range positional order [46]. Strict long range positional order is destroyed by the thermal fluctuations of the surfactant films around their average layer positions [48] so that quasi-Bragg singularities take the place of genuine Bragg peaks [47, 48, 49]. This behaviour is experimentally well established in lamellar phases which are not too dilute [50]. For these systems it is assumed that the topology of the multilamellar system is simple, with a negligible number

of saddle-like defects connecting adjacent layers. Then the Hamiltonian simplifies to

$$\mathcal{H} = 2\kappa \int_S dS H^2 \quad (2.1)$$

so that the physical parameters which specify the equilibrium state of a (symmetric) lamellar system are essentially reduced to the amphiphile concentration ϕ_s and the bending stiffness κ of the elastic surfactant film.

Models of smectic lamellar phases have so far been treated in harmonic approximation of the bending Hamiltonian¹ which allows for application of the equipartition theorem to determine the mode distributions of thermally undulating layers. Helfrich suggested two techniques in his original work [26]:

(a) The Landau - Peierls - de Gennes form of the bending energy associated with small local displacements $u(\vec{r}) = u(x, y, z)$ from perfectly equidistant lamellae reads [26]

$$g \approx \frac{1}{2} B u_z^2 + \frac{1}{2} \kappa [u_{xx}^2 + u_{yy}^2] \quad (2.2)$$

where B denotes the smectic elasticity modulus and κ is the bending constant as introduced in eqn. (2.1) (note that eqn. (2.2) is *not* scale-invariant). After Fourier expansion one can apply the equipartition theorem for quadratic forms so that the structure factor, $\nu(\vec{k}) = V^{-1} \langle |u(\vec{k})|^2 \rangle_0$, reads [26]

$$\nu(\vec{k}) = [B k_\rho^2 + \kappa k_z^4]^{-1} \quad (2.3)$$

From standard Gaussian theory (*cf.* Chapter 1) we know that the free energy density difference between confined ($B \neq 0$) and unconfined ($B = 0$) systems reads

$$\Delta f = \sum_{\vec{k}} \log \frac{\nu(B = 0, \kappa; \vec{k})}{\nu(B, \kappa; \vec{k})} \quad (2.4)$$

So far neither the interlayer spacing nor the steric hindrance from neighboring layers have entered. Helfrich chooses to introduce the spacing by imposing a cut-off k_0 in z - direction

$$\Delta f(B, \kappa, d) \sim \int_0^{k_c} \int_0^{k_0} dk_\rho dk_z \log \frac{k_\rho^4}{(k_z/\lambda)^2 + k_\rho^4}, \quad \lambda = \sqrt{\frac{\kappa}{B}} \quad (2.5)$$

and mimics the steric hindrance by adjusting self-consistently the smectic elasticity B , $B \stackrel{!}{=} d \frac{\partial^2 f}{\partial d^2}$. The result for the free energy per area is well-known [26]

$$\Delta f(\kappa, d) = \frac{3\pi^2}{128} \kappa^{-1} d^{-2} \quad (2.6)$$

¹The only exception known to us is the work by Golubović & Lubensky [51] which gives the first order correction to harmonic solutions.

(b) As the statistics of all layers is identical one can approximately consider a single membrane (or unit cell) between hard walls where the undulations are now expressed in Monge gauge $u(\vec{r}) = u(x, y)$, so that

$$g \approx \frac{1}{2} \kappa [u_{xx}^2 + u_{yy}^2] \quad (2.7)$$

It is usually argued that steric hindrance should be implemented by confining the membrane between hard walls. In reality, it seems more likely that two neighboring layers can indeed fuse at a high but not infinite energy cost. In any way, it has been so far impossible to surmount the mathematical difficulty of representing either saddle-like perforations or hard walls. In practice, one uses instead the harmonic potential

$$\langle u^2(\vec{r}) \rangle_0 = \mu d^2 \quad (2.8)$$

where μ is a constant of order unity. The equipartition theorem has to be applied to the energy modified by the hard wall constraint. Helfrich uses a phenomenological argument² to show that the ratio of free to constrained structure factors should be

$$\frac{\nu_{free}(\vec{k})}{\nu_{constrained}(\vec{k})} = \frac{k^4}{k^4 + \tilde{k}^4} \quad (2.9)$$

where $\nu(\vec{k}) = A^{-1} \langle |u(\vec{k})|^2 \rangle_0$. Gaussian theory yields for the difference in free energy per area between free and confined membrane, *cf.* eqn. (2.4)

$$\Delta f = \sum_{\vec{k}} \log \frac{\nu_{free}(\vec{k})}{\nu_{constrained}(\vec{k})} \quad (2.10)$$

Both methods (a) and (b) lead after evaluation of the integrals eqns. (2.5,2.10) eventually to the approximate repulsive entropic force (per volume) due to volume occupied by neighboring layers [26]

$$\Delta f \sim d^{-3} \quad (2.11)$$

Helfrich's seminal theory has experienced some discussion and a number of attempts for improvement. On the purely formal side neither the introduction of the cut-off at k_0 nor of the evaluation of B appear completely clear. The main problem here is that the

²The details of Helfrich's argument are given in [26]. Because this approach is not entirely satisfactory we will not present it here. Helfrich himself states that "It would be attractive to derive the general form of the function $\nu(\vec{k})$ by minimizing a free energy." This is exactly what the variational theory will achieve, for the most general case of the full non-linear Hamiltonian and the proper implementation of the constant surface area constraint.

Hamiltonian eqn. (1.2) is to a very good approximation scale-invariant while eqn. (2.2) breaks scale-invariance. Furthermore, in method (b) the phenomenological argument leading to eqn. (2.9) has been reformulated in the more recent literature [52].

Helfrich's theory in its original formulation operated in an ensemble characterized by fluctuating film area and fixed area of the associated projected surface, named open - framed ensemble in the classification of David & Leibler [53] whose experimental equivalent, black membranes [14], have to our knowledge never been investigated in confined situations. Therefore Helfrich's work has been reinterpreted [51] as a closed - unframed ensemble where the crumpling of the system is negligible under all circumstances. This is self-consistent only in the (low temperature) limit of large $\kappa \rightarrow \infty$. Only in this limit, the layer spacing d which is the proper, physical parameter associated with open - framed ensembles and surfactant concentration ϕ_s which naturally characterizes closed - unframed systems are essentially identical quantities, $d \sim \phi_s^{-1}$. This equivalence reveals immediately that the steric force law for the free energy density is nothing else but the scaling relation $f \sim \phi_s^3$ which can be directly derived from the scale invariance of the bending Hamiltonian and standard scaling arguments, as discussed in Chapter 1. The low temperature limit, however, should be exactly the one in which undulations are least important [54]. Naturally, a number of authors have therefore over the past years raised the issue of a more general treatment of closed - unframed ensembles beyond the low temperature limit [10, 55, 56]. This matter has gained particular urgency since the interpretation of the pioneering scattering experiments by Safinya *et al.* on smectic lamellar phases [47] was based on Helfrich's low temperature approximation while at the same time the experimental value of $\kappa \approx 1$ was quoted which should be well beyond the region of validity of Helfrich's calculation.

2.2 Variational Theory

The formulation of a generalized theory has to follow rigorously the rules set out in Chapter 1. This means that the surfactant concentration or film area is strictly fixed in accordance with eqn. (1.3) and as the bending modulus κ should not be restricted to the low temperature limit layer crumpling becomes an important factor in the theory. By fixing ϕ_s and κ only (but *not* crumpling or spacing), phase space outside the pure scaling regime becomes accessible and we can study in detail how *e.g.* equilibrium layer

crumpling C and average spacing d depend on ϕ_s and κ . We also do not *a priori* assume that the undulations always scale – as indicated by Helfrich’s scaling law $f \sim \phi_s^3$ – but have to determine the optimal state for every pair ϕ_s, κ variationally. To clarify the basic problem we have drawn in fig. (2-1) two possible configurations of a smectic lamellar phase at given κ and ϕ_s . Our task will be to formulate a theory which can determine which state is lower in free energy.

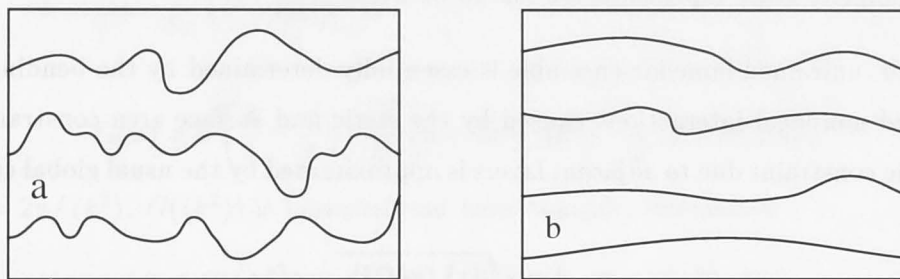


Figure 2-1: Sketch of two possible configurations of a smectic lamellar systems at given surfactant concentration. Due to surfactant conservation layer density and layer crumpling are coupled. (a) shows a configuration characterized by large interlayer spacing and strong crumpling, while (b) depicts a state with smooth undulations and small interlayer distance. Spacing and crumpling are measurable quantities in smectic phases.

Other physical quantities will arise naturally from the minimization of the free energy density. In particular, we will consistently evaluate the scattering structure factor, the renormalization of the bending modulus (which finds a very simple formulation in the variational theory), and the steric repulsion force for an ensemble characterized by the full, non-linear bending Hamiltonian.

The thermodynamics of lamellar surfactant phases can be conveniently studied using a model ensemble of essentially parallel, but thermally undulating interfaces. The mean positions of the undulating interfaces with surface area S are given by a set of flat, parallel surfaces with projected or base area A . The surface position of an individual undulating layer can be described by the displacement variable $u(\vec{r})$ normal to the projected surface (*cf.* eqn. (1.13) in Chapter 1)

$$u(\vec{r}) = \sum_{\vec{k}} u(\vec{k}) e^{i\vec{k}\vec{r}} \quad (2.12)$$

Although commonly used, the Monge representation of states, eqn. (2.12), is only an approximation as it is single-valued and does not describe surfaces with overhanging parts or topological defects, such as saddle structures which could connect neighbouring layers. However, even in the most swollen experimental samples [50, 10], the ratio of real to

projected surface area or crumpling ratio is $C = S/A \approx 1.2$. Usually the crumpling ratio is close to unity [57], and hence the single-valuedness should be a minor deficiency of the states eqn. (2.12). On theoretical grounds it has been suggested that topological changes can be neglected as long as the interlayer spacing is much smaller than the persistence length $d \ll \xi_k = r_m \exp(4\pi\kappa/3)$ [53] *i.e.* for membranes with not too small bending modulus κ . We restrict our study therefore to membranes with $\kappa \geq 1$. Below this value a more complete state representation has to be used.

The closed, unframed lamellar ensemble is essentially determined by the bending Hamiltonian and non-local interactions caused by the steric and surface area constraints. The local steric constraint due to adjacent layers is approximated by the usual global constraint [26]

$$d = \sqrt{\mu^{-1} \langle u(\vec{r})^2 \rangle_0} \quad (2.13)$$

where μ is a numerical factor³. We follow [26] and will set $\mu = 1/24$ (in our definition we operate with walls at $\pm d/2$) later for numerical calculations. Due to the incompressibility of the surfactant film [2], closed surfactant systems with surfactant volume fraction ϕ_s have an approximately constant surface to volume ratio

$$\phi_s \sim \frac{S}{V} = \frac{S}{A} d^{-1} = \text{const.} \quad (2.14)$$

i.e. in the closed - unframed ensemble the *total* surface area is kept constant (whereas the *individual* layer area and crumpling parameter may vary). The projected area to volume ratio A/V is not a conserved quantity.

Using Gaussian model states, the free energy \mathcal{F} (in units of $k_B T$) associated with the bending Hamiltonian \mathcal{H} can be approximated as shown in Chapter 1, $\mathcal{F} \leq F = -\sum_{\vec{k}} \log \sqrt{\nu(\vec{k})} + \langle \mathcal{H} \rangle_0$, where the subscript 0 refers to Gaussian states characterized by the Hamiltonian $\mathcal{H}_0 \sim \sum_{\vec{k}} \nu(\vec{k})^{-1} u(\vec{k}) u(-\vec{k})$. The entropic term has been derived from the partition function of the Gaussian ensemble (*cf.* Chapter 1) and the average of the bending energy $\langle \mathcal{H} \rangle_0$ can be calculated using the joint probability distribution $p(u_x, u_y, u_{xx}, u_{xy}, u_{yy})$ of the first and second derivatives of the height field $u(\vec{r})$ which is given by a multivariate Gaussian distribution (*cf.* Appendix). With the moments of the structure factor defined by

$$\langle k^n \rangle = \int_0^{k_c} k^{n+1} \nu(k) dk \quad (2.15)$$

³Note that with approximation eqn. (2.13) self-avoidance is *not* strictly obeyed.

where the cut-off k_c is of the order of an inverse molecular size, $k_c = \frac{2\pi}{r_c} = 1$ and the convenient notation $\langle k^0 \rangle = \langle 1 \rangle \sim \langle u^2 \rangle_0$ we can write (cf. Appendix)

$$\begin{aligned} \langle \mathcal{H} \rangle_0 &= \left\langle 2\kappa \int_A dA \frac{dS}{dA} H^2 \right\rangle_0 = 2\kappa A \left\langle \frac{dS}{dA} H^2 \right\rangle_0 \\ &= 2\kappa \left[\frac{1}{4} \langle k^4 \rangle \left\langle \left(1 + (\vec{\nabla}u)^2\right)^{-\frac{3}{2}} + \frac{3}{8} (\vec{\nabla}u)^4 \left(1 + (\vec{\nabla}u)^2\right)^{-\frac{5}{2}} \right\rangle_0 \right] \\ &= \frac{\kappa}{4\pi} \langle k^4 \rangle G(\langle k^2 \rangle) \end{aligned} \quad (2.16)$$

where

$$G(x) = x \left(\frac{3}{4} - \frac{x}{2} + \frac{\sqrt{\pi}}{8} (3 - 4x + 4x^2) \frac{e^x}{\sqrt{x}} (1 - \operatorname{erf}\sqrt{x}) \right) \quad (2.17)$$

with $x = 2\pi / \langle k^2 \rangle$. $G(\langle k^2 \rangle)$ is bounded and monotonically decreasing

$$0 \leq G(\langle k^2 \rangle) \leq 1, \quad G'(\langle k^2 \rangle) \leq 0 \quad \text{for} \quad \langle k^2 \rangle \geq 0 \quad (2.18)$$

For small $\langle k^2 \rangle$ it can be expanded into

$$G(\langle k^2 \rangle) = 1 - \frac{3}{4\pi} \langle k^2 \rangle + \frac{9}{8\pi^2} \langle k^2 \rangle^2 - O(\langle k^2 \rangle^3) \quad (2.19)$$

To quantify the surface area constraint we evaluate the crumpling ratio

$$C = \left\langle \frac{dS}{dA} \right\rangle_0 = \left\langle \left(1 + (\vec{\nabla}u)^2\right)^{1/2} \right\rangle_0 = \frac{e^x (\sqrt{\pi} - 2\Gamma(\frac{3}{2}, 0, x))}{2\sqrt{x}} \quad (2.20)$$

which can be expanded for $\langle k^2 \rangle \ll 1$

$$C(\langle k^2 \rangle) = 1 + \frac{1}{4\pi} \langle k^2 \rangle - \frac{1}{16\pi^2} \langle k^2 \rangle^2 + O(\langle k^2 \rangle^3) \quad (2.21)$$

2.2.1 Renormalization of the Bending Constant

In the harmonic approximation the differential operators $\frac{dS}{dA}$ and H are considered in the limit $u_x^2 + u_y^2 \rightarrow 0$ i.e. $\langle k^2 \rangle \rightarrow 0$. Then, $\frac{dS}{dA} \approx 1$ and $H \approx \frac{1}{2} [u_{xx}^2 + u_{yy}^2]$ so that the ensemble averages read

$$\langle \mathcal{H} \rangle_0 \approx \frac{\kappa}{4\pi} \langle k^4 \rangle, \quad C(\langle k^2 \rangle) \approx 1 \quad (2.22)$$

Comparison with the general expression eqn. (2.16) shows that the function $G(\langle k^2 \rangle)$ contains the non-linear coupling between modes i.e. yields the *general* effective, thermally softened bending constant [58]

$$\kappa_{eff} = G(\langle k^2 \rangle) \kappa \quad (2.23)$$

Therefore our variational method is equivalent to a Hartree approximation which replaces the non-linear Hamiltonian by a Gaussian with effective parameters which are determined self-consistently. We can compare this with the well established *approximate* renormalization of the bending constant in *free* membranes. There the approximate structure factor is known to be

$$\nu(k) = (\kappa k^4)^{-1} \quad (2.24)$$

Applying eqns. (2.17,2.19) to this case we retrieve the well-known first order renormalization correction of the bending constant

$$G(\langle k^2 \rangle) \approx 1 - \frac{3}{4\pi\kappa} \log \frac{k_c}{k_{min}} \quad (2.25)$$

in agreement with the results of [59, 60] (k_{min} is a lower frequency cut-off). For *closed* systems the exact form of the renormalization is – as we will see below – different. It is in general not possible to use the renormalization derived for a free membrane in a system characterized by other physical constraints.

2.2.2 Structure Factor and Free Energy

With the averages eqn. (2.16) and eqn. (2.20) the free energy density can be written as a functional of the structure factor $\nu(k)$ (using relation eqn. (2.13) for d)

$$f[\nu(k)] = \frac{F}{Ad} = \frac{1}{4\pi d} \left(\kappa \langle k^4 \rangle G(\langle k^2 \rangle) - \int_0^{k_c} k \log \nu(k) dk \right) \quad (2.26)$$

This expression has to be functionally minimized with respect to $\nu(k)$ under one constraint, $\phi_s \sim S/V = \text{const}$ which can be coupled to eqn. (2.26) by a Lagrange multiplier. The result will be a minimal $\nu(k)$ from which the equilibrium layer spacing and crumpling and the steric force law can be calculated as functions of ϕ_s and κ . We note that the free energy per area usually contains self-energy terms proportional to k_c^2 *i.e.* the number of degrees of freedom associated with the base surface. These terms represent an insignificant additive constant in the discussion of the free energy *per area*, but have to be omitted when going to the free energy *per volume*; we will continue this discussion later when this point becomes relevant for the calculation.

The minimization can be conveniently carried out by variationally minimizing

$$f[\nu(k)] = \frac{1}{4\pi D(\langle 1 \rangle)} \left(\kappa \langle k^4 \rangle G(\langle k^2 \rangle) - \int_0^{k_c} k \log \nu(k) dk + \lambda_1 C(\langle k^2 \rangle) + \lambda_2 D(\langle 1 \rangle)^2 \right) \quad (2.27)$$

under *two* constraints

$$d = D(\langle 1 \rangle) = \sqrt{\frac{\langle 1 \rangle}{2\pi\mu}} = \text{const}, \quad \frac{S}{V} = \frac{C(\langle k^2 \rangle)}{D(\langle 1 \rangle)} = \text{const} \quad (2.28)$$

The additional constraint on d will be removed later by $\partial f / \partial D = 0$. We prefer the notation $D(\langle 1 \rangle)$ to stress that the layer density is in this context not preset as in zero order theories, but a functional.

Differentiation turns the $\log \nu(\vec{k})$ term into $1/\nu(\vec{k})$ while the moments $\langle k^4 \rangle$, $\langle k^2 \rangle$, $\langle 1 \rangle$ yield factors of k^4 , k^2 and const , respectively⁴. Thus the general form of the consistent structure factor reads

$$\nu(k) = \frac{a}{k^4 - k_0^2 k^2 + \tilde{k}^4} \quad (2.29)$$

with

$$a = \kappa^{-1} G(\langle k^2 \rangle)^{-1} = \kappa_{eff}^{-1} \quad (2.30)$$

and

$$k_0^2 = - \left(\frac{\langle k^4 \rangle G'(\langle k^2 \rangle)}{G(\langle k^2 \rangle)} + \frac{\lambda_1}{\kappa} \frac{C'(\langle k^2 \rangle)}{G(\langle k^2 \rangle)} \right), \quad \tilde{k}^4 = \frac{\lambda_2 D(\langle 1 \rangle) D'(\langle 1 \rangle)}{\kappa G(\langle k^2 \rangle)} \quad (2.31)$$

where $a \geq 0$, $\tilde{k}^4 > 0$ while k_0^2 can assume any sign. For given surfactant concentration ϕ_s and bare bending stiffness κ the coefficient a is readily given by eqn. (2.30) because ϕ_s determines $C(\langle k^2 \rangle)$ which in turn determines $G(\langle k^2 \rangle)$. The coefficients k_0^2 , \tilde{k}^4 cannot be directly calculated from eqn. (2.31) but have to be evaluated from the non-linear equation system

$$\frac{a}{\sqrt{4\tilde{k}^4 - k_0^4}} \left(\arctan \frac{k_0^2}{\sqrt{4\tilde{k}^4 - k_0^4}} + \arctan \frac{2k_c^2 - k_0^2}{\sqrt{4\tilde{k}^4 - k_0^4}} \right) = 2\pi\mu d^2 \quad (2.32)$$

$$\pi\mu k_0^2 d^2 - \frac{a}{4} \log \frac{\tilde{k}^4}{k_c^4 - k_c^2 k_0^2 + \tilde{k}^4} = C^{-1}(\phi_s d) \quad (2.33)$$

$$\frac{\partial f}{\partial d} = 0 \quad (2.34)$$

where eqns. (2.32,2.33) correspond to eqns. (2.28) and C^{-1} denotes an inverse function. The function $f(k_0, \tilde{k}, d; \kappa, \phi_s)$ can be obtained by inserting the relations

$$\langle k^2 \rangle = \frac{k_0^2}{2} \langle 1 \rangle - \frac{a}{4} \log h_1$$

⁴See, for example, [2] where the structure factor for the roughening transition is derived in a very similar way, or also [61].

$$\langle k^4 \rangle = \frac{1}{2}(k_0^4 - 2\tilde{k}^4) \langle 1 \rangle - \frac{a}{4} k_0^2 \log h_1 + \frac{a}{2} k_c^2 \quad (2.35)$$

$$\int_0^{k_c} k \log \nu(k) dk = \frac{1}{2a}(k_0^4 - 4\tilde{k}^4) \langle 1 \rangle - \frac{1}{4} k_0^2 \log h_1 + \frac{1}{2} k_c^2 \log h_2 + k_c^2 \quad (2.36)$$

with the abbreviations

$$h_1 = \tilde{k}^4 / (k_c^4 - k_0^2 k_c^2 + \tilde{k}^4), \quad h_2 = a / (k_c^4 - k_0^2 k_c^2 + \tilde{k}^4)$$

and eqn. (2.30) into eqn. (2.26)

$$\begin{aligned} f(k_0, \tilde{k}, d; \kappa, \phi_s) &= \frac{1}{4\pi d} \left[\kappa \langle k^4 \rangle G(\langle k^2 \rangle) - \int k \log f(k) dk \right] \\ &= d^{-1} \left[\mu(2a)^{-1} \tilde{k}^4 d^2 - (8\pi)^{-1} k_c^2 (1 + \log \nu(k_c)) \right] \end{aligned} \quad (2.37)$$

Thus we have reduced the problem to the solution of three relatively simple equations. In particular, solution of eqn. (2.32) and eqn. (2.33) is straightforward and reduces $f(k_0, \tilde{k}, d; \kappa, \phi_s)$ to $f(d; \kappa, \phi_s)$ so that we are left with the single equation $\partial f(d; \kappa, \phi_s) / \partial d = 0$. At this point we have to consider the self-energy. It is a harmless energy offset in problems where the total projected area is constant. In the present calculation, however, the layer density is allowed to vary and the offset would cause a spurious d^{-1} term in the free energy. In order to subtract the self-energy we fix the quantities a , k_0 , \tilde{k} , and d at their physical values, consider the limit $k_c \rightarrow \infty$ and discard all diverging terms in the spirit of a field theoretical renormalization [6]. After subtracting the divergences the free energy density reads

$$f(k_0, \tilde{k}, d; \kappa, \phi_s) = d^{-1} \left[\mu(2a)^{-1} \tilde{k}^4 d^2 + (8\pi)^{-1} k_c^2 \log(1 - k_0^2 k_c^{-2} + \tilde{k}^4 k_c^{-4}) \right] \quad (2.38)$$

The equation system eqns. (2.32,2.33,2.34) with f given by eqn. (2.38) defines the solution of the problem to all orders in κ^{-1} .

2.2.3 Helfrich Limit and Crumpling Corrections

We start by solving analytically to first and second order in κ^{-1} . Since k_0/k_c and \tilde{k}/k_c are very small quantities we may expand the logarithmic term in eqn. (2.38) which then becomes independent of k_c and equal to $-(8\pi)^{-1} k_0^2$. Solving the simplified equation system yields the well-known first order results for the structure factor [26] (*cf.* Appendix for the derivation of these and the forthcoming results),

$$k_0^2 \approx 0, \quad \tilde{k}^2 \approx (8\mu)^{-1} \kappa^{-1} \phi_s^2 \quad (2.39)$$

the crumpling factor

$$C = \phi_s d \approx 1 + c_1 \kappa^{-1} - c_2 \kappa^{-2} \quad (2.40)$$

with [51],

$$c_1 = -\frac{1}{4\pi} \log[(8\mu)^{-\frac{1}{2}} \kappa^{-\frac{1}{2}} \phi_s] \quad (2.41)$$

the renormalization factor

$$G \approx 1 - g_1 \kappa^{-1} + g_2 \kappa^{-2} \quad (2.42)$$

with [51],

$$g_1 = -\frac{3}{4\pi} \log[(8\mu)^{-\frac{1}{2}} \kappa^{-\frac{1}{2}} \phi_s] \quad (2.43)$$

and the free energy density [51]

$$f(\kappa, \phi_s) \approx (128\mu)^{-1} \kappa^{-1} \phi_s^3 \quad (2.44)$$

which is exactly half the result given in Helfrich's original paper. Helfrich's formalism is equivalent to a purely Gaussian theory *i.e.* in Feynman - Hellman formalism (*cf.* Chapter 1) [26, 62]

$$\mathcal{F} \leq F = F_0 \quad (2.45)$$

While this captures the entropic contribution to the free energy, it neglects the bending energy term $\langle \mathcal{H} \rangle_0$. However, we see that the bending energy term eqn. (2.35) accounts to essentially half of the entropic term eqn. (2.36). The physical meaning is evident: apart from the entropic repulsion there is also a considerable energetic attraction because the undulations have to become smoother and thus less costly in bending energy when the layers approach each other. The strength of this attraction reduces the entropic repulsion. This also suggests that the force constant derived in Helfrich's method (a) is overestimated.

In second order, a k^2 term with positive coefficient

$$k_0^2 \approx \frac{3}{128\mu} \kappa^{-2} \phi_s^2 \quad (2.46)$$

emerges in the structure factor which should be observable in systems with low bending stiffness ($\kappa \approx 1$ [57, 47]) as a pronounced rounding or slight bump in the scattering structure factor at low k .

The second order corrections to the swelling law and renormalization are

$$c_2 = -\frac{3}{512} - \frac{1}{8\pi^2} \log^2[(8\mu)^{-\frac{1}{2}} \kappa^{-\frac{1}{2}} \phi_s] \quad (2.47)$$

and

$$g_2 = -\frac{9}{512} + \frac{9}{16\pi^2} \log^2[(8\mu)^{-\frac{1}{2}} \kappa^{-\frac{1}{2}} \phi_s] \quad (2.48)$$

Both contain non-logarithmic terms which are directly related to film area conservation.

The free energy density up to second order in κ^{-1} reads

$$f(\kappa, \phi_s) \approx b_1 \kappa^{-1} \phi_s^3 - b_2 \kappa^{-2} \phi_s^3 + b_3 \kappa^{-2} \phi_s^5 \quad (2.49)$$

with $b_1 = (128\mu)^{-1}$, $b_2 = 3(1024\pi\mu)^{-1}$, $b_3 = (512\pi\mu^2)^{-1}$. The most important point is here that the free energy density does not contain logarithmic renormalization terms which could originate from the non-linear part of the bending energy G and the crumpling factor C because these two contributions cancel each other in second order. This indicates that Helfrich's results remain largely unaffected even by second order terms. It might explain why Helfrich's high κ model can in fact be used for the interpretation of data taken in semi-rigid or even soft systems such as the ones studied by Safinya *et al.* at $\kappa \approx 1$. The second term on the rhs of eqn. (2.49) is identical to a term found by Golubović & Lubensky [51] in their perturbation analysis and can be rationalized as a non-local interaction term due to the surface area constraint. The last term in eqn. (2.49) is proportional to ϕ_s^5 ; Wennerström & Olsson [27] have recently discussed such terms – although derived in a different theory from higher order elasticity terms – in the context of the lamellar to sponge transition. This term becomes significant at high surfactant concentration.

2.2.4 Numerical Results: Free Energy, Structure Factor, Swelling, Renormalization

The above approximations turn out to be unreliable at low bending rigidity. We have therefore solved the equation system eqns. (2.32,2.33,2.34) numerically.

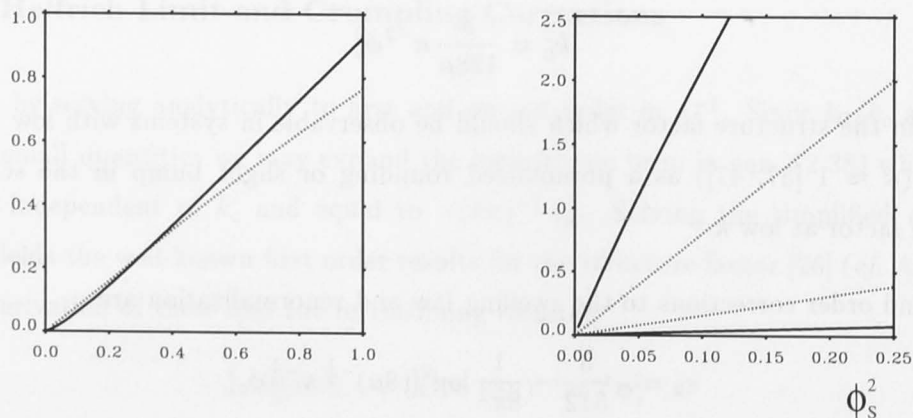


Figure 2-2: The coefficients k_0^2 and \tilde{k}^2 in the scattering structure factor eqn. (2.29) as functions of the bending constant κ and the surfactant concentration ϕ_s . (left) $k_0^2 \cdot 10^4$ vs κ^{-2} (solid line) and $\tilde{k}^2 \cdot 10^3$ vs κ^{-1} (dotted line) for $\phi_s = 0.1$. (right) $k_0^2 \cdot 2.5 \cdot 10^3$ vs ϕ_s^2 (solid line) and $\tilde{k}^2 \cdot 10^2$ vs ϕ_s^2 (dotted line) for $\kappa = 1$ (upper curves) and $\kappa = 5$ (lower curves).

In a series of figs. (2-2 - 2-4) we show numerical results which have maximal relative errors of 10^{-6} for k_0^2 and \tilde{k}^2 (fig. (2-2)), the crumpling C , the renormalization G , and the free energy density f for realistic values of κ and ϕ_s . The swelling factor $\phi_s d$ in fig. (2-3) shows the typical logarithmic dependence on ϕ_s – which has been verified in experiment [57] – for stiff film, $\kappa = 5$, but a systematic upward deviation for high dilution in the case of soft membranes, $\kappa \approx 1$. This deviation should be measurable and characteristic for soft lamellar phases. When comparing numerical and first order results we note significant differences in the case $\kappa = 1$; this casts some doubt on the first order fitting procedure used in [57] to estimate the value of the bending modulus in lamellar phases and we believe that the values for the bending moduli (of the soft systems) reported there could be underestimated by factors of up to $\approx 2 - 3$. Indeed, this correction factor seems to reconcile the results of the measurements of κ given in [57] with the results of alternative measurement techniques [63]. In fig. (2-3) we show the concentration dependence of the renormalization correction to the bending modulus. As expected, higher anharmonic terms lead in the case of soft membranes to strong deviations from the first order approximation.

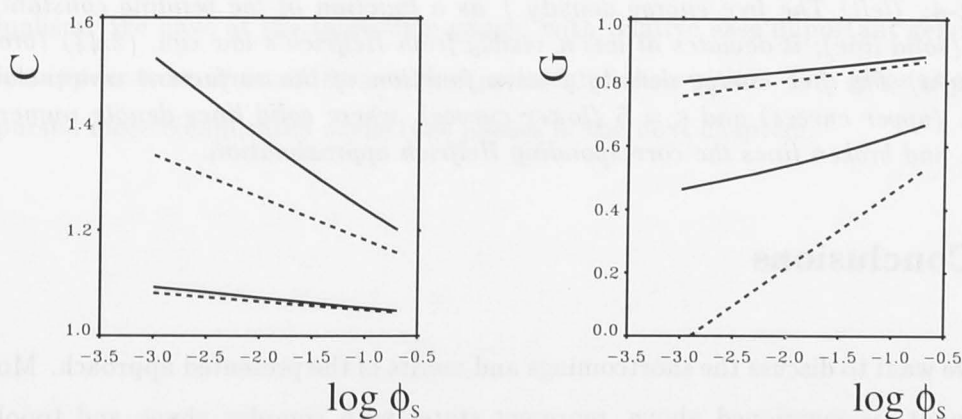


Figure 2-3: (left) The crumpling ratio $C = \phi_s d$ of ensembles of undulating membranes for $\kappa = 1$ (upper curves) and $\kappa = 5$ (lower curves) as a function of the surfactant concentration. Solid lines denote accurate numerical solutions, and broken lines the respective first order approximations, eqn. (2.41). The solid lines show a small deviation from the logarithmic law. (right) The renormalization of the bending constant G as a function

of surfactant concentration: numerical solutions (solid) and first order approximations (broken, eqn. (2.43)), for the $\kappa = 1$ (lower curves) and $\kappa = 5$ (upper curves).

Finally, in fig. (2-4) the free energy density as a function of the bending modulus and the surfactant concentration is shown. At given ϕ_s the steric repulsion is always lower than predicted by first order approximation. For a realistic regime, $\phi_s = 0.1$, $1 \leq \kappa \leq 10$, (fig. (2-4)) we find that the approximation is valid down to some $\kappa \approx 5$. For softer systems the complex interplay of anharmonic corrections to the Hamiltonian and the swelling corrections due to surface area conservation lead to deviations from the $1/\kappa$ - force law. However, as argued above, due to cancellation of renormalization and swelling terms up to second order in κ^{-1} the scaling $f \sim \phi_s^3$ is practically unchanged even for small $\kappa = 1$ (fig. (2-4)).

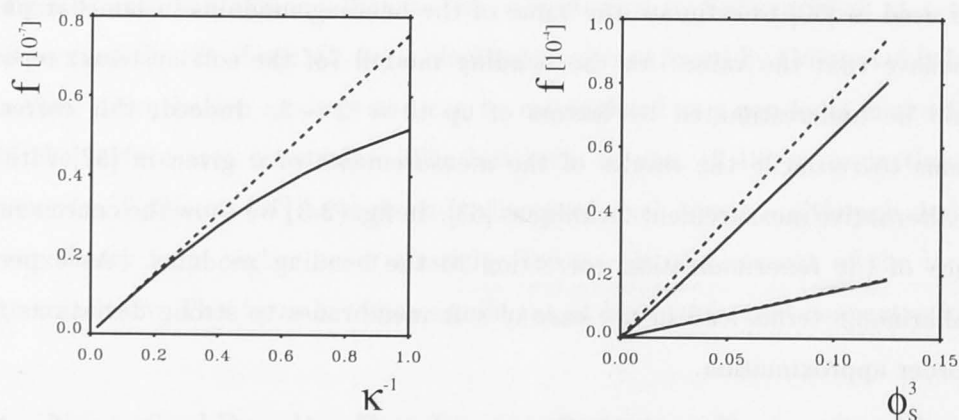


Figure 2-4: (left) The free energy density f as a function of the bending constant, at $\phi_s = 0.1$ (solid line); it deviates at low κ visibly from Helfrich's law eqn. (2.44) (broken line). (right) The free energy density f as a function of the surfactant concentration for $\kappa = 1$ (upper curves) and $\kappa = 5$ (lower curves), where solid lines denote numerical solutions, and broken lines the corresponding Helfrich approximation.

2.3 Conclusions

Finally, we want to discuss the shortcomings and merits of the presented approach. Monge gauge cannot, as mentioned above, represent states with complex shape and topology fluctuations [64]. Therefore the Gaussian curvature $\int K dS$ does not enter the calculation. Inclusion of this term leads to $\bar{\kappa}$ dependent contributions to the structure factor and free energy density,

$$f \sim b(\kappa, \bar{\kappa}) \phi_s^3 \quad (2.50)$$

and is likely to be crucial for the still poorly understood lamellar to sponge transition (*cf.* Chapter 4) [4]. This requires a sophisticated, non-perturbative generalization of the state representation which includes topological defects. Moreover, asymmetric lamellar phases – which contain, say, more water than oil so that two characteristic layers spacings are invoked – which certainly exist in ternary systems [4] and possibly also in binary phases cannot be discussed in the context of the presented theory. We will come back to the problem of topologically complex lamellar phases in the following chapters.

Nevertheless, the approach presented here is – within the validity of its assumptions – able to provide a simple and consistent description of multilamellar phases in terms of structure factor, swelling law, renormalization of the bending constant and the steric force law as functions of the surfactant concentration and the bending modulus. Its range of validity goes well beyond that of low temperature theories [51, 26]. The results are in agreement with known observations, and reveal new features which are related to the more accurate inclusion of layer crumpling, the constant area constraint and the usually neglected coupling terms in the bending Hamiltonian. These should be observable in the film structure factor and swelling law of soft and dilute smectic lamellar phases [50, 10]. Our results also show that Helfrich's first order steric force law is in fact also a good second order approximation, indicating that simple predictions of the Helfrich theory might be applicable even in semi-rigid regimes.

In the context of the development of this thesis we can state that application of the variational formalism has successfully reproduced a range of known results in one coherent formalism. We have at the same time gained with relative ease important generalization which appear to be in accordance with experimental observation. This gives us confidence to pursue more complicated surfactant phases in the next chapters.

2.A Appendix

Statistical Averages With the definition of the moments, eqn. (2.15), the covariance matrix A_{ij} contains the correlations of the first and second derivatives of the height field $u(\vec{r})$

	u_x	u_y	u_{xy}	u_{xx}	u_{yy}
u_x	$\frac{1}{4\pi} \langle k^2 \rangle$	0	0	0	0
u_y	0	$\frac{1}{4\pi} \langle k^2 \rangle$	0	0	0
u_{xy}	0	0	$\frac{1}{16\pi} \langle k^4 \rangle$	0	0
u_{xx}	0	0	0	$\frac{3}{16\pi} \langle k^4 \rangle$	$\frac{1}{16\pi} \langle k^4 \rangle$
u_{yy}	0	0	0	$\frac{1}{16\pi} \langle k^4 \rangle$	$\frac{3}{16\pi} \langle k^4 \rangle$

where each matrix element is the correlation bracket $\langle \dots \rangle_0$ which contains the derivative in the ordinate and abscissa. A practical calculation of the statistical average of various differential operators O is then based on a statistical integration over the Gaussian multivariate distribution eqn. (1.17) which reads here explicitly [45]

$$p = \frac{1}{\sqrt{(2\pi)^n |A|}} \int_{-\infty}^{+\infty} \dots \int_{-\infty}^{+\infty} \dots du_x du_y du_{xy} du_{xx} du_{yy} O \exp \left[-\frac{1}{2} \vec{x} A^{-1} \vec{x}^T \right]$$

where A is the correlation matrix defined above and $\vec{x} = (u_x, u_y, u_{xy}, u_{xx}, u_{yy})$. We will perform these integrations here explicitly and note that the same principle will be used for more complicated cases in the following two chapters.

With $u_x^2 + u_y^2 = v^2$

$$H = \frac{1}{2} \operatorname{div} \vec{n}, \quad \vec{n} = \frac{1}{2} [1 + v^2]^{-\frac{1}{2}} (u_x, u_y)^T, \quad dS/dA = [1 + v^2]^{\frac{1}{2}}$$

so that

$$\begin{aligned} \left\langle \frac{dS}{dA} H^2 \right\rangle_0 &= \left\langle \frac{4^{-1}}{[1 + v^2]^{\frac{3}{2}}} [(1 + u_x^2)^2 u_y^2 + (1 + u_y^2)^2 u_x^2 + 2(1 + u_x^2)(1 + u_y^2) u_{xx} u_{yy} + 4u_x^2 u_y^2 u_{xy}^2] \right\rangle_0 \\ &= \frac{1}{8\pi} \langle k^4 \rangle \left\langle (1 + v^2)^{-\frac{3}{2}} + \frac{3}{8} v^4 (1 + v^2)^{-\frac{5}{2}} \right\rangle_0 \end{aligned}$$

where we have used that *e.g.* $\langle u_x u_y \rangle_0 = 0$ and that all the correlation matrix elements of the second derivatives are proportional to $\langle k^4 \rangle$. The only non-trivial part is, with the

abbreviations $\sigma^2 = \langle k^2 \rangle / (4\pi)$ and $x = 1/(2\sigma^2)$,

$$\begin{aligned} \left\langle (1+v^2)^{-\frac{3}{2}} + \frac{3}{8}v^4(1+v^2)^{-\frac{5}{2}} \right\rangle_0 &= \frac{1}{2\pi\sigma^2} \int_{-\infty}^{+\infty} e^{-\frac{v^2}{2\sigma^2}} \left[(1+v^2)^{-\frac{3}{2}} + \frac{3}{8}v^4(1+v^2)^{-\frac{5}{2}} \right] du_x du_y \\ &= \frac{1}{\sigma^2} \int_0^\infty v e^{-\frac{v^2}{2\sigma^2}} \left[(1+v^2)^{-\frac{3}{2}} + \frac{3}{8}v^4(1+v^2)^{-\frac{5}{2}} \right] dv \\ &= \frac{1}{2\sigma^2} \int_0^\infty e^{-xt} \left[(1+t)^{-\frac{3}{2}} + \frac{3}{8}t^2(1+t)^{-\frac{5}{2}} \right] dt \\ &= x e^x \int_1^\infty e^{-xt} \left[t^{-\frac{3}{2}} + \frac{3}{8}(t-1)^2 t^{-\frac{5}{2}} \right] dt \\ &= x \left[\frac{3}{4} - \frac{x}{2} + \frac{\sqrt{\pi}}{8} (3-4x+4x^2) \frac{e^x}{\sqrt{x}} (1 - \operatorname{erf}\sqrt{x}) \right] \end{aligned}$$

which is eqn. (2.17) in the text.

The integral for the crumpling, eqn. (2.21), is straightforward

$$\left\langle (1+v^2)^{1/2} \right\rangle_0 = \frac{1}{\sigma^2} \int_0^\infty v e^{-\frac{v^2}{2\sigma^2}} (1+v^2)^{1/2} dv = x e^x \int_1^\infty e^{-xt} \sqrt{t} dt = \frac{e^x (\sqrt{\pi} - 2\Gamma(\frac{3}{2}, 0, x))}{2\sqrt{x}}$$

The technique outlined here will be re-applied in different contexts in Chapters 3 and 4.

Crumpling Corrections To zeroth order in crumpling we find

$$C \approx \phi_s d \iff d \approx \phi_s^{-1} \iff \langle k^2 \rangle \approx 0$$

it follows immediately that $k_0 \approx 0$. Thus d and k_0 are already fixed, and eqn. (2.32) determines \tilde{k}^2 which has a simple solution [26, 51], eqn. (2.39). The lowest order approximation to the free energy eqn. (2.44) follows without problem.

To calculate the next order we introduce

$$\tilde{q} = (\tilde{k}d)^2, \quad q_0 = (k_0d)^2, \quad q_c = (k_c d)^2$$

Then, eqns. (2.32,2.33) simplify to

$$\begin{aligned} \frac{a}{\sqrt{4\tilde{q}^2 - q_0^2}} \left(\arctan \frac{q_0}{\sqrt{4\tilde{q}^2 - q_0^2}} + \frac{\pi}{2} \right) &= 2\pi\mu \quad (2.A1) \\ \frac{4}{\mu} (\phi_s d - 1) - \frac{a}{2\pi\mu} (\log \tilde{q} - \log q_c) &= q_0 \end{aligned}$$

and the free energy density can be written⁵

$$f = d^{-3} \left(\frac{\mu}{2a} \tilde{q}^2 - \frac{1}{8\pi} q_0 \right) \quad (2.A2)$$

⁵The following four equations are due to M. Teubner.

Now we take the derivatives of eqns. (2.A1) with respect to d

$$\begin{aligned} \left(\frac{q_0}{\tilde{q}} + 8\pi\mu\frac{\tilde{q}}{a}\right)\tilde{q}' &= \left(1 + 2\pi\mu\frac{q_0}{a}\right)q_0' \\ q_0' &= \frac{4\phi_s}{\mu} + \frac{1}{2\pi\mu}\frac{a}{\tilde{q}}\tilde{q}' \end{aligned} \quad (2.A3)$$

and of the free energy density eqn. (2.A2)

$$f' = d^{-4} \left[-\frac{3\mu}{2a}\tilde{q}^2 + d \left(\frac{\mu}{a}\tilde{q}\tilde{q}' - \frac{1}{8\pi}q_0' \right) \right] = 0 \quad (2.A4)$$

Solving the linear equation system eqns. (2.A3) with respect to \tilde{q}' , q_0' , inserting \tilde{q}' and q_0' into eqn. (2.A4) and keeping the lowest order terms yields

$$q_0 = \frac{3}{2}\mu\tilde{q}^2$$

which leads to eqn. (2.46) when we use the first order approximation for \tilde{q} . Having gained \tilde{k}^2 to first and k_0^2 to second order, we see that the equation for the second moment is consistently up to second order

$$\langle k^2 \rangle = \pi\mu k_0^2 d^2 - \frac{a}{4} \log \frac{\tilde{k}^4}{k_c^4 - k_c^2 k_0^2 + \tilde{k}^4} \approx \frac{3\pi}{128\kappa^2} - \frac{a}{2} \log \tilde{k}^2$$

where we have to keep in mind that $a^{-1} \approx \kappa(1 - \frac{3}{4\pi}\langle k^2 \rangle)$ has to be included self-consistently. Note also that possible terms $\sim \kappa^{-2}$ in the expression for \tilde{k}^2 are not necessary to derive $\langle k^2 \rangle$ to second order. The consistent expressions for C and G up to second order can be gained from the expansions eqns. (2.19,2.21). Once \tilde{k}^2 , k_0^2 and the crumpling, which is directly related to d , are determined the free energy density eqn. (2.49) can be calculated by series expansion.

Random Interface Model of Sponge Phases

We have seen that application of the variational theory to the simple case of smectic lamellar phases allowed us to go beyond the harmonic approximation nearly exclusively used throughout the literature on fluctuating membranes. While this is important for lamellar phases, it should be even more so in the most distinct example of a fluctuating membrane phase, the bicontinuous sponge phase.

3.1 Introduction

A microscopic description of a ternary (binary) surfactant system with all the surfactant molecules located at the water/oil (inside/outside) interfaces begins with a Hamiltonian, $H(\psi)$ where ψ is a local composition variable with, for example, $\psi = -1$ corresponding to water (inside) and $\psi = 1$ corresponding to oil (outside). The Hamiltonian can, in principle, take into account all the microscopic interactions, including the long range interactions which give rise to the curvature energy of the surfactant film. If we restrict ourselves to two-body interactions it can be written as an infinite range Ising Hamiltonian¹

$$\mathcal{H}_I = \frac{1}{2} \sum_{i \neq j} V_{ij} \psi_i \psi_j \quad (3.1)$$

¹Unlike the models based on nearest or next nearest neighbor interactions mentioned in Chapter 1.

If we apply the Gaussian transformation of quadratic Hamiltonians [65] (sometimes also called Hubbard - Stratonovich transformation)

$$\exp \left[\frac{1}{2} \sum_{ij} \psi_i V_{ij} \psi_j \right] = \frac{1}{\sqrt{(2\pi)^n |V|}} \int_{-\infty}^{\infty} \prod_{i=1}^n ds_i \exp \left[-\frac{1}{2} \sum_{ij} s_i (V^{-1})_{ij} s_j + \sum_i s_i \psi_i \right] \quad (3.2)$$

– where the s_i are now unconstrained field variables with $-\infty < s_i < \infty$ – to the partition function associated with \mathcal{H}_I then we get the well-known result [65, 6]

$$\mathcal{Z}_I = \int_{-\infty}^{+\infty} \prod_{i=1}^n ds_i \exp \left[\sum_i \ln [2 \cosh s_i] + \frac{1}{2} s_i V_{ij} s_j \right] \approx \int_{-\infty}^{+\infty} \prod_{i=1}^n ds_i \exp X \quad (3.3)$$

Eqn. (3.3) is well-defined in the limit of vanishing lattice constant and $n \rightarrow \infty$ so that the exponent in the partition function can be replaced by

$$X = \int d\vec{r} \log [2 \cosh s(\vec{r})] - \frac{1}{2} \int \int d\vec{r} d\vec{r}' s(\vec{r}) V(\vec{r} - \vec{r}') s(\vec{r}') \quad (3.4)$$

where the first term is local and the second term contains interactions. Eqns. (3.3,3.4) represent the most general way of deriving a field theory from a spin model. They cannot be solved exactly. In standard continuum models of GL type one usually drops contributions higher than quartic in the local term and replaces the interaction term by phenomenological gradient terms. The most important effective free energy (which is, however, not a Hamiltonian) used for describing microemulsion sponge phases is due to Teubner & Strey (TS)

$$F_{TS}(s) = \int d\vec{r} \left[a_2 s^2 + c_1 (\nabla s)^2 + c_2 (\Delta s)^2 \right] \quad (3.5)$$

In the presented description of microemulsions, however, we relate the two-body interaction term (after Fourier transform)

$$\frac{1}{2} \sum_{\vec{r}, \vec{r}'} s(\vec{r}) V(\vec{r} - \vec{r}') s(\vec{r}') \leftrightarrow \frac{1}{2} \sum_{\vec{k}} V(\vec{k}) s(\vec{k}) s(-\vec{k}) \quad (3.6)$$

(where we will later use the definition $V(\vec{k}) \sim \nu^{-1}(\vec{k})$) directly to the bending Hamiltonian by the variational theorem. The local term is replaced by a mean-spherical constraint

$$\langle s^2(\vec{r}) \rangle_0 = 1 \quad (3.7)$$

which relaxes the local condition for the occupation variable $s^2(\vec{r}) = 1$ of the spin model to a global condition and was first suggested by Berlin & Kac in their discussion of ferromagnets [66]. Teubner effectively also used eqn. (3.7) but called it a normalization condition in [37]. The purpose of this constraint is to contain the overcounting of the entropy caused by the infinite range of the field variable s .

The random interface theory of sponge phases thus forms a link between the bending Hamiltonian and the effective free energies considered in other continuum models of sponge phases. Moreover, due to the geometrical coupling of the film to the bulk density, by $s(\vec{r}) = 0$, the random interface theory can – unlike bulk GL theories – also provide a description of the film properties of binary L_3 sponge phases.

GL theories for these phases contain, unlike eqn. (3.5), an explicit amphiphile degree of freedom. Roux, Coulon, Cates and co-workers proposed [12]

$$F_{RCC} = \int d\vec{r} \left[\frac{a}{2} \rho^2 + \frac{A}{2} \eta^2 + \frac{1}{4} \eta^4 + \frac{1}{2} \rho \eta^2 + \frac{\gamma_\rho}{2} |\vec{\nabla} \rho|^2 + \frac{\gamma_\eta}{2} |\vec{\nabla} \eta|^2 + \frac{\gamma_c}{2} \eta (\vec{\nabla} \eta \vec{\nabla} \rho) \right] \quad (3.8)$$

(henceforth called RCC model) where ρ denotes the local deviation of the amphiphile concentration from its mean value and η is the local difference between inside and outside (water and oil) concentrations. One of the strengths of this formulation is the small parameter space comprising a and A which corresponds to the natural number of parameters, κ and $\bar{\kappa}$ [12], so that it operates at the same level of complexity as the random interface approach. However, we see immediately that bulk and film degrees of freedom in eqn. (3.8) have a soft algebraic coupling in contrast to the random interface model where these degrees of freedom are geometrically coupled.

Both forms eqns. (3.5,3.8) were modified by Gompper & Schick by adding, combining or modifying a number of interaction terms [67] which makes the GL theories more suitable for fitting experimental data [13].

It is also worth mentioning that a claim to mediate between full-fledged field theories and the effective interface model has been made before by Gompper & Zschocke [68] who used a fit to the bending energy of spheres and cylinders by a GL free energy of essentially the form eqn. (3.5) to relate the elastic moduli to GL theory. We should note that this fit was achieved using assumptions such as a large number of phenomenological parameters, special functional forms of the GL parameters and – perhaps most seriously – the flat interface approximation [15]. In any way, the only practical application of this method known to us by Lerczak *et al.* [69], resulted for example in values of $\bar{\kappa} > 0$ which are in the context of the Hamiltonian eqn. (1.2) not stable².

²Lerczak *et al.* pointed out that this result might not be correct due to the flat interface approximation.

3.2 Structure and Thermodynamics

The constituting equations of the theory eqns. (1.2,1.3,3.7) are now motivated and we can proceed with the approximation scheme outlined in Section 1.3.

The free energy density and physical constraints can be written for isotropic systems for zero spontaneous curvature (*cf.* Appendix for details)

$$f[\nu(\vec{k})] = 2\kappa \left\langle \delta(s - \alpha) |\vec{\nabla}s| H^2 \right\rangle_0 + \bar{\kappa} \left\langle \delta(s - \alpha) |\vec{\nabla}s| K \right\rangle_0 - (4\pi^2)^{-1} \int_0^{k_c} dk k^2 \log \nu(k) \quad (3.9)$$

$$\phi_s = \frac{2}{\sqrt{3}\pi} e^{-\frac{\alpha^2}{2}} \langle k^2 \rangle^{\frac{1}{2}} \quad (3.10)$$

$$\langle 1 \rangle = 1 \quad (3.11)$$

where the film thickness is set to unity, $r_c = 1$, and with Teubner's results [37] for the mean-square and saddle-splay curvatures (*cf.* [37] and also Appendix)

$$\begin{aligned} \left\langle \delta(s - \alpha) |\vec{\nabla}s| K \right\rangle_0 &= \frac{1}{3\sqrt{3}\pi} e^{-\frac{\alpha^2}{2}} (\alpha^2 - 1) \langle k^2 \rangle^{\frac{3}{2}} \\ \left\langle \delta(s - \alpha) |\vec{\nabla}s| H^2 \right\rangle_0 &= \left\langle \delta(s) |\vec{\nabla}s| K \right\rangle_0 + \frac{2}{5\sqrt{3}\pi} \langle k^4 \rangle \langle k^2 \rangle^{-\frac{1}{2}} \end{aligned}$$

where α is the asymmetry parameter which is related to the, say, water volume fraction ϕ by [37]

$$\phi = (2\pi)^{-\frac{1}{2}} \int_{\alpha}^{\infty} ds e^{-\frac{s^2}{2}} = 2^{-1} \left[1 - \operatorname{erf}\left(\frac{\alpha}{\sqrt{2}}\right) \right] \quad (3.12)$$

For example, water / oil (inside / outside) symmetry, $\phi = 1/2$, corresponds to $\alpha = 0$ while there is bulk asymmetry for $\alpha \neq 0$. From eqn. (3.A4) we also see that α is directly related to the mean curvature of the interfaces, $\langle \delta(s - \alpha) |\vec{\nabla}s| H \rangle_0 \sim \alpha$. The moments are defined as

$$\langle k^n \rangle = (2\pi^2)^{-1} \int_0^{k_c} dk k^{n+2} \nu(k) \quad (3.13)$$

where $\langle 1 \rangle$ is the notation for $\langle k^0 \rangle$. The cut-off length is $k_c = \eta 2\pi r_c^{-1}$ where η is a constant $O(1)^3$. Finally, in the Appendix we discuss the constraint of self-avoidance which is practically fulfilled by our definition of random surfaces with the exception of

³Following de Gennes [46] we chose a cut-off related to the breakdown of linear elasticity theory. A choice of $\eta \approx 6$ inverse film thicknesses, corresponding to some 50 – 100 Å, avoids cumbersome factors of 2π and appears reasonable [70] and convenient. In any way, the detailed choice of k_c does not influence qualitative results.

'kissing' of two neighboring membranes (just before they fuse into a saddle-like structure) at one surface point.

It is worthwhile mentioning that eqn. (3.12) is actually more specialized than necessary. It assumes *one* interface separating the oil and water or inside and outside partitions. Equally well, one could allow *two* interfaces which, say, separate an oil layer confined by two monolayers from water on the other side of the two monolayers. Two interfaces would describe oil-swollen L_3 phases whose study has only just started [1, 71, 72]. Although for much of the remainder – except for the film scattering – of this chapter we will only discuss the conventional problems associated with one interface, we should keep in mind that a further minimization of eqn. (3.12) could determine the stability for example of oil-swollen L_3 phases *vs* asymmetric microemulsions.

We also should be aware that unlike the two dimensional theory in Chapter 2 where the field was the interface position, the field is now indirectly linked to the interface. We use the entropy derived from the mode distribution of the underlying three dimensional field to approximate the interfacial entropy. The equivalence of interfacial and field entropy is an active field of research in signal-processing. Curtis & Oppenheim [73] found that for band-limited, Fourier expandable, multidimensional signals (*i.e.* just the fields under discussion here) the level surfaces contain the same information (or entropy [74]) as the unleveled field. The equivalence has been illustrated by examples of recovering two dimensional images from one dimensional level crossings [73].

3.2.1 Structural Properties

Bulk Structure Factor

The functional minimization $\partial f[\nu]/\partial \nu$ can be performed by coupling the constraints eqns. (3.10,3.11) to the free energy density by Lagrange multipliers (technically exactly analogous to what was done in Chapter 2 to arrive at eqn. (2.29)) and the minimization yields the general result

$$\nu(k) = a [k^4 - bk^2 + c]^{-1} \quad (3.14)$$

where $a > 0$, $c \geq 0$ and b can assume any sign. This is just the bulk structure factor which was introduced in an *ad hoc* manner by Teubner & Strey who used it to fit numerous experimental bulk scattering data [11]. The random interface theory on the other hand

predicts this structure factor on the basis of the bending Hamiltonian and the coefficients a , b , c can be determined in terms of the parameters κ , ϕ_s and α^4 . In eqn. (3.9) the prefactor of the fourth moment $\langle k^4 \rangle$ depends only on fixed quantities κ , α and $\langle k^2 \rangle$ ($\langle k^2 \rangle$ is fixed due to eqns. (3.10,3.11)). Thus the value of a is readily determined (again fully analogous to the respective calculation in Chapter 2) as

$$a = a_0 \phi_s \kappa^{-1} e^{\alpha^2} \quad (3.15)$$

with $a_0 = 15/16 \pi^2$. The remaining coefficients have to be determined from the constraints eqns. (3.10,3.11) which read explicitly (for $k_c \approx 1$)

$$\int_0^1 dk \frac{k^2}{k^4 - bk^2 + c} = 2\pi^2 a^{-1} \quad (3.16)$$

$$\int_0^1 dk \frac{k^4}{k^4 - bk^2 + c} = 2\pi^2 a^{-1} \langle k^2 \rangle \quad (3.17)$$

The procedure to gain a , b , c was independently crosschecked by freely choosing, say, a then determining b , c from the constraints and finally explicitly numerically minimizing the free energy density. The result was that the minimal a coincided exactly with eqn. (3.15) which is gained analytically from variational minimization as it should.

After introducing the abbreviations

$$\epsilon = a(2\pi^2)^{-1} = \epsilon_0 e^{\alpha^2} \phi_s \kappa^{-1}, \quad \delta = \delta_0 \phi_s \kappa - 1 \quad (3.18)$$

where $\epsilon_0 = 15/32$, $\delta_0 = 8/5\pi^2$, and the new variable

$$c' = \sqrt{4c/b^2 - 1} \quad (3.19)$$

integration yields for eqns. (3.16,3.17)

$$(1 - ic')^{\frac{1}{2}} \operatorname{arctanh}\left(\frac{\sqrt{2}}{\sqrt{b(1 - ic')}}\right) - (1 + ic')^{\frac{1}{2}} \operatorname{arctanh}\left(\frac{\sqrt{2}}{\sqrt{b(1 + ic')}}\right) = i\sqrt{2}\sqrt{bc'}\epsilon^{-1}$$

$$(1 - ic')^{\frac{3}{2}} \operatorname{arctanh}\left(\frac{\sqrt{2}}{\sqrt{b(1 - ic')}}\right) - (1 + ic')^{\frac{3}{2}} \operatorname{arctanh}\left(\frac{\sqrt{2}}{\sqrt{b(1 + ic')}}\right) = 2\sqrt{2}\frac{ic'}{\sqrt{b}}\delta$$

This equation system cannot be solved exactly⁵. However, for small b , c' it can be expanded into

$$i\sqrt{b}c' \approx \frac{\pi\epsilon}{\sqrt{2}}, \quad \frac{\pi}{2^{3/2}}\frac{\sqrt{b}}{ic'} \approx \delta \quad (3.20)$$

⁴In binary systems α or equivalently ϕ are not fixed. We will come back to this below.

⁵Note that the seeming trivial solution $c' = 0$ is in fact not defined.

with the result

$$b \approx 2 \epsilon \delta, \quad c \approx \epsilon^2 \delta^2 + \frac{\pi^2}{4} \epsilon^3 \delta \quad (3.21)$$

For further discussion it is helpful to use the real space Fourier transform of eqn. (3.14) which reads [11]

$$g(r) \approx e^{-r/\xi} \frac{\sin k_0 r}{k_0 r} \quad (3.22)$$

where we note that the approximation $k_c \rightarrow \infty$ which was used to gain eqn. (3.22) is only good when the structure factor has a sharp peak at $0 \leq k \leq k_c$. Eqn. (3.22) contains the two characteristic scales which we discussed in the introductory chapter. With, $D = b/2 + \sqrt{c}$ [11]

$$k_0 = \frac{1}{\sqrt{2}} \begin{cases} \sqrt{D}, & D \geq 0 \\ \sqrt{-D}, & D \leq 0 \end{cases}, \quad \xi^{-1} = \frac{1}{\sqrt{2}} \sqrt{-\frac{b}{2} + \sqrt{c}} \quad (3.23)$$

so that for $\kappa^{-1} \ll 1$

$$k_0 \approx \epsilon^{\frac{1}{2}} \delta^{\frac{1}{2}} \left(1 + \frac{\pi^2}{32} \epsilon \delta^{-1} \right), \quad \xi^{-1} \approx \frac{\pi}{4} \epsilon \quad (3.24)$$

While the above approximations which encompass $\kappa^{-1} \ll 1$ will turn out very helpful sometimes even beyond their strict limit of validity we should also keep in mind that large κ will lead eventually to a phase transition towards ordered systems (Chapter 4) so that the asymptotic limit $\kappa^{-1} \rightarrow 0$ should not be overrated.

Film Structure Factor

Before proceeding with the physical consequences of various values of κ and ϕ_s on sponge structure, we want to introduce methods to calculate the film scattering signal from the interfaces. There are various ways of calculating the film structure factor, all of them of approximate character only.

In principle one would like to compute the scattering from an ensemble of layers with uniform physical thickness⁶ with given scattering length profile and density. The profile is usually taken to be of a simple square shape [39]. Hence – recalling the arguments used in Section 1.2 – we can write the relevant film-film correlation function as

$$\Gamma(r) = \left\langle \Theta_{\beta_-(\vec{r})\beta_+(\vec{r})}(0) \Theta_{\beta_-(\vec{r})\beta_+(\vec{r})}(r) \right\rangle_0 \quad (3.25)$$

⁶Experiments show that the fluctuation of the bi- or monolayer thickness is negligible, usually of the order of few Ångströms.

where Θ denotes the Heaviside step function. Gaussian random fields do not support a parallel family of surfaces (*i.e.* two neighboring level cuts are never strictly parallel) and therefore $\beta_-(\vec{r})$, $\beta_+(\vec{r})$ which are the two level cuts which describe the two interfaces at positions $\pm r_c/2$ around the mean layer position α have to vary in space in order to assure constant physical film thickness r_c . The functionality of $\beta_-(\vec{r})$, $\beta_+(\vec{r})$ is, however, not known. At best one can write them as a Taylor series which reads up to first order (for $\alpha = 0$)

$$\beta_{\pm}(\vec{r}) \approx \frac{r_c}{2} |\vec{\nabla}s(\vec{r})| \quad (3.26)$$

There are two ways of proceeding from here.

(a) The method briefly mentioned in the first chapter is based on replacing the $\beta_{\pm}(\vec{r})$, by their mean values $\beta_-(\vec{r}) \rightarrow \langle \beta_-(\vec{r}) \rangle = \beta_-$, $\beta_+(\vec{r}) \rightarrow \langle \beta_+(\vec{r}) \rangle = \beta_+$ so that the film thickness is not strictly uniform. This approximation was derived practically simultaneously and independently by Berk [75], us [42] and Lee *et al.* [76]. Due to the decoupling of field and gradient degrees of freedom the variation of the film thickness is a truly independent random process and was assumed implicitly [75, 76] or explicitly [42] not to be important in the interesting range of wave vectors far away from molecular scales $k \ll k_c$ (we will come back to this point below). Then

$$\begin{aligned} \Gamma^{\beta-\beta+}(r) &= \langle \Theta_{\beta-\beta+}(0) \Theta_{\beta-\beta+}(r) \rangle_0 \\ &= \int_{-\infty}^{+\infty} \int_{-\infty}^{+\infty} dx dy \frac{1}{2\pi\sqrt{1-g^2(r)}} e^{-\frac{x^2+y^2-2g(r)xy}{2(1-g^2(r))}} \Theta_{\beta-\beta+}(x) \Theta_{\beta-\beta+}(y) \quad (3.27) \\ &= \Gamma^{\beta-\beta+}(0) - \frac{1}{2\pi} \int_{g(r)}^1 dt \frac{1}{\sqrt{1-t^2}} \left[e^{-\frac{\beta_-^2}{1+t}} + e^{-\frac{\beta_+^2}{1+t}} - 2e^{-\frac{1}{2} \frac{1-t^2}{1-t^2} (\beta_-^2 - 2\beta_- \beta_+ t + \beta_+^2)} \right] \end{aligned}$$

The derivation of eqn. (3.27) is relatively simple; explanations are given in [42] and in greater detail in [75]. A numerically useful transformation $t = \sin \phi$ avoids the artificial singularity of the integrand

$$\Gamma^{\beta-\beta+}(r) = \Gamma^{\beta-\beta+}(0) - \frac{1}{2\pi} \int_{\arcsin(g(r))}^{\pi/2} d\phi \left[e^{-\frac{\beta_-^2}{1+\sin \phi}} + e^{-\frac{\beta_+^2}{1+\sin \phi}} - 2e^{-\frac{1}{2 \cos^2 \phi} [\beta_-^2 - 2\beta_- \beta_+ \sin \phi + \beta_+^2]} \right] \quad (3.28)$$

After normalization

$$\gamma^{\beta-\beta+}(r) = \frac{\Gamma^{\beta-\beta+}(r) - \Gamma^{\beta-\beta+}(\infty)}{\phi_s(1 - \phi_s)} = \frac{\Gamma^{\beta-\beta+}(r) - \phi_s^2}{\phi_s(1 - \phi_s)} \quad (3.29)$$

Teubner's specialized result for a one-step level cut [37] is immediately recovered by taking $\beta_+ \rightarrow \infty$ ($\lim_{\beta_+ \rightarrow \infty} \gamma^{\beta-\beta+} = \gamma^{\beta-}$). Berk's $2/\pi \arcsin[g(r)]$ term [34] is the limit of

eqn. (3.28) for $\beta_+ \rightarrow \infty$, $\beta_- = 0$. Lee *et al.* later used a slight variation of this approach and gave an approximate result

$$\Gamma(r) \sim \left[1 - (1 - \phi_s^2)^2 g^2(r) \right]^{-\frac{1}{2}} - 1$$

which was successfully used for fitting film scattering data in [76].

Because this approximation works with a finite film thickness we actually find the qualitatively correct sequence of scaling laws for the film scattering structure factor [77, 78]: in an intermediate range of wave vectors which are larger than the structural wave vector but smaller than the wave vector associated with the film thickness we will find that $\nu_f(k) \sim k^{-2}$ characteristic for the scattering from thin films. At wave vectors larger than the order of magnitude of the inverse film thickness, however, we expect the scattering to follow the standard Porod law, $\nu_f(k) \sim k^{-4}$.

As mentioned above the shortcoming of this approximation is that the film is not of perfectly uniform thickness. In experiment the effective fluctuations of the film in binary systems are of the order of a few Ångstroms only so that the detailed scattering in the high k region might not be well described. At the same time eqn. (3.27) could be a very good approximation for the film scattering from oil-swollen [71] or water-swollen [12] L_3 phases where the two surfactant monolayers enclose a thin film of oil or water. For oil-swollen systems it has been found experimentally that the film thickness has substantial fluctuations [71] due to fluctuations of the thickness of the confined oil film. We note that modelling with two level cuts gives us also simple access to complicated defects – which have attracted some recent attention [79, 80] – such as occasional seams between two or more oil-swollen films [79, 80] which are now allowed and energetically not too expensive. Clearly, a systematic study of oil-swollen systems which are intermediate between pure L_3 phases and microemulsions is of great interest [1] and eqn. (3.27) should therefore be pursued in any case.

Given that a physical correlation function $g(r)$ becomes small for large r a good approximation to the film correlation function for large r can be gained by expanding eqn. (3.27) (before integration) into a series for small $g(r)$. Then

$$\Gamma(r) = \Gamma[g(r)] \approx \phi_s^2 + I_1 g(r) + I_2 g^2(r) \quad (3.30)$$

where

$$I_1 = 1/(2\pi) \int_{\beta_-}^{\beta_+} \int_{\beta_-}^{\beta_+} dx dy e^{-\frac{1}{2}(x^2+y^2)} xy$$

$$I_2 = 1/(4\pi) \int_{\beta_-}^{\beta_+} \int_{\beta_-}^{\beta_+} dx dy e^{-\frac{1}{2}(x^2+y^2)} (x^2 - 1)(y^2 - 1)$$

where for small α (here $\beta_- = \alpha - \epsilon$, $\beta_+ = \alpha + \epsilon$)

$$I_1 \sim \alpha^2 \quad (3.31)$$

After normalization we see that the leading term goes like $g(r)$ so that the film spectrum has a term proportional to the bulk structure factor. However, it vanishes for symmetric sponge phases ($\alpha = 0$) defined by $\beta_- = -\beta_+$, $\beta_+ = \beta_-$. For the symmetric phase the leading term is

$$\Gamma(r) \sim g^2(r) \quad (3.32)$$

so that after Fourier transform

$$\nu_f(k) \sim \int dr r^2 j_0(kr) \Gamma(r) \quad (3.33)$$

the film scattering reads

$$\nu_f(k) \sim \Delta_0 + \frac{1}{4kk_0^2} \left[2 \arctan \frac{\xi k}{2} - \arctan \frac{\xi(k-2k_0)}{2} - \arctan \frac{\xi(k+2k_0)}{2} \right], \quad D \geq 0 \quad (3.34)$$

$$\nu_f(k) \sim \Delta_0 - \frac{1}{4kk_0^2} \left[2 \arctan \frac{\xi k}{2} - \arctan \frac{k}{2(\xi^{-1} - k_0)} - \arctan \frac{k}{2(\xi^{-1} + k_0)} \right], \quad D \leq 0 \quad (3.35)$$

where the constant Δ_0 takes into account the small overall error arising in the integration eqn. (3.33) due to the inaccuracy of eqn. (3.32) at small r . Mainly due to the phase space factor, r^2 , in the integration this error is never serious. It amounts to an overall, systematic deviation which can be approximated by the difference of eqn. (3.33) when evaluated with the exact or approximate $\Gamma(r)$ at zero wave vector, $\Delta_0 = \nu_f^{exact}(0) - \nu_f^{approx}(0)$. We have explicitly assessed this for the example $k_0 = 1$, $\xi^{-1} = 0.01$ and found that from $k = 0.0001k_0$ to $k = 0.01k_0$ the respective errors $\Delta_{k=0.01}$ $\Delta_{k=0.0001}$ differ by a mere 6%.

Eqn. (3.34) has two major parts, $\sim k^{-1} \arctan(\xi k)/2$ and $\sim k^{-1} \arctan \xi(k-2k_0)/2 + k^{-1} \arctan \xi(k+2k_0)/2$ which determine the behaviour of $\nu_f(k)$ around $k = 0$ and $k = 2k_0$. The first term is monotonic indicating strong low k scattering and the shape of the second term can range from monotonic to step-like depending on whether the values of $k_0\xi$ are small or large.

We will use eqns. (3.34,3.35) to discuss several physical regimes of k_0 , ξ (or κ , ϕ_s) in detail in the next section.

(b) Alternatively to method (a), one can use eqn. (3.26) and perform the limit of an infinitely thin layer, $r_c \rightarrow 0$. The film - film correlation function in this approximation is

the joint probability [81]

$$\Gamma(r) \sim r_c^{-2} \text{Prob} \left[|s(0)| \leq \frac{r_c}{2} |\vec{\nabla}s(0)|, |s(r)| \leq \frac{r_c}{2} |\vec{\nabla}s(r)| \right] \quad (3.36)$$

The limes $r_c \rightarrow 0$ accurately describes scattering from an interfacial system which has no thickness fluctuations. It is probably preferable to method (a) when discussing systems where the scattering comes only from the surfactant mono- or bilayers but certainly inadequate for oil- or water-swollen systems. The limes leads to⁷

$$\Gamma(r) = \left\langle \delta(s(0) - \alpha) \sqrt{\vec{\nabla}s^2(0)} \delta(s(r) - \alpha) \sqrt{\vec{\nabla}s^2(r)} \right\rangle_0 \quad (3.38)$$

In expression eqn. (3.38) the correlation matrix $A(r)$ of the Gaussian multivariate contains now gradient terms (*cf.* Appendix) and evaluation of eqn. (3.38) becomes far more difficult than by method (a). The formula for the correlation function reads after applying the delta functions and with the shorthand $\vec{s}_0 = (ds/dx(0), ds/dy(0), ds/dz(0))$, $\vec{s}_r = (ds/dx(r), ds/dy(r), ds/dz(r))$

$$\Gamma(r) = [2\pi]^{-4} |A(r)|^{-\frac{1}{2}} \int_{-\infty}^{\infty} \dots \int_{-\infty}^{\infty} d\vec{s}_0 d\vec{s}_r \sqrt{\vec{s}_0^2} \sqrt{\vec{s}_r^2} \exp \left[-\frac{1}{2} \vec{\lambda} A^{-1}(r) \vec{\lambda}^T \right] \quad (3.39)$$

where $\vec{\lambda} = (\alpha, \alpha, s_{z0}, s_{zr}, s_{x0}, s_{xr}, s_{y0}, s_{yr})$. This means that evaluation of eqn. (3.39) encompasses some eight integrations, if we include the exact evaluation of the various correlation functions (with finite k_c , *cf.* Appendix) and the final Fourier transform. In the best case, for symmetry $\alpha = 0$, the multiple integral can be reduced to a very complicated four-fold integral. This makes the exact evaluation of eqn. (3.39) untractable. However, we can do an expansion analogous to the one which lead to eqn. (3.30). After some calculation (in the Appendix) we find approximately

$$\Gamma(r) = \Gamma \left[g(r), \frac{\partial g(r)}{\partial r}, \frac{\partial^2 g(r)}{\partial r^2}, r^{-1} \frac{\partial g(r)}{\partial r} \right] \approx \sigma_r + \sigma_r \alpha^2 g(r) + 4\sigma_r^{-1} G_2(r) \quad (3.40)$$

where

$$G_2 = \sigma_r^2 g^2(r) - \frac{2}{3} \sigma_r g_1^2(r) + \frac{1}{9} g_2^2(r) \quad (3.41)$$

⁷To avoid confusion, we should note here that most recently Gompper & Hennes [82] and Gompper & Goos [83] tried to adopt the geometrical film coupling into their one parameter bulk GL model so that they are able to calculate film scattering. Unfortunately, these authors used the incorrect expression

$$\Gamma(r) \sim \langle \delta(s(r)) \delta(s(0)) \rangle_0 \quad (3.37)$$

where the integration measure is missing. The results for the film structure factor in [82, 83] are therefore not correct. Comments [84] and errata to the papers [82, 83] should clarify this situation.

where in leading order in r^{-1}

$$\begin{aligned} g(r) &\approx e^{-r\xi^{-1}} \frac{\sin k_0 r}{k_0 r} \\ g_1(r) &\approx e^{-r\xi^{-1}} \frac{1}{k_0 r} \left[k_0 \cos k_0 r - \xi^{-1} \sin k_0 r \right] \\ g_2(r) &\approx e^{-r\xi^{-1}} \frac{1}{k_0 r} \left[k_0^2 \sin k_0 r + 2k_0 \xi^{-1} \cos k_0 r - \xi^{-2} \sin k_0 r \right] \end{aligned}$$

The main effect of asymmetry, $\alpha \neq 0$, is the emergence of a linear term in $g(r)$ (there are in fact also a number of terms in α^2 which add to $G_2(r)$ but as they do not change the functional form we disregard them here) just as in method (a).

As the exact evaluation of $\Gamma(r)$ is not available we should restrict our attention to the small k regime. Then we see that the terms arising from $g^2(r)$, $g_1^2(r)$, $g_2^2(r)$ are of the form ($D \geq 0$)

$$\sim e^{-2r\xi^{-1}} r^{-2} \{ \sin^2 k_0 r, \cos^2 k_0 r, \sin k_0 r \cos k_0 r \}$$

After Fourier transform, eqn. (3.33), the leading contributions for small $k \approx 0$ are the same for the two squared terms $\sim \sin^2 k_0 r$, $\sim \cos^2 k_0 r$

$$\nu_f(k) \sim \Delta_0 + \frac{1}{2kk_0^2} \arctan \frac{\xi k}{2} \quad (3.42)$$

and show a (possible) step-pattern at $2k_0$ just as discussed in method (a). The mixed term $\sim \sin k_0 r \cos k_0 r$ leads after Fourier transform to

$$\sim k^{-1} \left\{ \log \left[1 + 4^{-1} \xi^2 (k + 2k_0)^2 \right] - \log \left[1 + 4^{-1} \xi^2 (k - 2k_0)^2 \right] \right\} \quad (3.43)$$

which can be neglected for $k \rightarrow 0$ but can have a peaked shape at $k \approx 2k_0$ for sufficiently large values of $k_0 \xi$. For $D \leq 0$ the situation is slightly more complicated. Then both squared and mixed terms

$$\sim e^{-2r\xi^{-1}} r^{-2} \{ \sinh^2 k_0 r, \cosh^2 k_0 r, \sinh k_0 r \cosh k_0 r \}$$

contribute at low k . None of these contributions shows any pattern at $2k_0$. Moreover, we will see in the stability discussion below that in practice only the contribution which leads after Fourier transform to eqn. (3.35) is relevant.

While it is not easy to decide how important fluctuations of the film thickness are in reality we can state that we have established major properties consistently by both methods (a) and (b) so that the following three patterns should be independent of the details of possible thickness fluctuations or the possible appearance of seams *etc.*

1. a characteristic arctangent form of the film scattering at low k for symmetric sponges
2. an additional term (of possible peak shape at k_0 , if $k_0\xi$ is large enough) for asymmetric sponges
3. a possible irregularity at $2k_0$ depending on the value of $k_0\xi$

In the following we will assign and discuss these and the corresponding bulk structure patterns in the context of physical scenarios characterized by the basic parameters κ , ϕ_s , ϕ .

Stability Analysis

Having established bulk and film structure factors we can now proceed with the discussion of several structural regimes as functions of the compositions and bending modulus. In all of these regimes we assume that $\epsilon \sim \phi_s/\kappa \ll 1$. This assumption is valid for 'good' microemulsions with large domain sizes. In the following we will make extensive use of eqn. (3.15), eqn. (3.18), eqn. (3.21) and eqn. (3.24) to distinguish several typical regimes.

(i) When $\delta \gg 1$, but $\epsilon\delta \ll 1$, corresponding to $\phi_s\kappa \gg 1$ but $\phi_s\kappa^{-1} \ll 1$ we find that $b \sim \phi_s^2$, $c \sim \phi_s^4$ so that the bulk scattering peak position k_0 and the correlation length ξ scale like

$$k_0 \sim \phi_s, \quad \xi \sim \kappa \phi_s^{-1} \quad (3.44)$$

This defines the scaling regime because it just fulfills the scaling relations eqn. (1.4) which we expected on fundamental grounds in the discussion of the scale invariance of the bending Hamiltonian. In this regime we have assumed $\kappa \gg 1$, so that

$$k_0 \gg \xi^{-1} \quad (3.45)$$

This means that there is short range order over several domains. In this regime the structure factor can be most conveniently written

$$\nu(k) = \frac{a}{(k^2 - \epsilon\delta)^2 + \frac{\pi^2}{4}\epsilon^3\delta} = \frac{a_0\phi_s\kappa^{-1}}{(k^2 - k_0^2)^2 + \frac{\pi^2}{4}\epsilon_0^3\delta_0\phi_s^4\kappa^{-2}} \quad (3.46)$$

For $\kappa^{-1} \rightarrow 0$ this converges towards the monodisperse limit where the Lorentzian eqn. (3.46) becomes a delta function. Its exact form is most easily derived from the correlation function

$$\nu(k) \rightarrow \frac{2\pi^2}{kk_0} [\delta(k - k_0) - \delta(k + k_0)] \quad (3.47)$$

Eqn. (3.47) fulfills the two constraints eqns. (3.10,3.11), $\langle 1 \rangle = 1$, $\langle k^2 \rangle = k_0^2$; moreover, $\langle k^4 \rangle = k_0^4$. There are angular fluctuations but no fluctuations in magnitude. The structure is completely determined by one mode, k_0 , which is in turn determined by the surfactant concentration, similar to the ACRS model. Indeed, the equations for the structural wave vector k_0 in the ACRS and the random interface model have strong resemblance in this limit

$$k_0^{ACRS} \sim \frac{\phi_s}{\phi(1-\phi)} \quad \text{and} \quad k_0 \sim \frac{\phi_s}{\phi(1-\phi) + \left(\frac{1}{\pi} - \frac{1}{4}\right)} \quad (3.48)$$

where we have used $\phi = 1/2 + 1/\sqrt{2\pi}\alpha + O(\alpha^3)$ to expand $\exp(-\alpha^2/2)$ in eqn. (3.10). It is perfectly thinkable that a theory based on such a structural premise can indeed provide a reasonable approximation to the free energy density even though the structural description is too crude. We will come back to this point later.

In the scaling regime proper (characterized by eqn. (3.46)) we see that the ratio of the bulk scattering intensity at zero wave vector and at the peak position, $\nu(0)/\nu(k_0)$, is independent of the surfactant concentration as indicated by experiments where it is measured as, for example, $\nu(0)/\nu(k_0) \approx 1/3 - 1/2$ in the microemulsions studied in [11]. We estimate that this ratio is given for bending moduli of $\kappa \approx 0.5$ which is of the expected order of magnitude⁸.

Swelling is another observable quantity. The relation between the structural length scale and the surfactant concentration in binary sponge phases (with $\phi_s = r_c S/V$)

$$d_0 = \frac{1}{2} \cdot 2\pi k_0^{-1} = \pi \frac{2}{\pi\sqrt{3}} \left(\frac{S}{V}\right)^{-1} \approx 1.15 r_c \phi_s^{-1} = \beta r_c \phi_s^{-1} \quad (3.49)$$

where the factor of 1/2 accounts for the fact that the bilayer periodicity is twice the bulk periodicity. Experimentally, values of, for example, $\beta \approx 1.2$ for $C_{12}E_5$ - water systems [85] or $\beta \approx 1.4$ for quasiternary CPCl - alcohol - brine mixtures [86] have been measured. Considering that the theoretical value of 1.15 has to rise once we go to interfaces which undulate more strongly, this result is satisfactory.

⁸and in fact outside the validity of the scaling regime. However, we will see below that extrapolations using the simple scaling relations are good even if applied beyond the strict limit of validity.

Finally, the dominant terms in the film structure factor, in the limit $k \rightarrow 0$, and for $\alpha = 0$ in the scaling approximation reads with method (a) simply

$$\nu_f(k) \approx \Delta_0 + \frac{1}{2kk_0^2} \arctan \frac{\xi k}{2} \quad (3.50)$$

For k of the order of k_0 the interesting terms (according to method (a)) are

$$\sim -\frac{1}{4kk_0^2} \left[\arctan \frac{\xi(k-2k_0)}{2} + \arctan \frac{\xi(k+2k_0)}{2} \right]$$

which cause a shoulder-like pattern a $k \approx 2k_0$ often seen in film scattering signals from microemulsions [87].

Method (b) yields in the asymptotic limit $\xi^{-1} \rightarrow 0$ a cancellation, $G_2(r) \rightarrow 0$, because $k_0^2 \rightarrow 3\sigma_r$. This means that the amplitude of the arctan term eqn. (3.50) is rather small and indicates that the low wave vector scattering from uniformly thick films could be distinguishable from the signal coming from non-uniform films. This seems to be in agreement with recent experiments [71]. A possible explanation is that the occasional seams in the system of non-uniform film thickness contribute strongly at low wave vector. In practice, however, all fits carried out by Chen *et al.* and us on grounds of method (a) were done for rather soft systems where $k_0\xi^{-1} \approx 2$. For these systems the asymptotic cancellation is not relevant (*cf.* regime (ii)).

We do not want to make predictions for higher k because we do not have accurate numerical evaluations of eqn. (3.39) available. It is clear from approximation eqn. (3.40), however, that for large $k_0\xi$ an irregularity at $2k_0$ can be expected which is 'at least' of shoulder shape as in method (a) (while peak shapes are also possible due to eqn. (3.43)).

For $\alpha \neq 0$ methods (a) and (b) give equivalent predictions for the correction linear in $g(r)$ when $\alpha \neq 0$. At low k a correction of the form $[-bk^2 + c]^{-1}$ ($b > 0$) is expected which would 'broaden' the arctangent shape in a way which is not accounted for by standard RCC theory which predicts an asymmetric contribution of Ornstein - Zernike form ($b < 0$, *cf.* regime (ii)), [12]. Because the bulk structure factor, eqn. (3.46), is peaked we expect a peak in the film structure factor at $k = k_0$ whose amplitude can be used as a direct measure of the order parameter, α ,

$$\nu_f(k) \sim \alpha^2 \quad (3.51)$$

similar to antiferromagnetic systems where the order parameter can be related to the height of the peak in the structure factor. Intuitively, the emergence of the peak is related to the periodicity of the asymmetric bulk components such as worms or vesicles.

In order to test this prediction, detailed small-angle scattering experiments of asymmetric sponges which are not too far in the vesicular region have to be performed. Ternary microemulsions might be less suited because the spontaneous curvature term can never be adjusted exactly to zero. To date most experiments in binary sponges seem to have operated in the small k regime. It would be interesting to gain detailed experimental data in the intermediate k range of slightly asymmetric sponges.

(ii) When the bending stiffness κ or the surfactant concentration ϕ_s are lowered, the scaling approximations of (i) become successively worse. We enter a new regime where $0 < \delta < 1$, corresponding to $\kappa \phi_s$ of order δ_0^{-1} , and both b and c become sensitive to the value of the bending modulus through their dependence on δ . The inverse correlation length and the structural wave vector are now related by

$$\xi^{-1} \gtrsim k_0 \quad (3.52)$$

There is no longer any one length scale dominating the structure in real space. As δ is decreased, b decreases and eventually both b and δ change sign. Our numerical results and a more precise analysis indicate that b becomes negative while c remains finite and positive. The locus at which $b = 0$ or $\xi^{-1} = k_0$ (sometimes called Lifshitz line [13]) can be determined in the $\phi - \phi_s$ plane by the equation system

$$\begin{aligned} \frac{1}{2} \ln \left(1 + c^{-\frac{1}{2}} - \sqrt{2}c^{-\frac{1}{4}} \right) - \frac{1}{2} \ln \left(1 + c^{-\frac{1}{2}} + \sqrt{2}c^{-\frac{1}{4}} \right) \\ + \arctan \left(1 + \sqrt{2}c^{-\frac{1}{4}} \right) - \arctan \left(1 - \sqrt{2}c^{-\frac{1}{4}} \right) &= 2\sqrt{2}c^{\frac{1}{4}}\epsilon^{-1} \\ \frac{1}{2} \ln \left(1 + c^{-\frac{1}{2}} - \sqrt{2}c^{-\frac{1}{4}} \right) - \frac{1}{2} \ln \left(1 + c^{-\frac{1}{2}} + \sqrt{2}c^{-\frac{1}{4}} \right) \\ + \arctan \left(1 - \sqrt{2}c^{-\frac{1}{4}} \right) - \arctan \left(1 + \sqrt{2}c^{-\frac{1}{4}} \right) &= 2\sqrt{2}c^{-\frac{1}{4}}\delta \end{aligned} \quad (3.53)$$

When b turns negative, the structure factor loses its peak at finite k_0 and decreases monotonically from its value at $k = 0$ with a width in \vec{k} space related to c *i.e.*

$$\nu(k) \sim \left[-bk^2 + c \right]^{-1} \quad (3.54)$$

$b < 0$, similar to the critical Ornstein - Zernike (OZ) scattering from a system close to phase separation [87].

The behaviour of the film scattering in the vicinity of the Lifshitz line follows qualitatively the pattern set by the bulk structure factor. The results of method (a) follow again eqn. (3.34). Similarly, with method (b) at $k_0 \approx \xi^{-1}$ we find that $g_1^2(r) \rightarrow 2k_0^2 g^2(r)$

and $g_2^2(r) \rightarrow 4k_0^4 g^2(r)$. In this regime we have no approximate analytical formulae for k_0^2 available. But *e.g.* from the example fig. (3-2) ($\phi_s = 0.05$) we see that close to the Lifshitz line $k_0^2 \approx 0.01 \langle k^2 \rangle$ so that $G_2(r)$ can be approximated

$$G_2(r) \approx 4\sigma_r^2 g^2(r) \quad (3.55)$$

which is equivalent to the result of method (a). Hence in this regime, for $\alpha = 0$, $k \ll k_0$

$$\nu_f(k) \sim \Delta_0 + \frac{1}{2k\xi^{-2}} \arctan \frac{\xi k}{2} \quad (3.56)$$

where ξ has to be related to ϕ_s or κ by eqns. (3.23,3.53). For asymmetry an additional term of OZ form, $\sim [-bk^2 + c]^{-1}$, ($b < 0$) appears. The asymmetry order parameter can therefore not be deduced from the film scattering in this regime. As in regime (i) the arctangent form of eqn. (3.56) is well-established. Similarly, the more complicated functional form comprising eqn. (3.56) and the OZ term has been used by RCC to fit experimental data. We will come back to this in more detail later.

For higher k values both methods (a) and (b) indicate that any irregularities around $2k_0$ become negligible. We confirm this also numerically for method (a) (*cf.* fig. (3-1), D).

(iii) Finally, at some critical value of $\delta \approx -\epsilon$, the coefficient c vanishes. The bulk structure factor then diverges as $k \rightarrow 0$, indicating an instability similar to that observed in phase separating systems at their critical point.

After redefining conveniently, $b \rightarrow -b$

$$b^{-\frac{1}{2}} \arctan(b^{-\frac{1}{2}}) = \epsilon^{-1}, \quad b^{\frac{1}{2}} \arctan(b^{-\frac{1}{2}}) = -\delta \quad (3.57)$$

which yields after division and multiplication for small b

$$b \approx -\epsilon\delta, \quad \frac{\pi^2}{4} \approx -\delta\epsilon^{-1} \quad (3.58)$$

and after some calculation we find that a good approximation⁹ for the instability line is

$$\phi_s \approx \pi^{-2} \left[\frac{8}{5}\kappa + \frac{15}{128}\kappa^{-1}e^{\alpha^2} \right]^{-1} \quad (3.59)$$

The situation concerning the film structure factor is similar to the one in (ii); both length scales, $|k_0|, \xi^{-1} \ll \sigma_r$ so that also in method (b) only the contribution in $g^2(r)$ has to be

⁹We checked for several values of α , and found relative errors of 10^{-4} and 10^{-2} , for $\kappa = 2.5$ and $\kappa = 0.5$, respectively. We may draw the conclusion that even low order perturbations to the scaling relations can give valid information beyond the scaling regime.

considered ($\alpha = 0$)

$$\nu_f(k) \sim \Delta_0 - \frac{1}{kk_0^2} \left[2 \arctan \frac{\xi k}{2} - \arctan \frac{k}{2(\xi^{-1} - k_0)} - \arctan \frac{k}{2(\xi^{-1} + k_0)} \right] \quad (3.60)$$

At the instability $c \rightarrow 0$, *i.e.* $k_0 \rightarrow \xi^{-1}$ (where k_0 has been redefined, $k_0 \rightarrow ik_0$) we observe a divergence at zero wave vector, as expected. For $\alpha \neq 0$ the monotonic bulk structure factor has to be added but cannot be observed as a peak specifying the asymmetry order parameter just as in (ii). In fig. (3-1) we show some examples of bulk and film structure factors in the various regimes

Film

Bulk

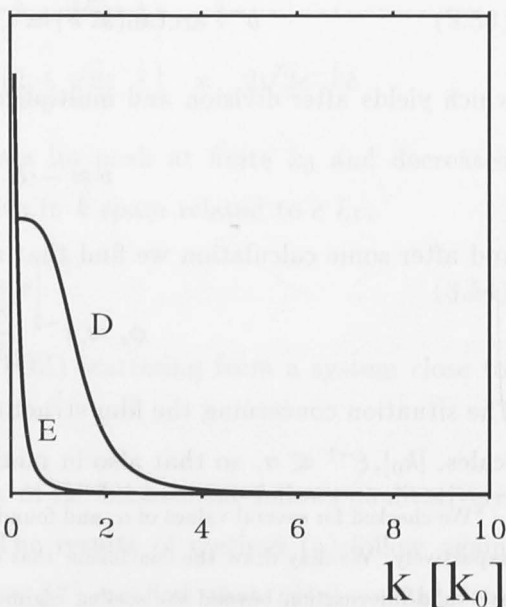
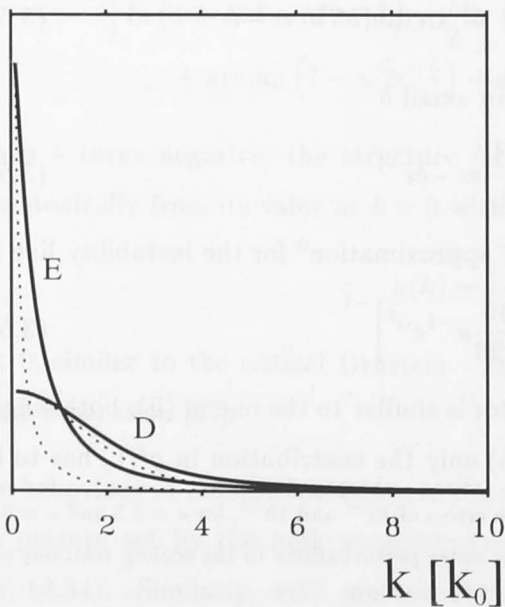
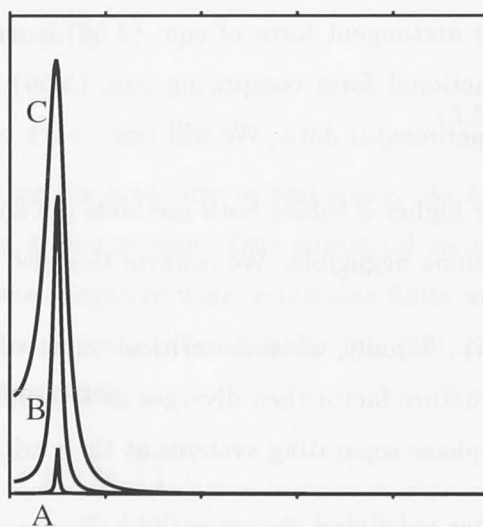
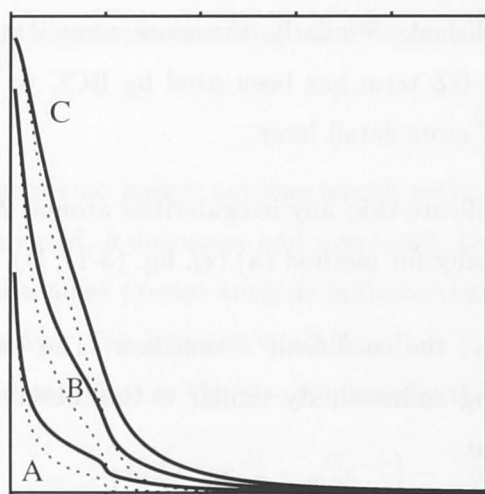


Figure 3-1: A selection of film and bulk structure factors, $\nu_f(k)$ vs k and $\nu(k)$ vs k (intensities in arbitrary units) where the film structure factors were evaluated using eqn. (3.28). The relevant parameters are given in the following table. For better visibility we have used multiplicative scale factors for film and bulk intensities of A, B, C, D, E (film: 1,4,11,2,1 ; bulk: 1,20,70,1,40). The dotted lines show the result when we used the approximations eqns. (3.34,3.35). The cut-off wavelength for the evaluation of the spectral moments was uniformly $k_c = 10k_0$.

	regime	k_0	ξ^{-1}
A	(i)	1.0	0.03
B	(i)	1.0	0.1
C	(ii)	1.0	0.25
D	(ii)	1.0	1.0
E	(iii)	$0.9i\xi^{-1}$	1.0

To summarize, and to stress the richness of structural behaviour which can arise from the relative variations of just two length scales we can also draw a scheme

$\kappa^{-1} \rightarrow 0$	$\phi_s \kappa^{-1} \ll 1$	$\phi_s \kappa^{-1} \ll 1$	$\phi_s \kappa^{-1} \ll 1$	
	$\phi_s \kappa \gg \delta_0^{-1}$	$\phi_s \kappa > \delta_0^{-1}$	$\phi_s \kappa \gtrsim \delta_0^{-1}$	$\phi_s \kappa \approx \delta_0^{-1}$
$\xi^{-1} \rightarrow 0$	$\xi^{-1} \ll k_0$	$\xi^{-1} \approx k_0$	$k_0 \in \mathfrak{S}$	$k_0 \rightarrow i\xi^{-1}$
ACRS	scaling	Lifshitz	disordered	phase separation
	\rightarrow	fluctuations	\rightarrow	
	\leftarrow	order	\leftarrow	

where order in this context refers, of course, to short range order.

While it is instructive to study the general patterns of film and bulk structure factors in terms of k_0 and ξ , we have also seen that the mapping $(k_0, \xi) \leftrightarrow (\phi_s, \kappa)$ allows us to address the more fundamental problem of predicting certain structural regimes for given physical parameters ϕ_s, κ . In fig. (3-2) we show therefore for specific examples of concentrations and moduli numerically exact solutions of the functional minimization problem. The structural wave vector k_0 is plotted as a function of either bending stiffness of surfactant concentration. Over much of the domain the scaling relations are obeyed

and only for very soft and/or very dilute systems scaling breaks down

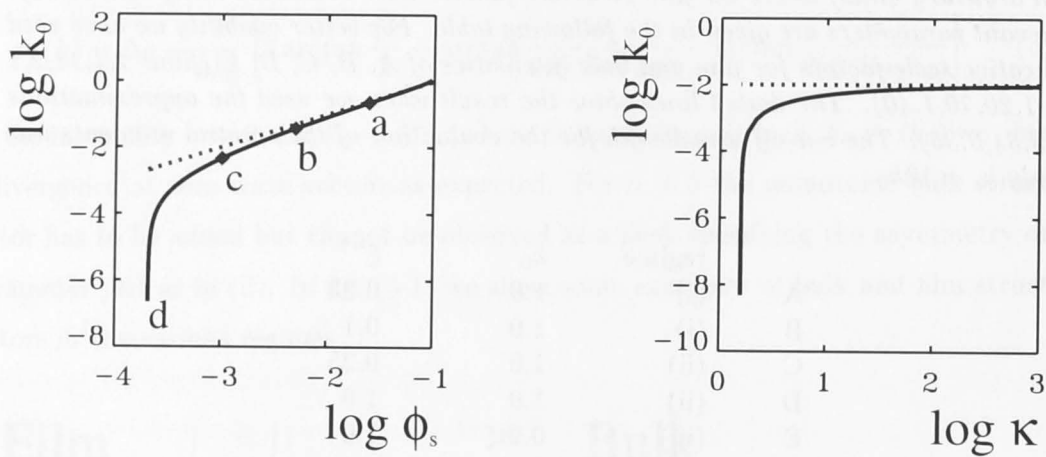


Figure 3-2: (left) Numerical evaluation of the structural wave vector k_0 vs ϕ_s (solid line) at a bending modulus $\kappa = 2.5$. For decreasing surfactant concentration k_0 leaves the scaling regime (i) where $k_0 = \pi/2\sqrt{3}\phi_s$ (dotted line) and approaches the unstable regime (iii) where the scaling behaviour has totally broken down. The values $\phi_s = 0.2, 0.1, 0.05, \approx 0.025$ are labeled a, b, c, d, respectively. Real space structures corresponding to these values are drawn in fig. (3-4). (right) Numerical evaluation of the structural wave vector k_0 vs κ (solid line) at a surfactant concentration $\phi_s = 0.05$. Similar to the left-hand graph we see that for a wide range of parameters scaling is obeyed to a good approximation while it breaks down at low bending stiffness.

It is easy to construct graphic images which represent possible configurations of a system determined by $\nu(k)$ (cf. Appendix). Sample a is given in a three dimensional representation in fig. (3-3) which reveals the fascinating complexity of the sponge phase in Gaussian approximation

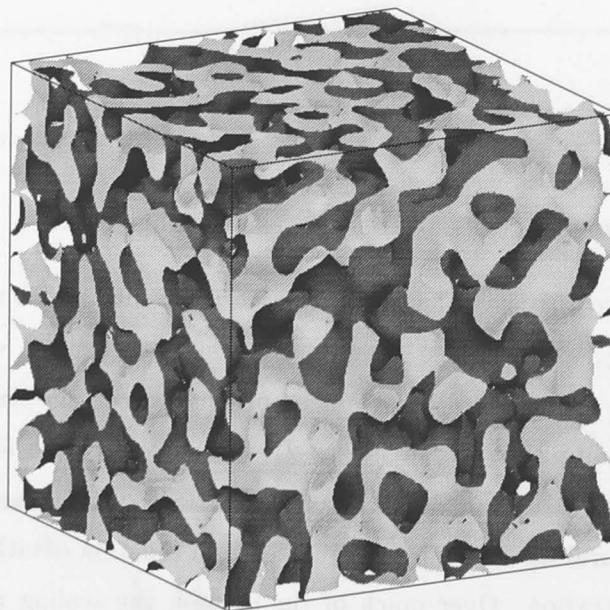


Figure 3-3: *Real space configuration corresponding to the ensemble denoted a in fig. (3-2). The side length of the sample cube is 3 (in reduced molecular units $r_m \cdot \phi_s$). 'Inside' and 'outside' of the interface are distinguished by brighter or darker gray shades.*

In fig. (3-4) we have taken the example systems of fig. (3-2) and plotted cross-sections through the corresponding real-space images in scaled units. As expected in the scaling region samples a and b show near perfect self-similarity while sample c is already more crumpled and has hence larger average domain sizes. Sample d is close to the instability $c = 0$ and is reminiscent of a mixture close to phase separation.

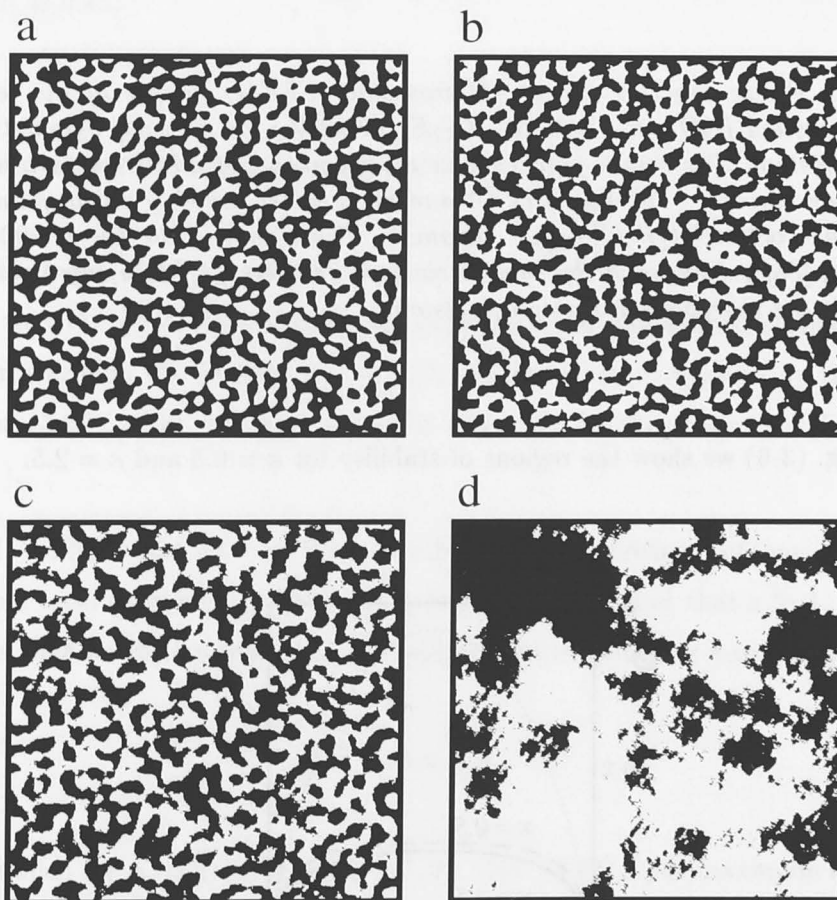


Figure 3-4: *Cross sections through real space structures corresponding to the points a, b, c, d in fig. (3-2). The side lengths of all images is equal (10 in reduced molecular units $r_m \cdot \phi_s$) to underline self-similarity and its breakdown.*

In the next figure, fig. (3-5), we show as a comparison freeze fracture microscopic images from a real system.

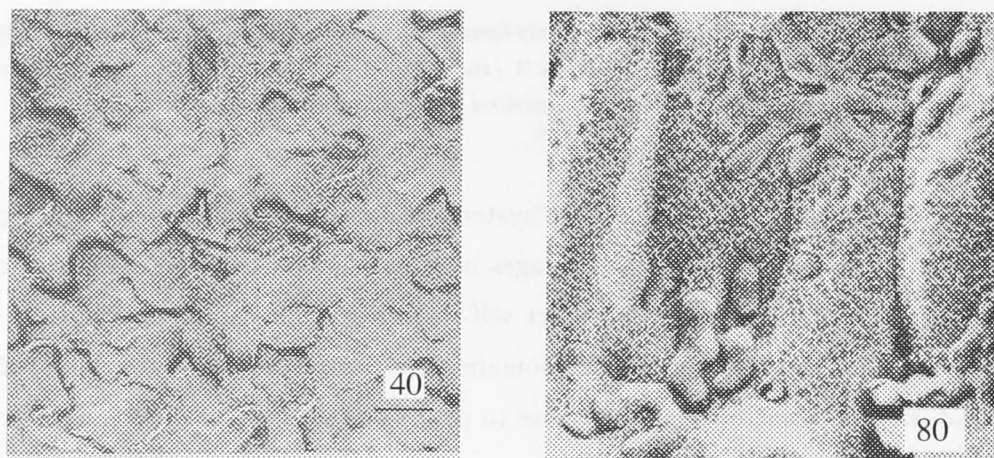


Figure 3-5: Freeze Fracture Electron Microscopic (FFEM) images of the ternary microemulsion system $H_2O - n - octane - C_{12}E_5$ (7 wt %) for a nearly symmetric and an asymmetric system. The octane patches have an irregular leopard-like pattern while water regions appear smooth. The numbers 40 and 80 give the water / oil asymmetry; here $\alpha = 100 \times [n - octane] / ([H_2O] + [n - octane])$. The length of the bar is 2000 Å (from Jahn & Strey [88]). Images of the symmetric type led Berk [34] to apply Cahn's scheme [35] to mimic the morphology of microemulsions.

Finally, in fig. (3-6) we show the regions of stability for $\kappa = 0.5$ and $\kappa = 2.5$.

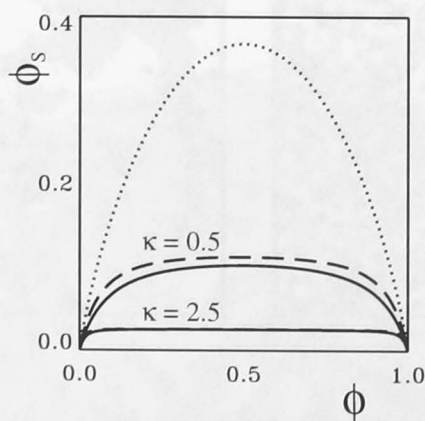


Figure 3-6: Stability diagram for sponge systems in the soft ($\kappa = 0.5$) and semi-rigid ($\kappa = 2.5$) regimes. The solid lines denote the instability $c = 0$ below which no sponge phase can exist. At the loci of the broken lines we have the Lifshitz line, $b = 0$. The upper dotted line marks the line of closest packing above which microemulsions cannot fulfill the geometrical constraints.

Apart from the previously discussed low ϕ_s instability there is also a stability boundary for high ϕ_s which is caused by a closest packing constraint which is only dependent on the cut-off k_c . The exact position of this line is given by the condition $c = -b - 1$ (a divergence at $k = k_c$) and can be approximated by

$$\phi_s \approx \frac{2}{\pi\sqrt{3}} e^{-\frac{\alpha^2}{2}} \quad (3.61)$$

For $\alpha = 0$, we find *e.g.* an upper boundary of $\phi_s \approx 0.37$, for any value of κ . The value of κ at which the region of stability of the microemulsion collapses entirely can then be given as $\kappa^* \approx 0.15$.

Bulk Structure Factor at Asymmetry

We want to briefly discuss the bulk structure factor for large asymmetry α . From fig. (3-6) we see that the region in which the structure factor is well-defined shrinks into a very narrow strip around the Lifshitz line, $b = 0$. Its lower bound is given by the instability $c = 0$, eqn. (3.57), while its upper bound is demarked by the closest packing constraint eqn. (3.61).

In general, we find that for $\alpha \neq 0$ the bending energy increases (*cf.* eqn. (3.A6)) while the entropic term decreases, as we expect. For $|\alpha| \gg 0$ we find that $c \gg 1$. Along $b = 0$ this means that we can approximate the bulk structure factor by a constant

$$\nu^{|\alpha| \gg 0}(k) \approx a/c = 6\pi^2 \quad (3.62)$$

which is fulfilled for $\phi_s \approx 2/(\sqrt{5}\pi) \exp(-\alpha^2/2)$. Eqn. (3.62) is the maximum entropy limit ('white noise'). Its real space correlation function

$$g(r) \sim -r^{-3} [k_c r \cos k_c r + \sin k_c r] \quad (3.63)$$

decays only algebraically, and one has to go to $|\alpha| \gg 0$ to reasonably decorrelate bulk regions. Remarkably, at modest $\alpha \gtrsim 1$ which is above the percolation threshold (*cf.* eqn. (3.12)) a statistical attraction between the isolated bulk regions persists. In fig. (3-7) we show a

cross section through a sample real space structure



Figure 3-7: Cross section through a real space structure with $\kappa = 2.5$, $\phi_s = 0.2$, $\phi = 0.14$ ($\alpha \approx 1.08$). The side length is 1.5 in reduced molecular units $r_m \cdot \phi_s$.

The image looks similar to the FFEM image of the asymmetric microemulsion in fig. (3-5)).

Discussion

Sponge phase structure has received an appreciable amount of experimental attention. In microemulsions most measurements restrict themselves to the bulk structure factor while in L_3 sponges only the film scattering signal can be measured. A few authors have also reported pairs of film and bulk scattering from microemulsions.

Perhaps the most important experimental work in the context of our results are due to Strey, RCC, Porte and their respective co-workers.

In experiment, a change in the bending stiffness κ can be achieved by changing the chain length of the amphiphile [19]. To our knowledge the only systematic investigation of a variation of chain length on microemulsion structure has been reported by Schubert & Strey [87]. There bulk and film spectra of the sequence of amphiphiles C_8E_3 , C_6E_2 , C_4E_1 have been measured very close to the three phase region (just inside the single-phase microemulsion region) with the result that the bulk (film) spectra gradually lost their peaks (shoulders) at k_0 ($2k_0$) (cf. fig. (4) in [87]) in qualitative agreement with our model predictions (cf. fig. (3-1)). In the same work Schubert & Strey also investigated in detail the effect of adding formamide to the mixture with results comparable to those of changing the chain length. However, as changing the formamide content is likely to strongly affect the spontaneous curvature, we have to refrain from a direct comparison

with our model predictions.

Schubert & Strey originally interpreted the change in chain length as a change in ‘amphiphilicity’, a term used by Gompper & Schick (we will discuss the Gompper & Schick theory in more detail below) to assign physical meaning to one of their phenomenological GL parameters. It measures the ‘tendency to create interfaces in an amphiphilic system’ [1]. C_4E_1 is in this context interpreted as a substance unfavorable to build up interfaces and closer to a state of molecular dispersion. At the same time, however, Schubert & Strey pointed out that it was clear from their and other experiments that even C_4E_1 had well-defined internal interfaces while the scattering indicated the absence of well-developed microemulsion structure. Schubert & Strey therefore conclude that the distinction between the two extremes, a well-defined microemulsion and a molecular dispersion is too simple. We have seen from the structure factors and real-space visualizations that this intermediate state between the two extremes can be sensibly interpreted as a state in which water and oil are separated by strongly non-scaling, crumpled interfaces which can be even torn up into smaller closed structures and at the same time still have clearly the character of a complex fluid with well-defined interfaces. In disagreement with [89] we do not find it necessary to depart from the Helfrich Hamiltonian in order to describe short chain amphiphilic systems but suggest that the interpretation of these complex fluids on grounds of the random interface model can reconcile the experimental findings of Schubert & Strey with a consistent theoretical picture.

The low wave vector region of film scattering from L_3 phases has been in detail examined in the pioneering work of RCC [12]. They find experimentally and on grounds of their GL theory, eqn. (3.8), that the generic form of the film structure factor at low k (not too close to criticality) is [77]

$$\nu_f^{symm}(k) \sim \frac{1}{1+k^2\xi_\rho^2} + \frac{B}{1+k^2\xi_\rho^2} \frac{\arctan k\xi_\eta/2}{k\xi_\eta/2} \quad (3.64)$$

$$\nu_f^{asymm}(k) \sim \frac{1}{1+k^2\xi_\rho^2} + \frac{B}{1+k^2\xi_\rho^2} \frac{1}{1+k^2\xi_\eta^2} \quad (3.65)$$

which has provided excellent fits to measured light scattering data [12, 77]. First of all, we note that the derivation of eqns. (3.64,3.65) was gained in the RCC model from the energy-energy correlation function in Gaussian approximation *i.e.* essentially from the square of the bulk correlation function, $g^2(r)$, which is also a significant term in our derivation. Not surprisingly, many general patterns of our results resemble the predictions of eqns. (3.64,3.65). If we stay for the moment with real k_0 the generic form of our film

scattering signal can be written approximately for low k

$$\nu_f(k) \sim \text{const} + \frac{\alpha^2}{k^4 - bk^2 + c} + \frac{1}{2kk_0^2} \arctan \frac{\xi k}{2} \quad (3.66)$$

We saw that in all regimes the arctangent function dominated the low k scattering for symmetric sponges ($\alpha = 0$) in our theory. For asymmetric sponges we find a low k contribution from the Lorentzian bulk structure factor which broadens the arctangent contribution and – for appreciably high κ – we also expect a peak at k_0 whose height is a measure of the asymmetry order parameter α (which is proportional to the mean curvature). It would be interesting whether experimental systems can be found which show this pattern. In regime (ii) for rather short correlation length this peak should not appear and instead we would find essentially an OZ correction for asymmetric sponges just as in eqn. (3.65). What differs between eqns. (3.64,3.65) and our calculation, however, is that because we refer to bulk degrees of freedom and couple the film geometrically the system is characterized by one correlation length ξ only, unlike the ξ_ρ, ξ_η used in eqns. (3.64,3.65). Another difference to the works of RCC is that we can relate the parameters in the film structure factor to fundamental physical variables, κ and ϕ_s . As we saw from the comparison to the measurements of Schubert & Strey our predictions work qualitatively satisfactory.

In principle we can also go beyond the low k region in the film structure factor. We saw that this is tractable with method (a) but very complicated with method (b). We know from experiment [87, 90] that film spectra from microemulsions tend to mostly show a hump-like pattern at $2k_0$ while film spectra from binary sponge phases more often show a pronounced peak [91, 92]. The hump-like pattern can be reproduced by method (a). Whether or not a peak can be produced by method (b) will have to await extensive numerical implementation of eqn. (3.39). In any case, we will see in Chapter 5 that the random interface approximation is – not surprisingly – inappropriate for $\kappa^{-1} \rightarrow 0$. Mode - mode correlations become then stronger and the region around $2k_0$ develops into a peak even in semi-rigid systems – as measured in many L_3 sponge phases.

Thus a large set of observed patterns in film and bulk scattering signals are derived by our theory in a unified way, with a minimum of assumptions and practically no adjustable parameters on the basis of the bending Hamiltonian. All results can be related to the basic parameters κ and ϕ_s . We can proceed from here by examining the intrinsic reasons for the typical sequence of structures upon variation of κ and ϕ_s . Whereas it is clear that lowering of the bending stiffness should ultimately lead to more disorder, it is less

obvious why this should happen upon lowering the surfactant concentration. If we write the crucial parameter δ (eqn. (3.18)) explicitly

$$\delta = \delta_0 \kappa \phi_s - k_c \quad (3.67)$$

we see that the solution of the problem is evident. Porte *et al.* already pointed out that scale-invariance of \mathcal{H} is not strictly accurate but that there is – apart from the surfactant concentration – a second important length scale, the microscopic length scale, r_c . The physical phenomenon which is induced by this additional length scale can be interpreted as follows: for any given finite κ there exists a small ϕ_s (and vice versa) for which the microscopic correction terms in eqn. (3.67) completely dominate the scaling term. These corrections are intimately related to the molecular length scale which is apart from the surfactant concentration the only other relevant length scale; the entropy gain from forming small objects on molecular scales (single molecules, micelles, small droplets or small sponges) overwhelms the energetic gain associated with the formation of microscopically smooth membranes, causes the breakdown of scaling and ultimately the instability. The effect becomes more severe, the smaller the surfactant concentration. This is in fact anti-intuitive. For example, Wennerström & Olsson argued [27] that corrections to the scaling of this type cannot be physical because the microscopic length scale should become relevant when the structural scale becomes comparable to the molecular scale *i.e.* at high surfactant concentration rather than at low surfactant concentration. However, it should be pointed out that it is well-known in the theory of critical phenomena that the microscopic length scale may well be important even close to criticality when intuitively only the diverging correlation length should play a role. The microscopic length scale causes in the case of critical phenomena the occurrence of anomalous dimensions [6] and in our case of surfactants in solutions it causes an instability towards phase separation.

We want to conclude this discussion with two brief remarks. Firstly, one should note that if we would operate in the context of the standard Monge gauge with its fixed topology (*e.g.* no expulsion of vesicles or overhanging membranes are possible) this effect has to be far weaker. Secondly, we have addressed so far only *limits* of stability without having discussed thermodynamic instabilities which might pre-empt these. Therefore the critical scaling which can be derived from eqn. (3.67), $\phi_s \sim \kappa^{-1}$, is only to be seen as a lower limit. Thermodynamic instabilities might well occur before that with a critical

$$\phi_s \sim \kappa^{-x}, \quad \text{with } x \leq 1 \quad (3.68)$$

so that the instability given by eqn. (3.67) can in fact be a precursor of a phase transition.

Having analysed in detail microemulsion structure, its relation to bending constant and surfactant concentration and the limits of stability of the bicontinuous phases we can now proceed with the consistent discussion of the thermodynamics.

3.2.2 Phase Transitions

Experimentally two types of transitions are observed in the isotropic region of the phase diagram. In ternary systems a multiphase sequence is seen at low surfactant concentration, *cf.* fig. (1-1), where the middle-phase sponge is in equilibrium with oil and/or water rich (*i.e.* highly asymmetric, $|\alpha| \gg 0$ dilute vesicle/micellar) phases. Binary sponge systems when diluted can undergo a phase transition from a symmetric sponge ($\alpha = 0$) to an asymmetric phase ($\alpha \neq 0$), called symmetric - asymmetric (S/A) transition, which can be first order (*e.g.* $C_{12}E_5$ - water [85]) or continuous (*e.g.* SDS - pentanol - brine [12, 93]). The relation of the free energies of symmetric and asymmetric systems is therefore crucial, if we want to approach critical phenomena in isotropic amphiphilic systems.

We can determine the minimal free energy density consistently by inserting the minimal structure factor which we gained by $\partial f[\nu]/\partial \nu$ into eqn. (3.9). Then asymmetric systems with $\alpha \neq 0$ can be studied either numerically, or – more conveniently – by means of a Landau expansion of the minimal free energy in the asymmetry order parameter α . The order parameter α is of direct physical importance since it is proportional to the mean curvature of the interface $\langle \delta(s - \alpha) |\vec{\nabla}s| H \rangle \sim \alpha$, eqn. (3.A4). The free energy density f can then be written

$$f = a_0(\kappa, \bar{\kappa}, \phi_s) + a_2(\kappa, \bar{\kappa}, \phi_s) \alpha^2 + a_4(\kappa, \bar{\kappa}, \phi_s) \alpha^4 + a_6(\kappa, \bar{\kappa}, \phi_s) \alpha^6 + O(\alpha^8) \quad (3.69)$$

In the previous section we had seen that the simple solutions eqns. (3.15,3.21) which are only valid for $\kappa \gg 1$ are very useful even outside their strict range of validity *e.g.* to approximately determine the limit of stability of the bicontinuous phase. Similarly, we can use eqns. (3.15,3.21) to approximate the free energy density f . To make this problem tractable we have to restrict ourselves to terms down to order κ^{-1} . We can expand the free energy density f with respect to τ where $\delta = \kappa^2 [\delta_0 \phi_s \kappa^{-1} - \tau^2]$ (eqn. (3.18)) and $\tau = \kappa^{-1}$. The expansion of the free energy density in τ is convergent

$$f = f_0 + \tau^2 f_2 + \tau^4 f_4 + O(\tau^6) \quad (3.70)$$

After this expansion we have to consistently collect terms in τ and κ . After tedious but

straightforward calculation and another expansion in ϕ_s we find

$$f_0 \approx -\frac{1}{36\pi^2} - \frac{1}{12\pi^2} \log\left(\frac{15\pi^2}{16} \phi_s \kappa^{-1} e^{\alpha^2}\right) + \quad (3.71)$$

$$\left[\frac{\pi^2}{8} e^{\alpha^2} (\alpha^2 - 1)(2\kappa + \bar{\kappa}) + \frac{3\pi^2}{10} \kappa e^{\alpha^2} + \frac{45\pi^2}{16384} \kappa^{-1} e^{2\alpha^2} \right] \phi_s^3 + O(\phi_s^4, \kappa^{-2})$$

$$\tau^2 f_2 \approx \left[-\frac{3}{8} e^{\alpha^2} - O(\kappa^{-2}) \right] \phi_s^2 + \frac{45}{128} \kappa^{-1} e^{2\alpha^2} \phi_s^3 + O(\phi_s^4, \kappa^{-2}) \quad (3.72)$$

$$\tau^4 f_4 \approx \left[\frac{15}{128\pi^2} \kappa^{-1} e^{\alpha^2} \right] \phi_s + O(\phi_s^4, \kappa^{-2}) \quad (3.73)$$

We have compared the above approximation for f with the exact calculation of f based on the coefficients eqns. (3.15,3.21) and confirmed very good convergence. For example, we found for $\kappa = 10$ the relative error to decrease from 5.5% to $7.5 \cdot 10^{-5}\%$ when going from $\phi_s = 0.3$ to $\phi_s = 0.01$. Similarly, the relative error for constant $\phi_s = 0.1$ developed from 15.5% to $10^{-3}\%$ when increasing κ from 1 to 10^5 .

The above expressions can then be inserted into eqn. (3.70) and expanded in α to yield the Landau coefficients a_0, a_2, a_4 etc.

Corrections to Scaling and Steric Repulsion

The leading terms comprising the symmetric term a_0 can be written

$$a_0 = f_s + f_c + f_h \quad (3.74)$$

with

$$f_s = \frac{\pi^2}{40} [2\kappa - 5\bar{\kappa}] \phi_s^3 \quad (3.75)$$

$$f_c = -\frac{3}{8} \phi_s^2 - \frac{1}{12\pi^2} \log \phi_s + \text{const} \quad (3.76)$$

$$f_h = \left[\frac{4\pi^2}{16384} + \frac{45}{128} \right] \kappa^{-1} \phi_s^3 \quad (3.77)$$

In leading order in the elastic moduli we recover the pure scaling form f_s of the free energy density. In this limit the free energy density is a monotonic function of ϕ_s and a change in surfactant concentration cannot yield phase transitions as the surfactant concentration is varied – as discussed above – in contrast to experimental observation.

The remaining terms can be split into the non-scaling corrections f_c and the scaling corrections f_h (both up to leading terms in the moduli). We note that the leading corrections f_c

(where *const* comprises terms which are not dependent on ϕ_s) are actually *singular*¹⁰ for $\phi_s \rightarrow 0$, but have small coefficients of order unity compared with the scaling term whose coefficient is order κ (assumed large). The term $\log \phi_s$ comes from $\log \xi^{-1}$ ($\xi \sim \kappa \phi_s^{-1}$, eqn. (3.44)) which measures the entropy associated with polydispersity given by the width of the correlation peak. This stands in contrast to the types of corrections which have been discussed so far in the literature and which vanish for $\phi_s \rightarrow 0$. A logarithmic correction based on the renormalization of the bending constant in planar geometry (low temperature Monge approximation, [15])

$$f \sim A\phi_s^3 + B\kappa^{-1}\phi_s^3 \log \phi_s \quad (3.78)$$

has been suggested by a number of authors [5, 12, 31]. Wennerström & Olsson, on the other hand, suggested higher order corrections of the type [27]

$$f \sim \phi_s^3 [A + B\phi_s^2] \quad (3.79)$$

which originate from higher order bending terms. Experimental verification has been attempted and seems to support a logarithmic correction in some systems [12] but not in others [91, 94]; the experimental difficulties are the smallness of the effect and the restricted swelling of samples due to instability either towards ordered phases at high surfactant concentration or towards vesicular systems at low surfactant concentration. We argue here that because the random interface model operates in a well-defined range of \vec{k} vectors down to a few molecular scales renormalization à la eqn. (3.78) should in any case have minor significance. Even if we would include these terms explicitly we see that both eqns. (3.78,3.79) are minor because logarithmic or higher order terms are weaker than the algebraic, low order ones found here. More generally, with regard to eqn. (3.78), we also put forward that there is some doubt whether the planar result eqn. (3.78) can be applied to the case of non-planar interfaces. This has most recently been shown by Morse & Milner who proved that for the case of spherical interfaces the renormalization has to be strongly modified [95]. It has also been argued *e.g.* by Wennerström & Olsson that the notion of renormalization is not straightforward in the case of sponge phases due to the absence of a well-defined reference surface [27].

Finally, there are scaling corrections which are themselves proportional to ϕ_s^3 . They are to leading order given by

$$f_h \approx \frac{45}{128} \kappa^{-1} \phi_s^3 \quad (3.80)$$

¹⁰Singular corrections are known in other systems, for example, the confluent singularity of the susceptibility in magnetic systems [6].

We see immediately that f_h has just the functionality analogous to the leading terms in eqn. (2.49) for smectic lamellar phases. This term can therefore be interpreted as a steric repulsion term of Helfrich type. It has been applied and discussed (but not derived) in the context of a coarse-grained lattice model by Golubović & Lubensky [32]. Eqn. (3.80) for sponge phases motivates its use in [32] and is to our knowledge the first systematic attempt to derive this term in sponge phases.

S/A Transition

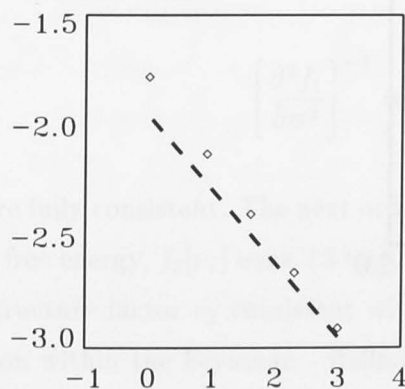
In standard Landau theory (ie for $a_4 > 0$ which we assume for the moment) the locus of the phase transition is determined by the quadratic coefficient. We find up to $O(1)$ in κ

$$a_2 = -\frac{1}{12\pi^2} - \frac{3}{8}\phi_s^2 + \frac{3}{10}\pi^2\kappa\phi_s^3 \quad (3.81)$$

(where we have now omitted steric repulsion terms because we assume them small). For small ϕ_s and large κ we can solve and see that the critical surfactant concentration ϕ_s^* - determined by $a_2(\kappa, \phi_s^*) = 0$ - reads

$$\phi_s^* \approx \left(\frac{5}{18\pi^4}\right)^{\frac{1}{3}} \kappa^{-\frac{1}{3}} \quad (3.82)$$

Because derivation of eqn. (3.82) is rather tedious it is in this case worthwhile to verify



our approximations by comparison with exact, numerical results. We show this in the log - log plot of ϕ_s vs κ in the inset. As expected the $\sim \kappa^{-\frac{1}{3}}$ law holds for large κ while corrections cause a steeper decay at small bending constant. If we compare with the structural instability, eqns. (3.67,3.68), we see as expected that the thermodynamic instability pre-empts in general the structural instability (but *cf.* the

following paragraphs for a more detailed discussion).

The transition at ϕ_s^* is only topological without changing the symmetry of the system (similar to the classical liquid - gas transition). In fig. (3-8) we show three dimensional images of systems in the asymmetric region of a specific example with $\kappa = 2.5$. We see

a sequence of structures from a worm-like structure to systems which are beyond the percolation threshold ($\alpha \approx 1$) and thus of more or less vesicular nature.

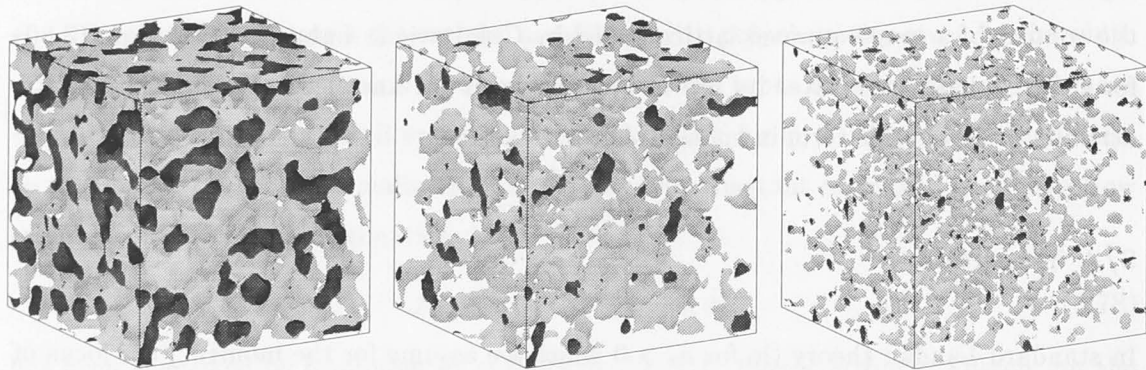


Figure 3-8: Real-space structures according to the structure factors variationally minimized for $\kappa = 2.5$, $\bar{\kappa} = 0, 0, -5$, $\phi_s = 0.9\phi_s^*, 0.4\phi_s^*, 0.4\phi_s^*$ and $\alpha \approx 0.54, 1.3, 1.7$ (from left to right) showing the evolution from a weakly asymmetric worm-like (left) to a strongly asymmetric vesicular phase (right). The sidelengths of the sample cubes are all equal to 50 film thicknesses.

The swelling behaviour around the transition should also show observable change. Fig. (3-9) shows a

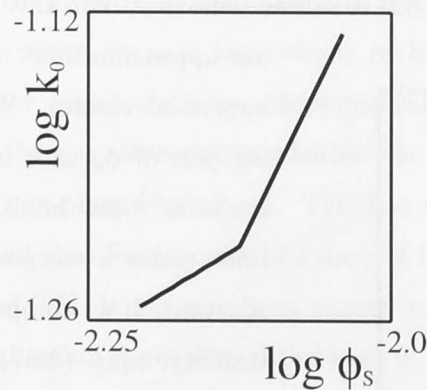


Figure 3-9: The structural wave vector k_0 over the surfactant concentration for $\kappa = 2.5$. The locus of the S/A transition is seen as a cusp.

log - log plot of the structural wave vector k_0 vs the surfactant concentration for $\kappa = 2.5$. At the transition the scaling changes visibly into a much weaker dependence. This seems

to be in agreement with experiments [78]. We find a similar cusp irregularity when plotting the correlation length ξ vs ϕ_s (not shown here). Thus our calculation indicates that near the phase transition the bulk correlation function remains analytic and in particular $\nu(k=0)$ is finite. At the same time the second derivative of the free energy density with respect to α at ϕ_s^* vanishes, which must lead to a divergence of the structure factor at $k=0$ due to the relationship between zero angle scattering and osmotic compressibility [5, 91]

$$\nu(k=0) \sim \phi \left[\frac{\partial \pi}{\partial \phi} \right]^{-1}, \quad \pi = -f + \phi \frac{\partial f}{\partial \phi} \quad (3.83)$$

This apparent contradiction can be explained by carefully considering the order of approximation to which $\nu(k)$ and $f[\nu(k)]$ have been calculated. Consider, for example, Landau theory where in the free energy (*e.g.* the uniform trunc of eqn. (3.8)) no gradient terms are necessary to predict phase transitions. Thus at this level a uniform order parameter distribution or flat correlation function is sufficient to make statements about phase transitions. Only the Ornstein - Zernike extension which introduces self-consistently gradient terms can also provide suitable structure factors [23]. We can argue similarly for the random interface model. In the limit of very large bending stiffness, $\kappa^{-1} \rightarrow 0$, the structure factor is essentially given to zeroth order by a delta function: $\nu_0 \sim \delta(k - k_0)$, although there still are random fluctuations in the direction of the wave vector. The first order free energy density, $f_1[\nu_0]$, is given by eqn. (3.75) and does not show any phase transition. The structure factor consistent with f_1 is given by eqn. (3.46) to first order in κ^{-1} and we see that then

$$\left[\frac{\partial^2 f_1}{\partial \alpha^2} \right]^{-1} = \nu_1(k=0) = a/c = 5/(3\pi^2) \kappa^{-1} \phi_s^{-3} \quad (3.84)$$

are fully consistent. The next order of approximation, using the structure factor ν_1 , yields a free energy, $f_2[\nu_1]$ eqns. (3.69,3.82) which does exhibit an S/A transition. However, the structure factor ν_2 consistent with $f_2[\nu_1]$ requires a very complex, higher-order calculation within the Feynman - Hellman variational theory [43]. Although f_2 clearly exhibits a phase transition at ϕ_s^* indicating $\nu_2(k=0) \rightarrow \infty$, the structure factor ν_1 is too approximate and only the next order of approximation, ν_2 , is expected to show the divergence at the right place. Eqn. (3.46) is therefore not accurate too close to the critical point. This, however, should not affect the qualitative properties of the results for the scattering away from the critical region.

Nature of the S/A Transition

The quartic coefficient up to $O(1)$ in the moduli reads

$$a_4 = -\frac{3}{16}\phi_s^2 + \frac{\pi^2}{80}[22\kappa + 5\bar{\kappa}]\phi_s^3 \quad (3.85)$$

If we would only take leading terms in the moduli into account, and remember the local stability constraint $-2\kappa \leq \bar{\kappa} \leq 0$, all coefficients a_{2n} , $n \geq 2$ including a_4 would always be positive. This would indicate that the S/A transition is in any case continuous. On the other hand, we see from eqn. (3.71) (and explicitly in eqn. (3.85)), that corrections could in fact change the sign of the higher Landau coefficients, if κ is low enough thus allowing for the possibility of first order S/A transitions and tricritical points [96, 12, 79]. The general form of the Landau free energy eqn. (3.69) is in fact the same as in the classical example of a tricritical system, the Blume - Emery - Griffiths model [97] of He^3/He^4 mixtures¹¹. There and also in [12] generic phase diagrams have been studied in detail.

First Order Coexistence

A more general possibility of a first order transition would be first order coexistence commonly observed in ternary microemulsions. A continuous S/A transition would create an equilibrium of two microemulsion sponge phases, one with more water than oil content and an analogous one with reversed oil / water ratio [31]. There is to our knowledge no experimental evidence for this. Similarly, there are also binary systems which show coexisting symmetric and asymmetric phases, *e.g.* [85]. This is physically realized when the critical surfactant concentration ϕ_s^* lies in the two-phase region predicted by first order coexistence.

Technically, first order coexistence can be most conveniently studied by the double tangent or (in the case of ternary microemulsions) double plane construction. This technique is discussed in detail in [2, 12, 31]. We can briefly explain the principle for the case of two phase co-existence in sponges (which is equivalent to three phase coexistence in microemulsions). After performing the minimization

$$\bar{f}(\phi_s, \kappa, \bar{\kappa}) = \min_{\alpha} f(\alpha, \phi_s, \kappa, \bar{\kappa})$$

¹¹ For a detailed discussion *cf.* [96].

equilibrium for two phases with concentrations ϕ_{s1} , ϕ_{s2} at constant total volume requires the equality of the chemical potentials μ and the osmotic pressures Π of the two phases [2, 12]

$$\left. \frac{\partial \bar{f}}{\partial \phi_s} \right|_{\phi_s = \phi_{s1}} = \left. \frac{\partial \bar{f}}{\partial \phi_s} \right|_{\phi_s = \phi_{s2}} = \mu_s, \quad \bar{f}(\phi_{s1}) - \phi_{s1} \left. \frac{\partial \bar{f}}{\partial \phi_s} \right|_{\phi_s = \phi_{s1}} = \bar{f}(\phi_{s2}) - \phi_{s2} \left. \frac{\partial \bar{f}}{\partial \phi_s} \right|_{\phi_s = \phi_{s2}} = \Pi$$

and results in

$$\bar{f}(\phi_{s1}) - \bar{f}(\phi_{s2}) = \mu_s (\phi_{s1} - \phi_{s2}) \quad (3.86)$$

which can be geometrically interpreted as the equation of a common tangent (with slope μ_s) along \bar{f} . In the case of binary sponges the two concentrations ϕ_{s1} , ϕ_{s2} mark two phase coexistence (graphically usually connected by a tie line) and in ternary systems the points $(\phi_1 = 1/2, \phi_{s1})$, (ϕ_2, ϕ_{s2}) , $(1 - \phi_2, \phi_{s2})$ establish the three phase triangle (*e.g.* the region denoted 3 in the phase diagram fig. (1-1)). The determination of possible two phase regions in ternary systems requires the analogous procedure, but now a more general common tangent plane is constructed

$$f(\phi_1, \phi_{s1}) - f(\phi_2, \phi_{s2}) = \mu (\phi_1 - \phi_2) + \mu_s (\phi_{s1} - \phi_{s2}) \quad (3.87)$$

where μ is the chemical potential related to ϕ . In practice one can carry out construction eqn. (3.86) numerically with the exact free energy density calculated from eqn. (3.9) with the minimal structure factors. We plot in fig. (3-10) the numerically determined free energy density \bar{f} for $\kappa = 2.5$, $\bar{\kappa} = 0$.

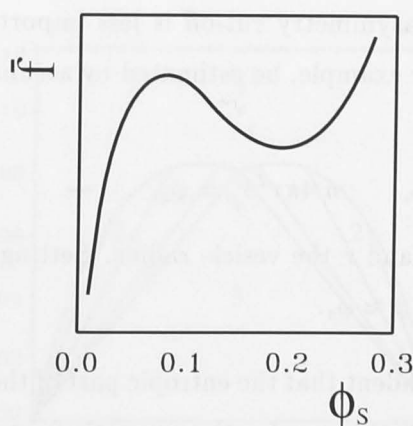


Figure 3-10: Typical free energy density $\bar{f}(\phi_s)$ for $\kappa = 2.5$, $\bar{\kappa} = 0$ used for the double tangent construction. The low ϕ_s cut-off occurs at $\phi \approx \phi_s$ (eqn. (3.89)).

There is a local minimum in the free energy which can be identified with the middle

phase microemulsion (or symmetric binary sponge). The situation of the 'deep minima' at high asymmetry is similar but less severe than that in the coarse-grained lattice model where the random mixing entropy diverged for $\phi \rightarrow 0$ [31]. In our case the minimum is also a boundary minimum but converges towards a finite value of the free energy density. This is due to a flaw common to all lowest order curvature theories when one moves into the vesicular region [31]. Linear elasticity is not fully adequate to estimate the energetic cost in the dilute phase. This happens formally in the random interface model due to the exponential term in α which converges to zero for strong asymmetry. It becomes extreme when we go to micellar dimensions which are clearly ill-described by eqn. (1.2). It essentially means that in this case we only minimize with respect to the entropy under the physical constraints. Then the ansatz for the structure factor reads $\nu(k) = [-bk^2 + c]^{-1}$. For small b a simple calculation shows that the two constraints can be solved approximately by $c = b \langle k^2 \rangle + (6\pi^2)^{-1}$ and $b \approx [-7(3 - 5 \langle k^2 \rangle)]/[6(15\pi^2 - 42\pi^2 \langle k^2 \rangle + 35\pi^2 \langle k^2 \rangle^2)]$. When $\alpha - i.e.$ the density and size of the vesicles - is adjustable, as it is in the three phase curve, we find just the maximum entropy solution as we should

$$b = 0, \quad c = [6\pi^2]^{-1}, \quad \alpha = \pm \left[\log \left[\frac{4}{5\pi^2} \phi_s^2 \right] \right]^{\frac{1}{2}}, \quad \bar{f} = - [12\pi^2]^{-1} \log [6\pi^2] \quad (3.88)$$

This is physically sensible in the context of our theory, and differs from coarse grained models where the random mixing entropy diverged towards $-\infty$ for large asymmetry [31]. In ACRS the choice of a molecular cut-off *i.e.* a maximal value of α was therefore crucial because the depth of the asymmetric minimum was very sensitive to it, *cf.* [31]. Here the situation is less complicated because the maximum entropy state is well-defined and the detailed definition of the asymmetry cut-off is less important. A sensible choice of the asymmetric cut-off can, for example, be estimated by assuming monodispersity of the isolated vesicles so that

$$n \frac{4\pi}{3} r^3 = \phi, \quad n 4\pi r^2 r_c = \phi_s \quad \rightarrow \quad \phi \approx \phi_s \quad (3.89)$$

where n is the vesicle density and r the vesicle radius. Setting a minimal radius to, say, $r \approx 3 \cdot r_c$ we find the minimal $\phi \approx \phi_s$.

While we can be relatively confident that the entropic part of the free energy density is not unreasonable this is clearly not the case for the energetic part. The assumption of linear elasticity breaks down below a certain vesicle radius [70]. This should be remedied *e.g.* by introducing higher order curvature invariants, for example, of the kind eqns. (3.A7,3.A8). This would introduce new phenomenological curvature moduli about which there is practically nothing known. However, higher order elasticity would also simply allow for a

wider range of Gaussian moduli beyond the constraint $-2\kappa \leq \bar{\kappa} \leq 0$. Within the context of a pure elasticity Hamiltonian the possibility of a positive value of $\bar{\kappa} > 0$ would be the simplest explanation why in some systems a continuous S/A transition is observed while in others the transition is first order: for a sufficiently positive $\bar{\kappa} > 0$ the deep minimum *e.g.* in fig. (3-10) vanishes while the continuous S/A transition (as given by eqn. (3.81)) is not affected by $\bar{\kappa}$ and remains then the only possible source of criticality.

It is therefore safe to say that our calculations indicate that a first order transition is 'more common' than a continuous one, if we define common as a system with negative saddle-splay modulus. This finds some support by the fact that ternary microemulsions show first order transitions and that continuous transitions in L_3 sponges are certainly also not the only possibility. The fact that - to our knowledge - continuous transitions in L_3 phases have only been observed in relatively complicated systems, SDS - pentanol - brine [12] and OBS - pentanol - brine [79], might support this argument.

For the standard case of negative $\bar{\kappa}$ we can carry out the double tangent construction *e.g.* for the case fig. (3-10). We consistently found in all cases we studied that at constant $\bar{\kappa}$ the relative position of the three phase point is still well described by the scaling law for the critical S/A transition $\phi_s \sim \kappa^{-\frac{1}{3}}$ so that this relation holds in our model independent of the nature of the transition. In fig. (3-11) we show an example for a microemulsion phase diagram for $\kappa = 5$. It shows the characteristic 2 - 3 - 2 multiphase sequence as in fig. (1-1)

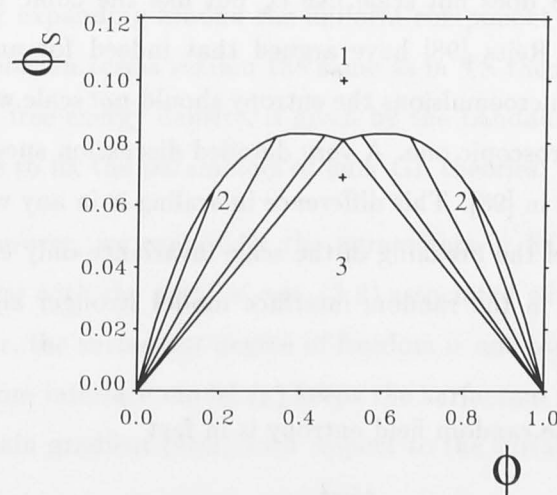


Figure 3-11: $\phi - \phi_s$ phase diagram with $\kappa = 5$, $\bar{\kappa} = -5$. The lower and upper crosses

denote the three phase point for $\bar{\kappa} = 0$ and $\bar{\kappa} = -10$, respectively. The cut-off scale used here was three times the usual cut-off.

Often measured three phase points are quite low in ϕ_s and we used the little freedom we have in terms of parameter adjustment to raise r_c to $3r_c$ in order to lower the three phase point. In principle, however, the butterfly shape is very typical no matter which parameters we use. Changes in κ or $\bar{\kappa}$ (or even r_c) only stretch or squeeze the basic butterfly shape.

3.2.3 Relation to Coarse Grained and Ginzburg - Landau Theories

Firstly, we can compare with the ACRS coarse-grained model. There a heuristic bending energy B and the random mixing entropy were used, *cf.* [31]. For small deviations from bulk symmetry, $\phi = 1/2$, we can use again $\alpha \sim \phi - 1/2$ and expand

$$B^{ACRS} \sim \phi_s^3 [c_1 + c_2 \alpha^2], \quad -S^{ACRS} \sim \phi_s^3 [c_3 - c_4 \alpha^2] \quad (3.90)$$

where the c_2, c_4 are positive numerical constants. If we set $\bar{\kappa} = 0$ in the random interface model, keep the leading terms in κ in the bending energy and the leading terms in the entropy and expand both in terms of α , we get for B and $-S$ the same functional forms with respect to the asymmetry parameter α (but with different c_n) so that the qualitative similarities of the two models in their thermodynamic predictions do not come as a surprise. However, $-S$ does not scale like ϕ_s^3 but like the cubic microscopic scale. Most recently Sturgeon & Reiss [98] have argued that indeed for an estimate of the configurational entropy of microemulsions the entropy should *not* scale with the structural length scale but with a microscopic one. A very detailed discussion specifically dedicated to this matter can be found in [98]. This difference in scaling is in any way not surprising because in the ACRS model the breaking of the scale invariance only enters through the renormalization of κ while in the random interface model stronger algebraic terms are present, as discussed above.

The first scaling term in the random field entropy is in fact

$$-S_h \approx \frac{45\pi^2}{1024} e^{2\alpha^2} \kappa^{-1} \phi_s^3 \quad (3.91)$$

which is a steric repulsion term which grows for increasing asymmetry order parameter.

We are now also in a position to determine the phenomenological Ginzburg - Landau parameters in the theory of Teubner & Strey and in the extended version due to Gmper & Schick.

In the TS model the parameters a_2 , c_1 , c_2 in eqn. (3.5) can be simply estimated by comparison of the coefficients in the structure factors [37]. Then

$$a_2 = \frac{c(\alpha, \phi_s, \kappa)}{a(\alpha, \phi_s, \kappa)}, \quad c_1 = \frac{b(\alpha, \phi_s, \kappa)}{a(\alpha, \phi_s, \kappa)}, \quad c_2 = \frac{1}{a(\alpha, \phi_s, \kappa)} \quad (3.92)$$

where the $a(\alpha, \phi_s, \kappa)$, $b(\alpha, \phi_s, \kappa)$, $c(\alpha, \phi_s, \kappa)$ have of course been determined in detail above.

Gmper & Schick generalized the functional of TS to include a number of experimental observations¹²

$$F_{GS}(s) = \int d\vec{r} [f(s) + g(s)(\nabla s)^2 + c(\Delta s)^2] \quad (3.93)$$

where we have kept the original notation of [13] for the GL parameters. Unlike eqn. (3.5) the local and gradient terms are now not purely quadratic or constant. In order to model transitions between the microemulsion and the oil- or water-rich phases, GS assumed special functional forms where $f(s)$ and $g(s)$ are of convenient piece-wise parabolic and piece-wise constant form, respectively (*cf. e.g.* [13] for details). We can derive the analogous functions by expanding around the uniform component ($k \rightarrow 0$). The coefficients of gradient and Laplacian terms remain the same as in TS theory while the constant term, the uniform bulk free energy density, is given by the Landau expansion eqn. (3.69). It is therefore possible to fix the parameters of bulk GL theories.

At this stage, however, we cannot fix the parameters in RCC GL theory. Our results can only be related with the parts of eqn. (3.8) associated with the asymmetry degree of freedom. However, the surfactant degree of freedom is not comparable in the two models because the random interface model (a) keeps the surfactant concentration constant and (b) does not contain gradient terms with respect to the surfactant concentration.

¹²We note that the causality is reversed in comparison to the random interface model: experimental patterns are *input*, not results.

3.3 Discussion and Outlook

The shortcomings and merits of the random interface model should be briefly summarized and discussed in the context of alternative models.

Random interface theory represents a useful connection between standard field theoretical models and the membrane description of amphiphilic phases. It combines the advantages of both approaches. On the one hand it allows a genuine continuum description of fluctuating surfactant solutions while it stays close enough to the membrane description to refer to the natural parameters κ , $\bar{\kappa}$, ϕ_s , ϕ without need to introduce the abstract parameters of GL theory. Perhaps the most attractive feature of random interface theory is its ability to unify predictions on structure and thermodynamics of fluctuating membranes and to stay at the same time fundamental enough to allow for comparison to experiment.

The model can successfully and consistently predict two of the most established characteristics of the sponge structure factors: the Teubner - Strey form of the bulk structure factor and low wave vector scattering with an unusual arctangent form of the film structure factor. The evolution of the bulk and film structure factors upon change of κ and ϕ_s – characterized by the loss of a scaling structural length scale – agrees with experiment, provides an insightful basis for their interpretation and sheds some light on the subtle mechanism driving the entropic instability underlying the sponge - dilute transitions: the important role of the microscopic length scale.

Consistently, evaluation of the free energy density resulted in the typical symmetric - asymmetric transitions in L_3 sponge phases and microemulsions which are in general first order or under appropriate conditions sometimes continuous in agreement with experiments. The asymmetry order parameter (essentially the mean curvature) in L_3 sponge phases was predicted to be measurable using the film structure factor of asymmetric phases.

However, there are also a number of imperfections in the theory. Firstly, second order Feynman - Hellman theory is needed to bring the structure factor better in line with the criticality implied by the free energy density. Maybe more urgently, it would be very interesting to see how the 'softening' of the geometric coupling of bulk and amphiphile degrees of freedom would affect our predictions. In this case the uniform order parameter α would be replaced by a spatially varying $\alpha(\vec{r})$ which would be again assumed to have

a Gaussian mode distribution. Then we could explicitly diagonalize and proceed by minimizing not only the bulk structure factor but also the structure factor associated with the amphiphile. It is not unlikely that structure factors which correspond to uniform α are in general not the minimal solution. Non-uniform α would slightly soften the film - bulk coupling, enlarge topological phase space and stress the role of $\bar{\kappa}$. Secondly, the type of occurring transitions cannot be reliably predicted mainly because of the failure of any linear bending energy model to accurately estimate the energy of small vesicles or even micelles.

We also want to briefly discuss a few aspects of the above work in the context of established or alternative literature.

Maybe most notable throughout this chapter (and the remainder of the thesis) is the absence of any reference to the well-established de Gennes - Taupin persistence length ξ_p [29] which is used extensively throughout the literature on flexible membrane models. While this notion has sparked pioneering insights into the mechanisms which underly fluctuating membrane systems we should note that it is – similar to the related issue of the renormalization of the bending constant – derived in the approximation of quasi-flat membranes [15]. It is therefore very useful in the context of phases which are essentially twodimensional (smectic lamellar) but might be less applicable to topologically complex systems. For example, in the *AOT* system studied by Porte *et al.* [5] the persistence length is several orders of magnitude larger than the structural length, casting doubt on the utility of the concept for such structures. Instead of a persistence length ξ_p we used a correlation length ξ which contains information about both the correlations along the surface and correlations to neighboring surfaces. This seems a natural and physically sensible extension of the persistence length concept for topologically complex structures in three dimensions.

The models most similar to the random interface description are GL models. The relationship to the bulk (one - parameter) GL models due to Teubner & Strey (extended by Gompper & Schick) is clear: these GL models are, roughly speaking, low wave vector expansions of the random interface formulation. Our approximate random interface description provides a physical basis for the assumptions which are necessary to create these GL models. This is for example demonstrated by our ability to fix the GL parameters in terms of the natural parameters which originate from the bending Hamiltonian. The relationship to the two - parameter RCC GL model is more tentative with respect

to the amphiphile degree of freedom. The best modelling of the amphiphile degree of freedom remains certainly a point of discussion (*cf.* above); geometric coupling might be too strong.

In conclusion we can state that the results of this chapter – despite weaknesses – can be taken as satisfactory evidence that the random interface description of sponge phases is a solid approximation to the challenging and still outstanding problem of the exact solution of the bending Hamiltonian.

It encourages the further investigation and application of the model. Some possible directions are

1. systematic study of the evolution from a binary L_3 sponge to a microemulsion: Gompper & Schick pointed out in [1] that an investigation of the intermediate structures with two kinds of internal interfaces has received hardly any attention. While the random interface model can readily treat the curvature energy (by simply adding the curvature energy of two interfaces with half the bending modulus of a bilayer) and the scattering properties of such systems given by eqn. (3.27), a refined approach to the entropic contribution remains an obstacle to a full thermodynamic treatment. Recent experimental interest in these systems [72] adds urgency to the topic.
2. systems with non-zero spontaneous curvature, *e.g.* vesicle phases which are of technological importance.
3. inclusion of direct interactions *e.g.* of electrostatic type: similar to the unsatisfactory situation in the field of steric interaction where only Helfrich could offer a low temperature theory for simple smectic lamellar phases, most works on direct interactions of electrostatic and vdW type are also restricted to the relatively easy case of smectics. Most recently, Menes & Safran [99] have treated interacting microemulsions for the case of high bulk asymmetry. A consistent treatment near symmetry is still missing.

In the next chapter we will discuss some aspects of another important topic: the relative stability of the sponge and lamellar phases.

3.A Appendix

Statistical Averages We follow the straightforward statistical method explained in Chapter 2. However, a few non-standard variations to the procedure have to be explained.

The correlation matrix is now

	s	s_x	s_y	s_z	s_{xx}	s_{yy}	s_{zz}	s_{xy}	s_{xz}	s_{yz}
s	$\langle 1 \rangle$	0	0	0	$-\langle k^2 \rangle / 3$	$-\langle k^2 \rangle / 3$	$-\langle k^2 \rangle / 3$	0	0	0
s_x	0	$\langle k^2 \rangle / 3$	0	0	0	0	0	0	0	0
s_y	0	0	$\langle k^2 \rangle / 3$	0	0	0	0	0	0	0
s_z	0	0	0	$\langle k^2 \rangle / 3$	0	0	0	0	0	0
s_{xx}	$-\langle k^2 \rangle / 3$	0	0	0	$\langle k^4 \rangle / 5$	$\langle k^4 \rangle / 15$	$\langle k^4 \rangle / 15$	0	0	0
s_{yy}	$-\langle k^2 \rangle / 3$	0	0	0	$\langle k^4 \rangle / 15$	$\langle k^4 \rangle / 5$	$\langle k^4 \rangle / 15$	0	0	0
s_{zz}	$-\langle k^2 \rangle / 3$	0	0	0	$\langle k^4 \rangle / 15$	$\langle k^4 \rangle / 15$	$\langle k^4 \rangle / 5$	0	0	0
s_{xy}	0	0	0	0	0	0	0	$\langle k^4 \rangle / 15$	0	0
s_{xz}	0	0	0	0	0	0	0	0	$\langle k^4 \rangle / 15$	0
s_{yz}	0	0	0	0	0	0	0	0	0	$\langle k^4 \rangle / 15$

The difference to the calculation of averages in the appendix of the second chapter is that now the integration is performed over the volume V rather than the base area A , and that the implicit forms of the differential operators are needed. In detail [100]

$$\frac{dS}{dV} = |\vec{\nabla}s|$$

$$H = \frac{1}{2} \operatorname{div} \vec{n} \quad (3.A1)$$

$$K = \sum_{cycl} \frac{\vec{x}_i}{|\vec{x}_i|} \left(\frac{\partial \vec{n}}{\partial x_j} \times \frac{\partial \vec{n}}{\partial x_k} \right)$$

with $\vec{n} = \vec{\nabla}s / |\vec{\nabla}s|$.

Now, as shown in the introduction chapter, the volume averages can be identified with the ensemble averages over some differential operator O and therefore

$$\langle \delta(s - \alpha) |\vec{\nabla}s| O \rangle_0 = \int_{-\infty}^{\infty} \dots \int_{-\infty}^{\infty} ds ds_i ds_{ij} P(s, s_i, s_{ij}) \delta(s - \alpha) |\vec{\nabla}s| O \quad (3.A2)$$

where we have used the Dirac delta function to restrict the integrations to the interface. Six of the ten integrations are easy because their section of the covariance matrix

is diagonal. The problem is then reduced to a four-fold Gaussian integral with simple arguments. The considerable computational work can be surmounted by symbolic software packages. We will use the same method with varying covariance matrices in this and the next chapter. All these cases follow the same principle. In the present chapter we find

$$\frac{S}{V} = \frac{2}{\pi} \sqrt{\frac{\langle k^2 \rangle}{3}} e^{-\frac{\alpha^2}{2}} \quad (3.A3)$$

$$\left(\frac{S}{V}\right)^{-1} \langle \delta(s - \alpha) |\vec{\nabla}s|H \rangle_0 = \frac{1}{2} \sqrt{\frac{\pi}{6 \langle k^2 \rangle}} \alpha \quad (3.A4)$$

$$\left(\frac{S}{V}\right)^{-1} \langle \delta(s - \alpha) |\vec{\nabla}s|K \rangle_0 = \frac{1}{6} \langle k^2 \rangle (\alpha^2 - 1) \quad (3.A5)$$

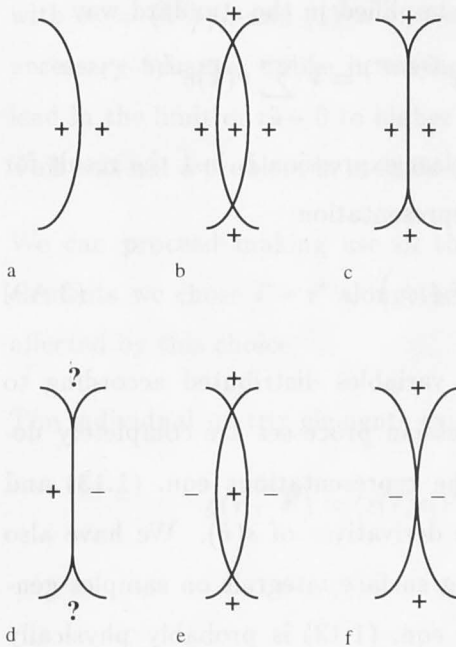
$$\left(\frac{S}{V}\right)^{-1} \langle \delta(s - \alpha) |\vec{\nabla}s|H^2 \rangle_0 = \left(\frac{S}{V}\right)^{-1} \langle \delta(s - \alpha) |\vec{\nabla}s|K \rangle_0 + \frac{1}{5} \langle k^4 \rangle \langle k^2 \rangle^{-1} \quad (3.A6)$$

$$\left(\frac{S}{V}\right)^{-1} \langle \delta(s - \alpha) |\vec{\nabla}s|H^3 \rangle_0 = \sqrt{\frac{\pi}{6 \langle k^2 \rangle}} \alpha \left[\frac{2979}{5600} \langle k^4 \rangle + \frac{433}{3360} (\alpha^2 - 3) \langle k^2 \rangle^2 \right] \quad (3.A7)$$

$$\left(\frac{S}{V}\right)^{-1} \langle \delta(s - \alpha) |\vec{\nabla}s|HK \rangle_0 = -\sqrt{\frac{\pi}{6 \langle k^2 \rangle}} \alpha \left[\frac{161}{300} \langle k^4 \rangle + \frac{1}{6} (\alpha^2 - 3) \langle k^2 \rangle^2 \right] \quad (3.A8)$$

It was Teubner who originally derived eqns. (3.A3,3.A4,3.A5,3.A6) in a very similar way which is outlined in detail in [37] but will not be used here. All our results agree with Teubner's original results [37]. Furthermore, as a crosscheck, Eqn. (3.A3) - eqn. (3.A8) will be independently, numerically verified at the start of the Appendix to Chapter 5.

Self - Avoidance The self-avoidance of random surfaces is not completely self-evident. There is the possibility of zero crossing which are not of first order *i.e.* coincide with extrema, saddle-points *etc.* We have drawn a collection of possible local structures in the inset below, where '+' and '-' symbolize $s(\vec{r}) > 0$ and $s(\vec{r}) < 0$, respectively, and the lines are the zero crossings.



We consider first local extrema, cases a - c. There $dS/dV = \sqrt{s_x^2 + s_y^2 + s_z^2} \delta(s)$ so that for vanishing gradient $dS/dV = 0$. Hence there is no surface area assigned to such cases, and we can immediately exclude the possibility of configurations a - c. While zero gradients are still possible on lines and points, they do not enter relevant calculations. Seams of the type d can also be excluded because the regions labeled by the question marks do not allow unambiguous assignment of positive or negative field values. The saddle-point cases e and f are more interesting. For general random fields they cannot be excluded. However, in our case of

a Fourier expandable, bandlimited ($k \leq k_c, k_c$ finite) Gaussian random process we know that the field is infinitely often continuously differentiable at any point in space. Therefore discontinuities of the normal derivatives along any intersection of a plane and the nodal surface should not exist. This is not the case at the intersection points in e and therefore configurations of type e are not allowed. However, continuity conditions are fulfilled in f. It represents the case of two membranes which 'kiss' at one point. This is the only allowed type of intersection in our model.

The problem of the order of zero crossings has been to some extent addressed in the literature on random fields [101, 36] in the context of general random processes. It is stated there that zero crossings which are simultaneously saddle-points or extrema can in practice be neglected. However, we are not aware of a rigorous proof for the complete absence of these phenomena in general random fields.

Representation and Visualization of Gaussian Fields As we have seen, statistical averages involving the random process $s(\vec{r})$ and/or its derivatives are given by a correlation matrix whose matrix elements always have similar form, for example, for $\langle s(\vec{r}) s(\vec{r}') \rangle_0$

$$\left\langle \sum_{\vec{k}} s(\vec{k}) e^{i\vec{k}\vec{r}} \sum_{\vec{k}'} s(\vec{k}') e^{i\vec{k}'\vec{r}'} \right\rangle_0 = \sum_{\vec{k}, \vec{k}'} \langle s(\vec{k}) s(\vec{k}') \rangle_0 e^{i\vec{k}\vec{r} + i\vec{k}'\vec{r}'}$$

Due to the absence of mode correlations this can be simplified in the standard way

$$\sum_{\vec{k}, \vec{k}'} \langle s(\vec{k}) s(\vec{k}') \rangle_0 e^{i\vec{k}\vec{r} + i\vec{k}'\vec{r}'} = \sum_{\vec{k}} \langle s(\vec{k}) s(-\vec{k}) \rangle_0 e^{i\vec{k}(\vec{r} - \vec{r}')} = V \sum_{\vec{k}} \nu(\vec{k}) e^{i\vec{k}(\vec{r} - \vec{r}')}$$

Teubner [37], on the other hand, has shown that the last expression is just the result for the calculation of $\langle s(\vec{r}) s(\vec{r}') \rangle_0$ with the alternative representation

$$s(\vec{r}) = \sqrt{\frac{2}{N}} \sum_{\vec{k}}^N \cos(\vec{k}_i \vec{r} + \phi_i) \quad (3.A9)$$

where now the \vec{k} vectors are by definition random variables distributed according to the spectral density $\nu(\vec{k})$. Because (zero mean) Gaussian processes are completely determined by their two-point correlation function the representations eqn. (1.13) and eqn. (3.A9) are equivalent. The same holds for the derivatives of $s(\vec{r})$. We have also verified this independently, numerically by calculating surface integrals on samples generated by eqns. (1.13, 3.A9) (*cf.* Chapter 5). While eqn. (1.13) is probably physically somewhat more insightful and preferable for analytic purposes, eqn. (3.A9) can be used in visualization and simulation because it requires a lower number of waves N to achieve 'good statistics' ($N = 100$ is sufficient for most visualization purposes). A simple subdivision of the area enclosed by $k^2 \nu(\vec{k})$ into equal parts results in a faithful representation of the statistical weights. In eqn. (1.13), however, one has to choose a sufficient number of vectors \vec{k} and then distribute sufficiently many $s(k)$ according to the Gaussian eqn. (1.14). This requires usually a value of N which is orders of magnitudes higher than that needed for eqn. (3.A9).

Film Scattering For approximation (b) the correlation matrix reads

	$s(0)$	$s(r)$	$s_z(0)$	$s_z(r)$	$s_y(0)$	$s_y(r)$	$s_x(0)$	$s_x(r)$
$s(0)$	$\langle 1 \rangle$	$g(r)$	0	$g_1(r)$	0	0	0	0
$s(r)$	$g(r)$	$\langle 1 \rangle$	$-g_1(r)$	0	0	0	0	0
$s_z(0)$	0	$-g_1(r)$	σ_r	$g_2(r)$	0	0	0	0
$s_z(r)$	$g_1(r)$	0	$g_2(r)$	σ_r	0	0	0	0
$s_y(0)$	0	0	0	0	σ_r	$g_3(r)$	0	0
$s_y(r)$	0	0	0	0	$g_3(r)$	σ_r	0	0
$s_x(0)$	0	0	0	0	0	0	σ_r	$g_3(r)$
$s_x(r)$	0	0	0	0	0	0	$g_3(r)$	σ_r

with $\sigma_r = \langle k^2 \rangle / 3$ and $\langle 1 \rangle = 1$. Note that evaluation of $\Gamma(r)$ with finite k_c is in general necessary because, unlike in method (a), the matrix elements involving gradient terms lead in the limit of $r \rightarrow 0$ to higher order moments *e.g.* $\langle k^2 \rangle$ which *diverge* for infinite k_c . This was not a problem in method (a) where the error associated with infinite k_c is small.

We can proceed making use of the isotropy of the system: in evaluating the matrix elements we chose $\vec{r} - \vec{r}'$ along the z - direction; as the system is isotropic, $\Gamma(r)$ is not affected by this choice.

The individual matrix elements can be derived in the usual way. For example,

$$\begin{aligned} g(\vec{r} - \vec{r}') &= \langle s(\vec{r})s(\vec{r}') \rangle_0 = \left\langle \sum_{\vec{k}\vec{k}'} s(\vec{k})s(\vec{k}') e^{i\vec{k}\vec{r}} e^{i\vec{k}'\vec{r}'} \right\rangle_0 \\ &= \sum_{\vec{k}} \langle s(\vec{k})s(-\vec{k}) \rangle_0 e^{i\vec{k}(\vec{r}-\vec{r}')} \\ &\rightarrow [2\pi]^{-3} \int_{-\infty}^{\infty} \int_{-\infty}^{\infty} \int_{-\infty}^{\infty} d\vec{k} \nu(\vec{k}) \end{aligned}$$

where we could chose $\vec{r}' = 0$ due to translational invariance. With $\vec{r} = (0, 0, r)$ we can continue

$$\begin{aligned} g(r) &= [2\pi]^{-3} \int_{-\infty}^{\infty} \int_{-\infty}^{\infty} \int_{-\infty}^{\infty} d\vec{k} \nu(k) e^{ik_z r} \\ &= [2\pi]^{-2} \int_0^{\infty} \int_{-1}^1 dk dt k^2 \nu(k) e^{ikrt} \\ &= [2\pi^2]^{-1} \int_0^{\infty} dk k^2 \nu(k) \frac{\sin kr}{kr} \\ &\approx e^{-r\xi^{-1}} \frac{\sin k_0 r}{k_0 r} \end{aligned}$$

And also

$$\begin{aligned} g_1(r) &= \langle s_z(\vec{r})s(\vec{r}') \rangle_0 = -\langle s(\vec{r})s_{z'}(\vec{r}') \rangle_0 \\ &= \sum_{\vec{k}} \langle s(\vec{k})s(-\vec{k}) \rangle_0 i k_z e^{i\vec{k}(\vec{r}-\vec{r}')} \\ &= [2\pi]^{-2} \int_0^{\infty} \int_{-1}^1 dk dt i k t k^2 \nu(k) e^{ikrt} \\ &= \frac{\partial}{\partial r} \int_0^{\infty} \int_{-1}^1 dk dt k^2 \nu(k) e^{ikrt} \\ &= \frac{\partial}{\partial r} g(r) \\ &\approx e^{-r\xi^{-1}} (k_0 r)^{-1} [k_0 \cos k_0 r - r^{-1} \sin k_0 r - \xi^{-1} \sin k_0 r] \end{aligned}$$

Similarly,

$$\begin{aligned} g_2(r) &= \langle s_z(\vec{r})s_{z'}(\vec{r}') \rangle_0 = -\frac{\partial^2}{\partial r^2}g(r) \\ &\approx e^{-r\xi^{-1}}(k_0r)^{-1}[-2r^{-2}\sin k_0r - 2\xi^{-1}r^{-1}\sin k_0r + 2k_0r^{-1}\cos k_0r \\ &\quad -\xi^{-2}\sin k_0r + 2k_0\xi^{-1}\cos k_0r + k_0^2\sin k_0r] \end{aligned}$$

Finally [102],

$$\begin{aligned} g_3(r) &= \langle s_x(\vec{r})s_{x'}(\vec{r}') \rangle_0 = \langle s_y(\vec{r})s_{y'}(\vec{r}') \rangle_0 \\ &= \sum_{\vec{k}} \langle s(\vec{k})s(-\vec{k}) \rangle_0 i^2 k_x(-k_x) e^{i\vec{k}(\vec{r}-\vec{r}')} \\ &= 2^{-1}[2\pi]^{-2} \int_0^\infty \int_{-1}^1 dk dt k^4(1-t^2)\nu(k)e^{ikrt} \\ &= 2^{-1}\frac{\partial^2}{\partial r^2}g(r) + 2^{-1}[2\pi]^{-2} \int_0^\infty \int_{-1}^1 dk dt k^4\nu(k)e^{ikrt} \\ &= e^{-r\xi^{-1}}(k_0r)^{-1} [r^{-2}\sin k_0r + \xi^{-1}r^{-1}\sin k_0r - k_0r^{-1}\cos k_0r] \\ &= -r^{-1}\frac{\partial}{\partial r}g(r) \end{aligned}$$

which has, unlike the other matrix elements, no first order contribution in r^{-1} .

Because we only use the above expressions to make statements for the limit $k \rightarrow 0$ *i.e.* $r \rightarrow \infty$ we have indeed used the form of $g(r)$ derived from the approximate Fourier transform with infinite k_c . With these matrix elements we can expand the integrand in eqn. (3.39) in powers of g , g_1 , g_2 , g_3 . Each integral contains then a diagonal matrix and the integration can be performed. We can define

$$F(O) = [2\pi]^{-4}|A(\infty)|^{-\frac{1}{2}} \int_{-\infty}^\infty \dots \int_{-\infty}^\infty d\vec{s}_0 d\vec{s}_r O \sqrt{\vec{s}_0^2} \sqrt{\vec{s}_r^2} \exp \left[-\frac{1}{2} \vec{\lambda} A^{-\frac{1}{2}}(\infty) \vec{\lambda}^T \right]$$

The integral of the zeroth order term is simply the normalization $(S/V)^2$ ($g = g_1 = g_2 = g_3 = 0$). The integral associated with the linear terms is taken over the operator

$$O = \sigma_r^{-2} \left[\alpha^2 \sigma_r^2 g - \alpha \sigma_r s_{zr} g_1 + \alpha \sigma_r s_{z0} g_1 + s_{zr} s_{z0} g_2 \right]$$

All odd integrals *i.e.* integrals over odd contributions such as s_{zr} , s_{z0} , $s_{zr}s_{z0}$ vanish, so that essentially

$$O \sim \alpha^2 g$$

The integral G_2 is a more complicated. Again, after elimination of all odd components we are left with (for $\alpha = 0$)

$$O \sim g_2^2 + 2\sigma_r g_1^2 + \sigma_r^2 g^2 + \sigma_r^{-2} s_{z0}^2 s_{zr}^2 g_2^2 - 2\sigma_r^{-1} s_{zr}^2 g_2^2 - 2s_{zr}^2 g_1^2$$

Using spherical coordinates these integrals can be reduced to simple one-dimensional Gaussian integrals. After further simplification we arrive at the equation for G_2 , eqn. (3.41).

Sponge - Lamellar Instability

Having determined the structure corresponding to the minimum of phase (3.42) we return to the stability analysis of the sponge phase. We will use the stability analysis in the next section to determine the stability of the sponge phase against other phases.

Experimentally, it has been established that the appearance of both hexagonal and orthorhombic sponge phases is accompanied by a nearly lamellar phase (cf. [11, 12] and [15, 17]) where the observed transition from sponge to lamellar can be explained by increasing the surfactant concentration along length or decreasing surfactant amount which is the wavelength of the bending energy mode. One can be quite confident in assuming that the fundamental parameters χ and κ of the system are not significantly affected by the presence of a second phase. It is therefore a natural requirement for any model of amphiphilic phase to assume a consistent formulation of the sponge - lamellar transition.

4.1 Introduction

The classical literature on the sponge - lamellar transition is sparse. It begins mainly around the work of Brinkmann [10]. Parts of [11, 12] and a more general lecture note [13, 14].

While Brinkmann and Hildebrand [11] derive field phase diagrams which depend strongly on experimental data on which they comment with confidence in principle, the corresponding lecture notes [13, 14] offer a phase diagram for equilibrium and its phase which qualitatively resembles observed data. However, the phase diagram

Using spherical coordinates these integrals can be reduced to single integrals over the angle θ and the radial coordinate r .

$$\int_{\mathbb{R}^3} \frac{1}{|\mathbf{r}|} \delta(\mathbf{r} - \mathbf{r}') d\mathbf{r} = \int_0^\infty \int_0^\pi \int_0^{2\pi} \frac{1}{r} \delta(r - r') \delta(\theta - \theta') \delta(\phi - \phi') r^2 \sin\theta dr d\theta d\phi$$

Figure 1.10

$$\begin{aligned} &= \int_0^\infty \int_0^\pi \int_0^{2\pi} \frac{1}{r} \delta(r - r') \delta(\theta - \theta') \delta(\phi - \phi') r^2 \sin\theta dr d\theta d\phi \\ &= \int_0^\infty \int_0^\pi \int_0^{2\pi} \frac{1}{r} \delta(r - r') \delta(\theta - \theta') \delta(\phi - \phi') r^2 \sin\theta dr d\theta d\phi \\ &= \int_0^\infty \int_0^\pi \int_0^{2\pi} \frac{1}{r} \delta(r - r') \delta(\theta - \theta') \delta(\phi - \phi') r^2 \sin\theta dr d\theta d\phi \\ &= \int_0^\infty \int_0^\pi \int_0^{2\pi} \frac{1}{r} \delta(r - r') \delta(\theta - \theta') \delta(\phi - \phi') r^2 \sin\theta dr d\theta d\phi \end{aligned}$$

where \mathbf{r} and \mathbf{r}' are the position vectors of the points \mathbf{r} and \mathbf{r}' respectively.

Because of the delta functions in the integrand, the only contribution to the integral comes from the point $\mathbf{r} = \mathbf{r}'$. The integral over the angles θ and ϕ is therefore trivial and the integral over r is also trivial, giving the result $4\pi r^2$.

$$\int_{\mathbb{R}^3} \frac{1}{|\mathbf{r}|} \delta(\mathbf{r} - \mathbf{r}') d\mathbf{r} = 4\pi r^2$$

The integral of the inverse square of the distance from the origin over the entire space is also divergent. The integral associated with the inverse square of the distance is

$$G(\mathbf{r}) = \int_{\mathbb{R}^3} \frac{1}{|\mathbf{r} - \mathbf{r}'|} d\mathbf{r}'$$

All the integrals in this section are divergent, but we can still define them in a regularized way.

The integral $G(\mathbf{r})$ is very singular. As a result, the integrals of all odd components are left with (for $n > 0$)

$$\int_{\mathbb{R}^3} \frac{r_i}{|\mathbf{r} - \mathbf{r}'|} d\mathbf{r}' = 0$$

Sponge - Lamellar Instability

Having discussed the isotropic sponge and microemulsion phases and their entropic instability towards dilute phases, we will now turn our attention to the energy driven instability of the sponge towards ordered phases.

Experimentally, it is a well-established fact that the appearance of both binary and ternary sponge phases is intimately related to nearby lamellar phases (*cf.* fig. (1-1) and [85, 22]) where the observed transition from sponge to lamellae can be triggered by increasing surfactant concentration, chain length or decreasing alcohol content which – in the language of the bending energy model – can be again interpreted as variations in the fundamental parameters ϕ_s , κ and $\bar{\kappa}$. It is therefore a natural requirement for any model of amphiphilic phases to attempt a consistent formulation of the sponge - lamellar transition.

4.1 Introduction

The theoretical literature on the sponge - lamellar transition is sparse. It evolves mainly around the work of Brazovskii [103], Porte *et al.* [22] and coarse grained lattice models [31, 89].

While microscopic and standard GL theories yield phase diagrams which do not compare well to experimental data or which defy comparison with experiment in principle, the coarse-grained lattice model [31] yielded a phase diagram for microemulsions and L_3 phases which qualitatively resembled measured ones. However, the free energy density

of the lamellar phase considered there was heuristically taken as Helfrich's free energy of steric repulsion which is not consistent with the description of the free energy density of the coarse-grained sponge phase¹. The more self-consistent extension of the coarse grained lattice model by Golubović & Lubensky remedied this inconsistency, but on the expense of an extended parameter space for which comparison to observation is not possible [32]. Porte *et al.*'s work [22] is semi-quantitative and although it leads to very useful insights into the role of the saddle-splay curvature which compare well to experiment (*cf.* below and the following chapter) it would not suffice for our present problem.

Finally, some recent attention has been given to the Brazovskii model, which was applied by Cates [104] and by Morse & Milner to surfactant phases [105]. However, we have to note again that neither of these approaches can lead to a quantitative treatment.

In general the body of theoretical work on the stability of the sponge towards lamellar phases is currently not considered satisfactory; an up to date account of experimental facts and the (mostly open) theoretical problems they pose has been given by Strey [4] who lists the relative stability of the sponge and lamellar phase, the typical shape of the lamellar region (as in fig. (1-1)), and the vanishing of the one phase microemulsion region upon change in surfactant chain length as outstanding problems. Furthermore, both experimentalists and theorists have pointed out numerous times that no current approach can do justice to the fact that topological changes are a crucial factor for the S/L transition so that the Gaussian curvature term should by no means be dropped in an approach to the S/L transition [106, 107, 27, 22, 108]. This is for example demonstrated by the experiments of Porte *et al.* who varied systematically the saddle-splay modulus with the result that sponge phases are only stable for a special, narrow range of saddle-splay moduli (*cf.* also next chapter). Another startling point is the stability of L_3 phases towards L_α up to relatively high surfactant concentration $\phi_s \approx 30\%$ [85] which has also been related to the stabilizing effect of saddle-splay curvature [106, 79].

In this chapter we will discuss the stability of the sponge phase towards the lamellar phase consistently within the frame of the random interface model. Detailed attention will be given to the role of Gaussian elasticity and surfactant concentration.

¹In our discussion this would be equivalent to using the results of Chapters 2 and 3 to study the relative stability of sponges and lamellae.

4.2 Nematic Lamellar Phase

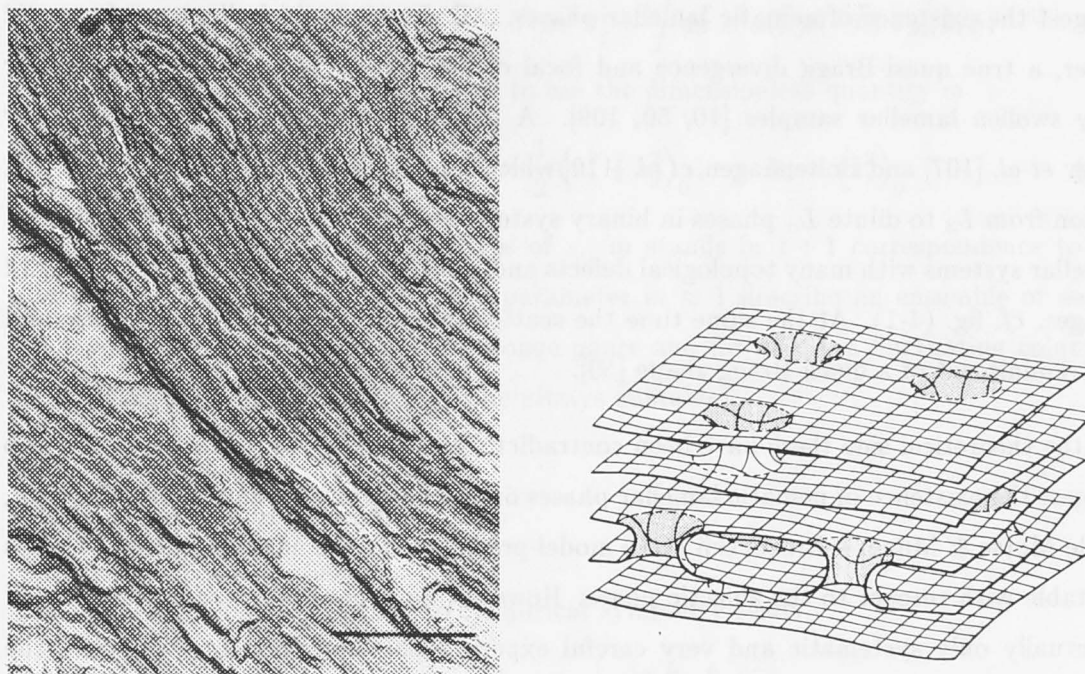


Figure 4-1: (left) *FFEM image from a dilute lamellar phase with many saddle defects.* (right) *Schematic picture of such a state (from [107]).*

In Chapter 1 we briefly mentioned the model by Huse & Leibler who postulated two different lamellar phases of nematic and smectic type. A very simple model of smectic phases was discussed in Chapter 2. Smectic lamellar phases show long range orientational and quasi long range positional order, while nematic phases are characterized by long range orientational order but only short range positional order. The ground state of nematic phases is highly degenerate and can be imagined as an ensemble of freely moving flat layers so that an infinite number of zero temperature configurations is possible (paramagnet with molecular lattice constant in one dimension). For all these configurations the bending energy is zero. The smectic phase in contrast has a unique periodic ground state. The bending Hamiltonian eqn. (1.2) alone does not justify such a unique ground state. If we operate purely on the basis of eqns. (1.2,1.3) we would expect on entropic grounds only the nematic lamellar phase to exist. In reality, small perturbations possibly caused by direct interactions appear to be sufficient to override the entropy gain, lift the nematic ground state degeneracy and cause smectic order, at least in rather concentrated samples [47].

For dilute systems – where we would naturally assume that direct interactions should be negligible – the situation is more ambiguous and there are some indications which suggest the existence of nematic lamellar phases. All experimental indicators of smectic order, a true quasi-Bragg divergence and focal conics texture cannot be confirmed for very swollen lamellar samples [10, 50, 109]. A detailed experimental investigation by Strey *et al.* [107] and Boltenhagen *et al.* [110] which focussed specifically on the transition region from L_3 to dilute L_α phases in binary systems suggests the existence of disordered lamellar systems with many topological defects and short-range positional order on FFEM images, *cf.* fig. (4-1). At the same time the scattering from these systems is diffuse and not reminiscent of a quasi-Bragg shape [50].

On the theoretical side there have been contradictory statements by Huse & Leibler who suggest the existence of nematic lamellar phases on the basis of the bending Hamiltonian, while Morse & Milner's Brazovskii (GL) model predicts that the nematic phase is always unstable with respect to the smectic phase. However, both models are rather crude and eventually only systematic and very careful experimental measurements will yield the final answer to the question of the existence of the nematic lamellar phase. In any way, investigation of its relative stability towards the sponge phase – which can be performed consistently within the random interface model – should shed some light on this hardly understood transition. It will certainly provide a reliable *upper limit* for the stability of the sponge phase. Although the sponge - nematic transition can possibly be pre-empted by a sponge - smectic transition the sponge phase can under no circumstances exist beyond the limits predicted by the sponge - nematic instability.

If we want to extend the random interface formalism towards anisotropic phases with cylindrical symmetry we have to break the rotational invariance of the isotropic distribution $p[s(k)] \sim \exp\left[-\frac{|s(k)|^2}{2\nu(k)}\right]$, where $s(k)$ is the Fourier transform of the random field $s(r)$. In a nematic lamellar phase the symmetry breaking can be expressed by

$$m_{ij} = \left\langle s_i s_j - \frac{1}{3} \delta_{ij} (\vec{\nabla} s)^2 \right\rangle_0 \quad (4.1)$$

analogous to the (uniaxial²) nematic order parameter introduced by Maier & Saupe [112, 46, 96, 105]. If we – without loss of generality – do the usual simplification to align the z - axis of the coordinate system with the direction of lamellar ordering [96, 105], m_{ij} is diagonal and a more convenient, scalar quantity can be used as the order parameter. For

²Biaxial nematics could exist [111] but are rather exotic and not considered here.

example, in Maier - Saupe's original treatment $Q = \langle s_z^2 \rangle - \frac{1}{2} \langle s_x^2 + s_y^2 \rangle$ was used, *cf.* also [105]

$$\sigma_z - \sigma_\rho \sim \int d\vec{k} k^2 \nu(\vec{k}) [1 - 3 \cos^2 \theta] \sim \int d\vec{k} k^2 s(\vec{k}) s(-\vec{k}) Y_{20}(\theta, \phi)$$

For our purposes it is most convenient to use the dimensionless quantity m

$$m = 1 - \frac{\sigma_\rho}{\sigma_z}, \quad \sigma_\rho = \frac{1}{2} \langle s_x^2 + s_y^2 \rangle_0, \quad \sigma_z = \langle s_z^2 \rangle_0 \quad (4.2)$$

where the s_i are again first derivatives of s . m stands in 1 : 1 correspondence to the above definition. Values of the order parameter $m \approx 1$ describe an ensemble of nearly flat layers, for $m = 0$ we regain the sponge phase and for $m < 0$ a fluctuating columnar phase is described (which we find to be always unstable).

4.2.1 Statistical Averages

The mode distribution assigned to cylindrical symmetry reads

$$p[s(k_\rho, k_z)] \sim \exp \left[-\frac{|s(k_\rho, k_z)|^2}{2\nu(k_\rho, k_z)} \right] \quad (4.3)$$

With this symmetry we can define the correlation matrix and perform the Gaussian integrals to find the surface averages (*cf.* Appendix):

Mean Square Curvature

$$\left\langle \delta(s - \alpha) \sqrt{(\vec{\nabla}s)^2 H^2} \right\rangle_0 = H_1(\sigma_\rho, \sigma_z) \langle k_\rho^4 \rangle + H_2(\sigma_\rho, \sigma_z) \langle k_\rho^2 k_z^2 \rangle + H_3(\sigma_\rho, \sigma_z) \langle k_z^4 \rangle + H_4(\sigma_\rho, \sigma_z) \quad (4.4)$$

with

$$H_1(\sigma_\rho, \sigma_z) = \frac{1}{4\pi\sqrt{\sigma_z}} e^{-\frac{\alpha^2}{2}} m^{-2} \left[-\frac{3}{8} - \frac{3}{8}m + \left(\frac{3}{8} + \frac{1}{4}m + \frac{3}{8}m^2 \right) m^{-\frac{1}{2}} \operatorname{arctanh}(m^{\frac{1}{2}}) \right]$$

$$H_2(\sigma_\rho, \sigma_z) = \frac{1}{4\pi\sqrt{\sigma_z}} e^{-\frac{\alpha^2}{2}} m^{-2} \left[3 - m + (-3 + 2m + m^2) m^{-\frac{1}{2}} \operatorname{arctanh}(m^{\frac{1}{2}}) \right]$$

$$H_3(\sigma_\rho, \sigma_z) = \frac{1}{4\pi\sqrt{\sigma_z}} e^{-\frac{\alpha^2}{2}} m^{-2} \left[-1 + \frac{5}{3}m + (1 - m)^2 m^{-\frac{1}{2}} \operatorname{arctanh}(m^{\frac{1}{2}}) \right]$$

$$H_4(\sigma_\rho, \sigma_z) = \frac{\sigma_z^{\frac{3}{2}}}{12\pi} e^{-\frac{\alpha^2}{2}} (\alpha^2 - 1) m^{-2} \left[9m^2 - 7m^3 + 3m^2 (1 - m)^2 m^{-\frac{1}{2}} \operatorname{arctanh}(m^{\frac{1}{2}}) \right]$$

where we have used the definition

$$\langle k_\rho^n k_z^m \rangle = (4\pi^2)^{-1} \int \int dk_\rho dk_z k_\rho^{n+1} k_z^m \nu(k_\rho, k_z) \quad (4.5)$$

for the moments of the structure factor. For $m \rightarrow 0$ eqn. (4.4) converges towards its isotropic form $(S/V)_{isotropic} [1/6(\alpha^2 - 1) \langle k^2 \rangle + 1/5 \langle k^4 \rangle / \langle k^2 \rangle]$ (cf. Chapter 3 and [37]) as it should, with

$$\sigma_z = \frac{1}{2}\sigma_\rho \rightarrow \frac{1}{3}\langle k^2 \rangle, \quad \langle k_\rho^4 \rangle \rightarrow \frac{8}{15}\langle k^4 \rangle, \quad \langle k_\rho^2 k_z^2 \rangle \rightarrow \frac{2}{15}\langle k^4 \rangle, \quad \langle k_z^4 \rangle \rightarrow \frac{1}{5}\langle k^4 \rangle$$

Saddle-Splay Curvature

$$\left\langle \delta(s - \alpha) \sqrt{(\vec{\nabla}s)^2} K \right\rangle_0 = e^{-\frac{\alpha^2}{2}} (\alpha^2 - 1) \frac{1}{\pi} \sigma_z^{\frac{3}{2}} (1 - m) \quad (4.6)$$

where the isotropic limit can be taken without problem. On the other hand, in the absence of in-plane fluctuations, $\sigma_\rho \rightarrow 0$, we see that $\langle \delta(s - \alpha) \sqrt{(\vec{\nabla}s)^2} K \rangle_0 \rightarrow 0$ corresponding to flat interfaces without connections.

Surface to Volume Ratio

$$S/V = \left\langle \delta(s - \alpha) \sqrt{(\vec{\nabla}s)^2} \right\rangle_0 = e^{-\frac{\alpha^2}{2}} \frac{\sqrt{\sigma_z}}{\pi} \left[1 + (1 - m) m^{-\frac{1}{2}} \operatorname{arctanh}(m^{\frac{1}{2}}) \right] \quad (4.7)$$

which goes to $\rightarrow (S/V)_{isotropic}$ for $m \rightarrow 0$ (cf. Chapter 3 and also [37]).

4.2.2 Structure Factor

The free energy density is here of the same functional form as eqn. (3.9) but with expressions eqn. (4.4) - eqn. (4.7) for the surface averages

$$f[\nu(k_\rho, k_z)] = 2\kappa \left[H_1 \langle k_\rho^4 \rangle + H_2 \langle k_\rho^2 k_z^2 \rangle + H_3 \langle k_z^4 \rangle + H_4 \right] + \bar{\kappa} \left\langle \delta(s - \alpha) \sqrt{(\vec{\nabla}s)^2} K \right\rangle_0 - \frac{1}{8\pi^2} \int \int dk_\rho dk_z k_\rho \log \nu(k_\rho, k_z) \quad (4.8)$$

Completely analogous to Chapters 2 and 3 we can functionally minimize $\partial f[\nu]/\partial \nu = 0$ to gain the optimal structure factor which reads

$$\nu(k_\rho, k_z) = \left[ak_\rho^4 + bk_\rho^2 k_z^2 + ck_z^4 - dk_\rho^2 - ek_z^2 + g \right]^{-1} \quad (4.9)$$

The coefficients a, \dots, g have to be determined by minimization. In the case of a, b, c this can be done immediately due to the simple form of eqn. (4.8)

$$a = 4\kappa H_1, \quad b = 4\kappa H_2, \quad c = 4\kappa H_3 \quad (4.10)$$

while the remaining coefficients can be determined by the two constraints $\langle 1 \rangle = 1$, $\phi_s = \text{const}$ and the definition of the order parameter $m = 1 - \sigma_\rho / \sigma_z$

$$(4\pi^2)^{-1} \int \int dk_\rho dk_z k_\rho \nu(k_\rho, k_z) = 1 \quad (4.11)$$

$$(4\pi^2)^{-1} \int \int dk_\rho dk_z k_\rho^3 \nu(k_\rho, k_z) = 2(1-m)\pi^2 e^{\alpha^2} \phi_s^2 \left[1 + (1-m)m^{-\frac{1}{2}} \text{arctanh}(m^{\frac{1}{2}}) \right]^{-2}$$

$$(4\pi^2)^{-1} \int \int dk_\rho dk_z k_\rho k_z^2 \nu(k_\rho, k_z) = \pi^2 e^{\alpha^2} \phi_s^2 \left[1 + (1-m)m^{-\frac{1}{2}} \text{arctanh}(m^{\frac{1}{2}}) \right]^{-2}$$

The equation system eqn. (4.11) can be solved numerically or approximately for small values m in the spirit of a Landau expansion.

To solve eqn. (4.11) perturbatively in m we expand all relevant quantities up to fourth order

$$x \approx x_0 + x_1 m + x_2 m^2 + x_3 m^3 + x_4 m^4 \quad (4.12)$$

with $x = a, b, c, d, e, g, \sigma_\rho, \sigma_z, \nu$ and where the index $_0$ refers to the sponge state, $m = 0$.

Some of the series are readily given:

$$\sigma_\rho \approx e^{\alpha^2} \pi^2 \phi_s^2 \left[\frac{1}{2} - \frac{1}{6} m - \frac{1}{10} m^2 - \frac{121}{1890} m^3 - \frac{608}{14175} m^4 \right] \quad (4.13)$$

$$\sigma_z \approx e^{\alpha^2} \pi^2 \phi_s^2 \left[\frac{1}{4} + \frac{1}{6} m + \frac{7}{60} m^2 + \frac{16}{189} m^3 + \frac{128}{2025} m^4 \right] \quad (4.14)$$

$$a \approx e^{-\alpha^2} \frac{4\kappa}{\pi^2 \phi_s} \left[\frac{4}{15} + \frac{8}{315} m + \frac{32}{1575} m^2 + \frac{296}{17325} m^3 + \frac{70012}{4729725} m^4 \right] \quad (4.15)$$

$$b \approx e^{-\alpha^2} \frac{4\kappa}{\pi^2 \phi_s} \left[\frac{8}{15} - \frac{8}{315} m - \frac{16}{1575} m^2 - \frac{16}{3465} m^3 - \frac{10456}{4729725} m^4 \right] \quad (4.16)$$

$$c \approx e^{-\alpha^2} \frac{4\kappa}{\pi^2 \phi_s} \left[\frac{4}{15} - \frac{16}{315} m - \frac{4}{225} m^2 - \frac{64}{7425} m^3 - \frac{23572}{4729725} m^4 \right] \quad (4.17)$$

To calculate the remaining coefficients and the structure factor we can write

$$\nu_i = w_i - n_0^{-2} n_i \quad (4.18)$$

with the recursion sequence

$$w_1 = 0$$

$$w_2 = n_0^{-3} n_1^2$$

$$w_3 = n_0^{-4} \left[-n_1^3 + 2n_0 n_1 n_2 \right]$$

$$w_4 = n_0^{-5} \left[n_1^4 - 3n_0 n_1^2 n_2 + n_0^2 n_2^2 + 2n_0^2 n_1 n_3 \right]$$

where

$$n_i = a_i k_\rho^4 + b_i k_\rho^2 k_z^2 + c_i k_z^4 - d_i k_\rho^2 - e_i k_z^2 + g_i$$

The particularly simple form of the coefficients of the structure factor can be fully exploited by performing the integrations on the lhs of eqn. (4.11) in spherical coordinates with according integration limits in cylindrical coordinates $\int_0^{\sqrt{kc^2-kz^2}} \int_{-k_c}^{k_c} \dots dk_z dk_\rho$. Eqn. (4.18) also shows that the 3×3 equation systems which determine the successive sets of coefficients $d_1, e_1, g_1, \dots, d_4, e_4, g_4$, are inhomogeneous linear equation systems. The calculation of the coefficients is therefore reduced to the evaluation of (solvable) radial integrals and linear equation systems

$$\begin{pmatrix} -\frac{2}{3}V_{24} & -\frac{1}{3}V_{24} & V_{22} \\ -\frac{8}{15}V_{26} & -\frac{2}{15}V_{26} & \frac{2}{3}V_{24} \\ -\frac{2}{15}V_{26} & -\frac{1}{5}V_{26} & \frac{1}{3}V_{24} \end{pmatrix} \begin{pmatrix} d_i \\ e_i \\ g_i \end{pmatrix} = \begin{pmatrix} L_{i1} \\ L_{i2} \\ L_{i3} \end{pmatrix} \quad (4.19)$$

where

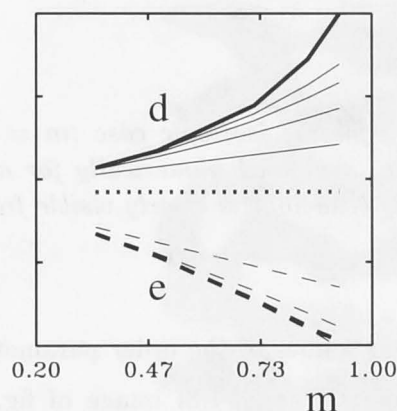
$$\begin{aligned} V_{mn} &= (2\pi^2)^{-1} \int_0^{k_c} dk n_0^{-m} k^n \\ L_{i1} &= W_i - \lambda_{i1} \\ L_{i2} &= -2\sigma_{\rho i} + W_i - \lambda_{i2} \\ L_{i3} &= -\sigma_{zi} + W_i - \lambda_{i3} \\ W_i &= (2\pi^2)^{-1} \int \int dk_\rho dk_z k_\rho w_i \\ \lambda_{i1} &= \frac{V_{26}}{15} [8a_i + 2b_i + 3c_i] \\ \lambda_{i2} &= \frac{V_{28}}{105} [48a_i + 8b_i + 6c_i] \\ \lambda_{i3} &= \frac{V_{28}}{105} [8a_i + 6b_i + 15c_i] \end{aligned}$$

Finally, the expansion coefficients d_i, e_i, g_i are

$$\begin{aligned} d_i &= 4^{-1} V^{-1} V_{26}^{-1} [4L_{i1} V_{24} V_{26} + L_{i2} (5V_{24}^2 - 9V_{22} V_{26}) + L_{i3} (6V_{22} V_{26} - 10V_{24}^2)] \\ e_i &= -2^{-1} V^{-1} V_{26}^{-1} [-2L_{i1} V_{24} V_{26} + L_{i2} (5V_{24}^2 - 3V_{22} V_{26}) + L_{i3} (12V_{22} V_{26} - 10V_{24}^2)] \\ g_i &= V^{-1} [L_{i1} V_{26} - L_{i2} V_{24} - L_{i3} V_{24}] \end{aligned}$$

for $i = 1, \dots, 4$ and with $V = -V_{24}^2 + V_{22} V_{26}$. Together with eqn. (4.15) - eqn. (4.17) for the a_i, b_i, c_i we have thus determined the coefficients of the structure factor up to fourth order in m where the expansion coefficients are given as one-dimensional, radial integrals. These integrals are exactly solvable. To check the perturbation results we can compare with exact, independently calculated, numerical solutions (to all orders in m) of

the equation system eqn. (4.11). The inset shows a comparison of the relevant structure factor coefficients d and e in the approximate and exact calculations (the expansions for a, b, c are trivial and g which is related to the mean-spherical constraint shows only very small change) for $\kappa = 5, \phi_s = 0.1$. The thick lines show results of the exact calculations and the thinner lines successive approximation to first, ..., fourth order. The dotted line is the isotropic result (zeroth order.) The agreement is satisfactory but deteriorates for increasing m . 'Exact' numerical solution (to all orders in m) of eqn. (4.11) vs the simpler perturbation theory is a choice in which neither option can fully satisfy. The former turns out to be a demanding computational task. Even with the simplification of taking constant integration limits - *i.e.* integrating over a cylindrical volume - when one of the integrations can be carried out analytically the remaining numerical integration suffers at large order parameter from an emerging very sharp peak in the structure factor which can flip into a divergence for small changes in the parameters. Only a sophisticated algorithm (Powell hybrid method) could be used to solve eqn. (4.11) and yet showed increasingly bad convergence properties for m approaching saturation, $m \rightarrow 1$; in fact we never succeeded in surpassing some $m \approx 0.95$. At the same time, the cylindrical integration limits slightly break the rotational symmetry in the sponge case (especially for the entropic part, *cf.* fig. (4-5)), $m = 0$, which in practice shifts the central minimum of the free energy density (fig. (4-5)) from $m = 0$ to small values of m . The perturbation expansion on the other hand retains the spherical integration region and is computationally far less complicated. However, it is well known that Landau expansion of the free energy density is strictly speaking invalid for cases of strongly first order transitions so that results gained from the perturbation analysis might then not be reliable. Nevertheless, for most of the remainder of this chapter it was a necessity to use perturbative results; these were checked for some selected cases by exact calculations with satisfactory success.



Before we proceed with phase transitions it is instructive to consider briefly examples of nematic lamellar structure. In fig. (4-2) we show angle averaged structure factors for the case $\kappa = 5, \phi_s = 0.1, \alpha = 0$ for order parameter values $m = 0$ and $m = 0.9$.

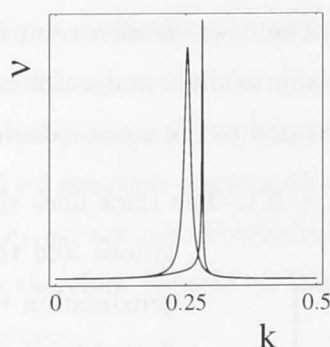


Figure 4-2: Angle averaged structure factors $\nu(k)$ for the isotropic case ($m = 0$, left curve) and a nematic state ($m = 0.9$, right curve) evaluated numerically for $\kappa = 5$, $\phi_s = 0.1$, $\alpha = 0$. The expected difference in swelling behaviour is clearly visible from the peak positions.

Corresponding real-space representations for different values of the order parameter are given in fig. (4-3). The image for $m = 0.9$ resembles the FFEM image of fig. (4-1) (particularly when looking at more detailed zooms of fig. (4-1)). Although uniaxial order is clearly discernible, there are still many topological defects, *cf.* fig. (4-4). These become progressively fewer for higher values of the order parameter $m \rightarrow 1$ when the structure factor approaches the form expected for lamellar order ($\sigma_\rho \rightarrow 0$)

$$\nu(k_\rho, k_z) = c \left[k_z^2 - \frac{1}{2c}(e - bk_\rho^2) \right]^2 - \frac{1}{4c}(e - bk_\rho^2)^2 + ak_\rho^4 - dk_\rho^2 + g$$

For small $k_z \rightarrow 0$ we find that for $e^2/(4c) - g \approx 0$ a delta function shape at $k_z^2 \approx e/(2c)$ emerges while at the same time due to $be/(2c) - d \approx 0$ the fluctuation in k_ρ - direction converges towards a delta function centered at $k_\rho \approx 0$.



Figure 4-3: Two dimensional cuts through real-space structures gained from structure factors for $\kappa = 5$, $\phi_s = 0.1$, $\alpha = 0$ for various values of m . The image for $m = 0$ was generated using cylindrical coordinates (unlike the spherical coordinates used for fig. (3-

4) in Chapter 3) to check the plotting algorithm. It is also worthwhile mentioning that the morphologies of structures with high m are similar to those observed in anisotropic carbonate rocks [113].

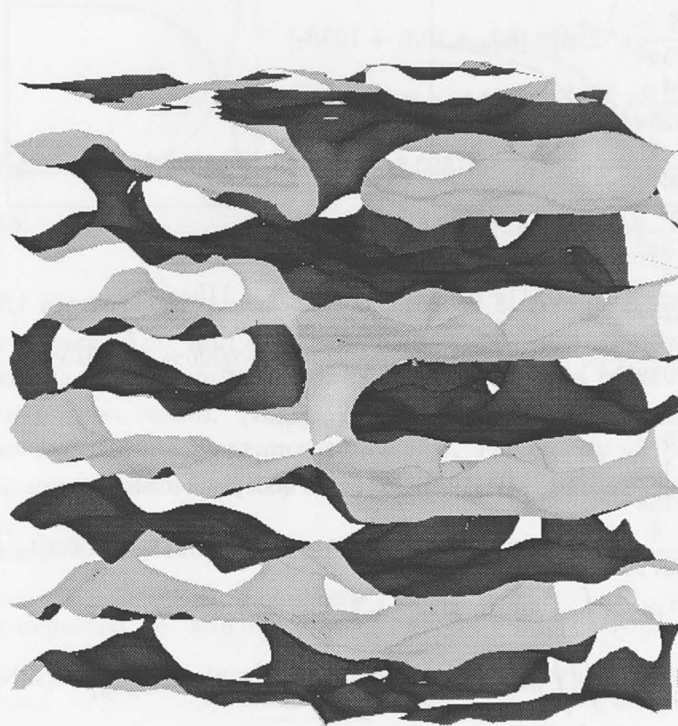


Figure 4-4: Three dimensional representation corresponding to the sample $m = 0.9$ in fig. (4-3). The sides of the interfaces in contact with either the in- or outside (water or oil) have different grey shades. Several defects can be seen.

4.3 Stability of the Sponge Phase

Having calculated the coefficients of the structure factor, we can insert into the free energy density eqn. (4.8) to find the Landau expansion up to fourth order

$$f \approx f_0 + f_2(\kappa, \bar{\kappa}, \alpha, \phi_s)m^2 + f_3(\kappa, \bar{\kappa}, \alpha, \phi_s)m^3 + f_4(\kappa, \bar{\kappa}, \alpha, \phi_s)m^4 \quad (4.20)$$

The linear term vanishes as usual³. For the other terms we find

$$\begin{aligned} f_2(\kappa, \bar{\kappa}, \alpha, \phi_s) &= -\frac{\pi^2}{60}\phi_s^3 e^{\alpha^2}(\alpha^2 - 1)\bar{\kappa} + 2\kappa[h_{12} + h_{22} + h_{32}] - \frac{1}{2}s_2 \\ f_3(\kappa, \bar{\kappa}, \alpha, \phi_s) &= \frac{\pi^2}{975}\phi_s^3 e^{\alpha^2}(\alpha^2 - 1)[2\kappa - 17\bar{\kappa}] + 2\kappa[h_{13} + h_{23} + h_{33}] - \frac{1}{2}s_3 \\ f_4(\kappa, \bar{\kappa}, \alpha, \phi_s) &= \frac{\pi^2}{37800}\phi_s^3 e^{\alpha^2}(\alpha^2 - 1)[134\kappa - 599\bar{\kappa}] + 2\kappa[h_{14} + h_{24} + h_{34}] - \frac{1}{2}s_4 \end{aligned} \quad (4.21)$$

³We have checked this explicitly to assure that our calculation is correct.

where the h_{ij} and s_i are

$$\begin{aligned}
 h_{12} &= \frac{4}{1575\pi^2} e^{-\alpha^2} \phi_s^{-1} [8\beta_0 + 10\beta_1 + 105\beta_2] \\
 h_{13} &= \frac{4}{17325\pi^2} e^{-\alpha^2} \phi_s^{-1} [74\beta_0 + 88\beta_1 + 110\beta_2 + 1155\beta_3] \\
 h_{14} &= \frac{4}{4729725\pi^2} e^{-\alpha^2} \phi_s^{-1} [17503\beta_0 + 20202\beta_1 + 24024\beta_2 + 30030\beta_3 + 315315\beta_4] \\
 h_{22} &= \frac{8}{1575\pi^2} e^{-\alpha^2} \phi_s^{-1} [-2\gamma_0 - 5\gamma_1 + 105\gamma_2] \\
 h_{23} &= \frac{8}{17325\pi^2} e^{-\alpha^2} \phi_s^{-1} [-10\gamma_0 - 22\gamma_1 - 55\gamma_2 + 1155\gamma_3] \\
 h_{24} &= \frac{8}{4729725\pi^2} e^{-\alpha^2} \phi_s^{-1} [-1307\gamma_0 - 2730\gamma_1 - 6006\gamma_2 - 15015\gamma_3 + 315315\gamma_4] \\
 h_{32} &= \frac{4}{1575\pi^2} e^{-\alpha^2} \phi_s^{-1} [-7\delta_0 - 20\delta_1 + 105\delta_2] \\
 h_{33} &= \frac{4}{51975\pi^2} e^{-\alpha^2} \phi_s^{-1} [-112\delta_0 - 231\delta_1 - 660\delta_2 + 3465\delta_3] \\
 h_{34} &= \frac{4}{4729725\pi^2} e^{-\alpha^2} \phi_s^{-1} [-5893\delta_0 - 10192\delta_1 - 21021\delta_2 - 60060\delta_3 + 315315\delta_4] \\
 s_2 &= (2\pi^2)^{-1} \frac{1}{2} \iint dk_z dk_\rho k_\rho n_0^{-2} [n_1^2 - 2n_0 n_2] \\
 s_3 &= (2\pi^2)^{-1} \frac{1}{3} \iint dk_z dk_\rho k_\rho n_0^{-3} [-n_1^3 + 3n_0 n_1 n_2 - 3n_0^2 n_3] \\
 s_4 &= (2\pi^2)^{-1} \frac{1}{4} \iint dk_z dk_\rho k_\rho n_0^{-4} [n_1^4 - 4n_0 n_1^2 n_2 + 2n_0^2 n_2^2 + 4n_0^2 n_1 n_3 - 4n_0^3 n_4]
 \end{aligned}$$

with

$$\begin{aligned}
 \beta_i &= (2\pi^2)^{-1} \iint dk_\rho dk_z k_\rho k_\rho^4 \nu_i \\
 \gamma_i &= (2\pi^2)^{-1} \iint dk_\rho dk_z k_\rho k_\rho^2 k_z^2 \nu_i \\
 \delta_i &= (2\pi^2)^{-1} \iint dk_\rho dk_z k_\rho k_z^4 \nu_i
 \end{aligned}$$

All double integrals have exact (but very lengthy) solutions. Higher order terms are in principle also available, but become excessively complex.

From eqn. (4.21) we see that negative values of $\bar{\kappa}$ destabilize the sponge as expected. Quantitatively we find that at constant ϕ_s and inside / outside symmetry, $\alpha = 0$, the stability of the sponge depends sensitively on the value of $\bar{\kappa}$. The transition turned out to be strongly first order in all cases; we give an example for $\kappa = 8$ in fig. (4-5)

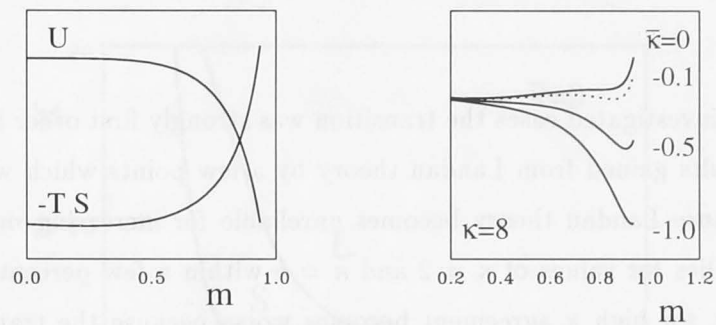


Figure 4-5: (left) Elastic energy and entropy for $\kappa = 8$, $\bar{\kappa} = 0$, $\phi_s = 0.1$, $\alpha = 0$ vs the nematic order parameter. Note that due to the cylindrical integration region the maximum in the entropic part is slightly shifted towards $m \approx 0.2$ instead of $m = 0$ as it should be for a spherical integration region. (right) The characteristic free energy behaviour of a strongly first order transition for various values of $\bar{\kappa}$. For clarity we omitted the artefact for $m < 0.2$. The approximate value of $\bar{\kappa}$ where the S/L transition occurs is highlighted as a dotted curve.

where we see the expected de- and increase of energetic and entropic contributions and the typical secondary minimum in the free energy density when plotted over the order parameter.

Surprisingly, strongly negative values of $\bar{\kappa}$ destroy the sponge even for soft membranes $\kappa \approx 1$ while in a narrow region of only slightly negative $\bar{\kappa}$ sponges appear to exist up to quite large values of $\kappa \approx 10$. In fig. (4-6) we show a $\kappa - \bar{\kappa}$ phase diagram for $\phi_s = 0.1$, $\alpha = 0$.

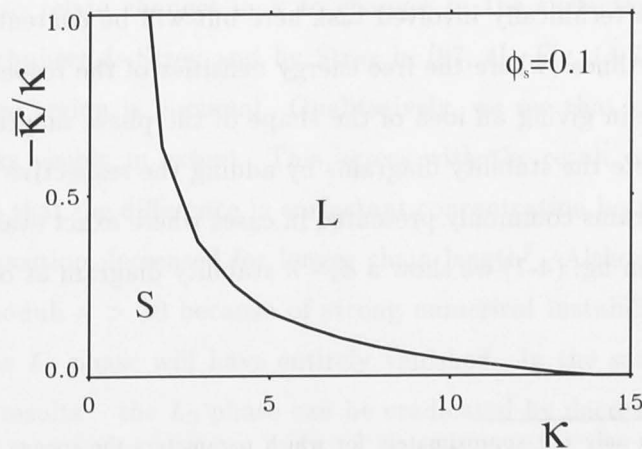


Figure 4-6: $\kappa - \bar{\kappa}$ phase diagram at $\phi_s = 0.1$, $\alpha = 0$. S and L denote sponge and lamellar phase.

As in any of the investigated cases the transition was strongly first order it was necessary to check the results gained from Landau theory by a few points which were determined numerically because Landau theory becomes unreliable for increasing m . Agreement is satisfactory and lies for values of $\kappa = 2$ and $\kappa = 5$ within a few percent of the Landau values. However, for high κ agreement becomes worse because the transition becomes stronger. The maximum of sponge existence $\kappa \approx 13$ in the plot should actually be $\kappa \approx 10$.

In the next chapter – where a Monte Carlo simulation is presented which can probe a phase space much larger than considered by the approximate random interface theory – we will see that our results for the $\kappa - \bar{\kappa}$ diagram are with slight modifications valid: a more ordered sponge ('molten cubic phase') can take the place of the ideally random one discussed here thus broadening the region of sponge stability in the $\kappa - \bar{\kappa}$ diagram. This will be discussed in more detail and in the context of Porte's theoretical conjectures [22] in the next chapter.

To gain phase diagrams in representations containing ϕ_s or ϕ is more complicated. Upon increase in ϕ_s we observe again a strongly first order transition (accompanied by phase coexistence). To determine the concentrations of the coexisting phases accurate knowledge of the free energy density is needed which is definitely beyond the scope of the Landau expansion⁴ and requires extensive numerical effort in order to work with a spherical integration region and to surmount the current limit of $m \approx 0.95$ in the numerical scheme. We will not tackle this technically involved task here but will be content with providing the respective stability lines (where the free energy densities of the respective phases are minimal) which suffice in giving an idea of the shape of the phase diagram. However, it is quite easy to complete the stability diagrams by adding the respective tie lines to gain 'schematic' phase diagrams commonly presented in cases where exact evaluation becomes too complicated [32]. In fig. (4-7) we show a $\phi_s - \kappa$ stability diagram at $\alpha = 0$ for a value of $\bar{\kappa} = 0$.

⁴Landau expansion can only tell approximately for which parameters the sponge becomes unstable; the values of the free energy density of the stable, nematic state is not reliable.

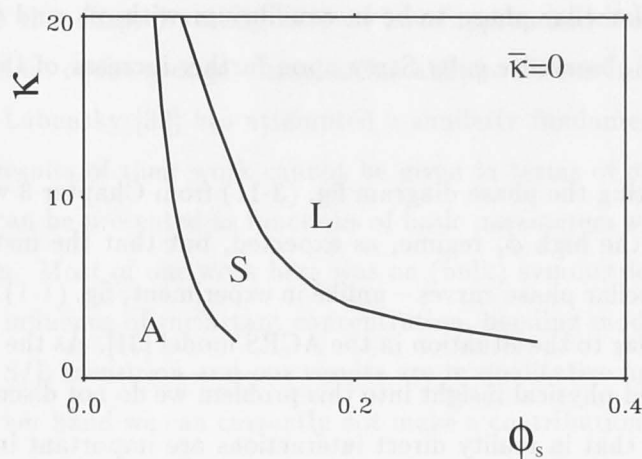


Figure 4-7: $\phi_s - \kappa$ stability diagram for $\bar{\kappa} = 0$ where A, S and L denote asymmetric (droplet) sponge, symmetric sponge and lamellar phases, respectively. The instability towards the A phase is based on eqn. (3.82) in Chapter 3. The computational effort to go beyond $\kappa = 20$ was not surmountable due to the strong instability of the (near) delta function shaped structure factor towards a singularity.

Alternatively, we could have plotted in fig. (4-7) ϕ_s vs the ‘temperature’ $\kappa^{-1} = T$ as e.g. in [31]. Then we would see that the phase sequence A - S - L resembles qualitatively experimental $\phi_s - T$ phase diagrams, e.g. the one for $C_{12}E_5$ in [85]. However, a change in temperature affects also the saddle-splay curvature so that in a genuine $\phi_s - T$ phase diagram the detailed shape of L_3 region could be quite different from that predicted by a $\phi_s - \kappa^{-1}$ plot.

It is more safe to relate changes in κ to changes in the surfactant chain length as investigated by Schubert & Strey and by Strey in [87, 4]. Fig. (4-7) is plotted for $\bar{\kappa} = 0$ where the sponge region is maximal. Qualitatively, we see that upon increase in κ the L_3 region shrinks visibly in extent. This agrees with the result of Strey who found (in microemulsions) that the difference in surfactant concentration between the middle phase and the S/L transition decreased for longer chain length⁵. Although we could not deal with bending moduli $\kappa > 20$ because of strong numerical instability it is clear that for some $\kappa > 20$ the L_3 phase will have entirely vanished. In the same way – as we know from our above results – the L_3 phase can be eradicated by decreasing $\bar{\kappa}$. At high κ the

⁵In [4] the respective concentration ranges for $C_{10}E_5$ and $C_{12}E_4$ were 12 and 2%.

asymmetric and lamellar regions collide and we expect a direct A/L transition (as mentioned *en passant* in [106]). In microemulsions this situation would mean that we would expect a very dilute lamellar phase to be in equilibrium with oil- and water-rich phases. This has been in fact observed *e.g.* by Strey upon further increase of the chain length to $C_{14}E_5$ [4].

Finally, when re-plotting the phase diagram fig. (3-11) from Chapter 3 we found that the lamellar region is in the high ϕ_s regime, as expected, but that the instability line from microemulsion to lamellar phase curves – unlike in experiment, fig. (1-1) – upwards rather than downwards similar to the situation in the ACRS model [31]. As the random interface description cannot add physical insight into this problem we do not discuss it any further. One might speculate that in reality direct interactions are important in the asymmetric region, a question most recently considered by Menes & Safran [99] and that the pure bending Hamiltonian is not sufficient to provide the details of the phase behaviour.

4.4 Smectic Lamellar Phase

The most straightforward way of modelling a smectic lamellar phase in the random interface formalism is by introducing an order parameter similar to a sublattice magnetization in antiferromagnets, μ , which off-sets the Gaussian field in, say, z - direction

$$p[s(k_\rho, k_z)] \sim \exp \left[- \frac{[s(k_\rho, k_z) - \mu \delta(k_z^2 - k_0^2)]^2}{2\nu(k_\rho, k_z)} \right] \quad (4.22)$$

so that the overall magnetization is still zero. For $\mu = 0$ we recover the nematic lamellar phase. For non-zero μ the average of the k_0 mode makes sure that the nematic ground state degeneracy is lifted and basic long-range order is imposed which is for $1/\kappa > 0$ softened into quasi long-range order by the presence of fluctuations. However, there is a basic difficulty in eqn. (4.22) in that it models the Bragg mode as a single sinusoidal mode so that translational symmetry is broken. Although we have to postpone the solution of this problem to future work, we have heuristically determined the free energy density for small $\mu \neq 0$ and found that indeed the nematic phase is stable with respect to the smectic, indicating – as mentioned above – that a description beyond mere curvature elasticity is necessary to appropriately approach the nematic - smectic transition.

4.5 Conclusion

We can conclude this chapter stating that we have approached the challenging task of a consistent treatment of the sponge - lamellar instability. To our knowledge only the work of Golubović & Lubensky [32] has attempted a similarly fundamental treatment. However, while the results of their work cannot be given in terms of observable parameters, our predictions can be presented as functions of basic parameters with simple experimental interpretation. Most of our work here was on (bulk) symmetric structures. We have investigated the influence of surfactant concentration, bending modulus and saddle-splay modulus on the S/L transition and our results are in qualitative agreement with experiment. On the other hand we can currently not make a contribution to the explanation of the unusual shape of the lamellar phase region in ternary phase diagrams, fig. (1-1) and [4]. Some success in this direction was most recently achieved by Menes & Safran [99] using a theory which includes direct interactions.

4.A Appendix

We set up the correlation matrix

	s	s_x	s_y	s_z	s_{xx}	s_{yy}	s_{zz}	s_{xy}	s_{xz}	s_{yz}
s	$\langle 1 \rangle$	0	0	0	$-\frac{1}{2} \langle k_\rho^2 \rangle$	$-\frac{1}{2} \langle k_\rho^2 \rangle$	$-\langle k_z^2 \rangle$	0	0	0
s_x	0	$\frac{1}{2} \langle k_\rho^2 \rangle$	0	0	0	0	0	0	0	0
s_y	0	0	$\frac{1}{2} \langle k_\rho^2 \rangle$	0	0	0	0	0	0	0
s_z	0	0	0	$\langle k_z^2 \rangle$	0	0	0	0	0	0
s_{xx}	$-\frac{1}{2} \langle k_\rho^2 \rangle$	0	0	0	$\frac{3}{8} \langle k_\rho^4 \rangle$	$\frac{1}{8} \langle k_\rho^4 \rangle$	$\frac{1}{2} \langle k_\rho^2 k_z^2 \rangle$	0	0	0
s_{yy}	$-\frac{1}{2} \langle k_\rho^2 \rangle$	0	0	0	$\frac{1}{8} \langle k_\rho^4 \rangle$	$\frac{3}{8} \langle k_\rho^4 \rangle$	$\frac{1}{2} \langle k_\rho^2 k_z^2 \rangle$	0	0	0
s_{zz}	$-\langle k_z^2 \rangle$	0	0	0	$\frac{1}{2} \langle k_\rho^2 k_z^2 \rangle$	$\frac{1}{2} \langle k_\rho^2 k_z^2 \rangle$	$\langle k_z^4 \rangle$	0	0	0
s_{xy}	0	0	0	0	0	0	0	$\frac{1}{8} \langle k_\rho^4 \rangle$	0	0
s_{xz}	0	0	0	0	0	0	0	0	$\frac{1}{2} \langle k_\rho^2 k_z^2 \rangle$	0
s_{yz}	0	0	0	0	0	0	0	0	0	$\frac{1}{2} \langle k_\rho^2 k_z^2 \rangle$

where the z - direction of the coordinate system is aligned with the direction of nematic ordering. Due to symmetry all derivatives which yield odd powers of k_i vanish. In the isotropic case the matrix simplifies and we recover the matrix used in the Appendix of Chapter 3.

Because of the decoupling of first and zeroth/second derivatives the averages over the respective parts of the differential operators eqn. (3.A1) can be done separately. For example, for the average over the mean square curvature we find that the differential operator reads after some calculation

$$\begin{aligned}
 \sqrt{(\vec{\nabla}s)^2} H^2 &= \frac{1}{4\sqrt{(\vec{\nabla}s)^2}} \left[s_{xx}^2 (s_y^2 + s_z^2)^2 + s_{yy}^2 (s_x^2 + s_z^2) + s_{zz}^2 (s_x^2 + s_y^2) \right. \\
 &\quad + 4s_{xy}^2 s_x^2 s_y^2 + 4s_{xz}^2 s_x^2 s_z^2 + 4s_{yz}^2 s_y^2 s_z^2 \\
 &\quad + 2(s_x^2 s_y^2 + s_x^2 s_z^2 + s_y^2 s_z^2) (s_{xx} s_{yy} + s_{xx} s_{zz} + s_{yy} s_{zz}) \\
 &\quad \left. + 2(s_x^4 s_{yy} s_{zz} + s_y^4 s_{xx} s_{zz} + s_z^4 s_{xx} s_{yy}) \right]
 \end{aligned}$$

so that the ensemble average has the form

$$\left\langle \delta(s - \alpha) \sqrt{(\vec{\nabla}s)^2} H^2 \right\rangle_0 = \left\langle \frac{s_z^4}{\sqrt{(\vec{\nabla}s)^2}} \right\rangle_0 \left[\frac{1}{2} \langle \delta(s - \alpha) s_{xx}^2 \rangle_0 + \frac{1}{2} \langle \delta(s - \alpha) s_{xx} s_{yy} \rangle_0 \right]$$

$$\begin{aligned}
& + \left\langle \frac{s_x^2 s_z^2}{\sqrt{(\vec{\nabla} s)^2}^5} \right\rangle_0 \left[\langle \delta(s - \alpha) s_{xx}^2 \rangle_0 + \langle \delta(s - \alpha) s_{xx} s_{yy} \rangle_0 \right. \\
& + 2 \langle \delta(s - \alpha) s_{xx} s_{zz} \rangle_0 + 2 \langle \delta(s - \alpha) s_{xz}^2 \rangle_0 \left. \right] \\
& + \left\langle \frac{s_x^4}{\sqrt{(\vec{\nabla} s)^2}^5} \right\rangle_0 \left[\frac{1}{2} \langle \delta(s - \alpha) s_{xx}^2 \rangle_0 + \frac{1}{6} \langle \delta(s - \alpha) s_{xx} s_{yy} \rangle_0 \right. \\
& + \frac{1}{3} \langle \delta(s - \alpha) s_{xy}^2 \rangle_0 + \frac{4}{3} \langle \delta(s - \alpha) s_{xx} s_{zz} \rangle_0 + \frac{2}{3} \langle \delta(s - \alpha) s_{zz}^2 \rangle_0 \left. \right]
\end{aligned}$$

The averages over the zeroth/second derivatives are not difficult because the respective arguments of the multivariate Gaussian are only quadratic. The averages over the first derivatives are more complicated. A set of the successive transformations, $\rho = s_x^2 + s_y^2$, $s_z^2 = y$, $y = \rho x$, is required. For example,

$$\begin{aligned}
\left\langle \frac{s_z^4}{\sqrt{(\vec{\nabla} s)^2}^5} \right\rangle_0 & \sim \int_0^\infty \int_0^\infty d\rho ds_z \frac{s_z^4}{(s_z^2 + \rho)^{\frac{5}{2}}} e^{-\frac{s_z^2}{2\sigma_z}} e^{-\frac{\rho}{2\sigma_\rho}} \\
& = \frac{1}{2} \int_0^\infty \int_0^\infty d\rho dy y^{\frac{3}{2}} (y + \rho)^{-\frac{5}{2}} e^{-\frac{y}{2\sigma_z}} e^{-\frac{\rho}{2\sigma_\rho}} \\
& = \frac{1}{2} \int_0^\infty \int_0^\infty d\rho dx x^{\frac{3}{2}} (1 + x)^{-\frac{5}{2}} e^{-\frac{\rho x}{2\sigma_z}} e^{-\frac{\rho}{2\sigma_\rho}} \\
& = \frac{1}{2} \int_0^\infty dx x^{\frac{3}{2}} (1 + x)^{-\frac{5}{2}} \left[\frac{x}{2\sigma_z} + \frac{1}{2\sigma_\rho} \right]^{-1} \\
& = \frac{2\sigma_\rho(\sigma_\rho - 4\sigma_z)\sigma_z}{3(\sigma_\rho - \sigma_z)^2} + \frac{2\sigma_\rho\sigma_z^{\frac{5}{2}} \arctan \sqrt{\frac{\sigma_\rho - \sigma_z}{\sigma_z}}}{(\sigma_\rho - \sigma_z)^{\frac{5}{2}}}
\end{aligned}$$

the other two terms $\left\langle \frac{s_x^2 s_z^2}{\sqrt{(\vec{\nabla} s)^2}^5} \right\rangle_0$ and $\left\langle \frac{s_x^4}{\sqrt{(\vec{\nabla} s)^2}^5} \right\rangle_0$ and all gradient terms appearing in the calculation of $\langle \delta(s - \alpha) \sqrt{(\vec{\nabla} s)^2} K \rangle_0$, $\langle \delta(s - \alpha) \sqrt{(\vec{\nabla} s)^2} H \rangle_0$ or $\langle \delta(s - \alpha) \sqrt{(\vec{\nabla} s)^2} \rangle_0$ can be done analogously. To gain the formulas eqn. (4.4) - eqn. (4.7) we finally apply the definition of the order parameter $m = 1 - \sigma_\rho/\sigma_z$.

$$\begin{aligned}
 & \frac{1}{2} \left(\frac{\partial^2 \phi}{\partial x^2} + \frac{\partial^2 \phi}{\partial y^2} \right) + \dots \\
 & \dots \\
 & \dots
 \end{aligned}$$

The average over the wavelength is not affected by the presence of the perturbation. The perturbation is assumed to be small and the average is taken over one period of the perturbation.

$$\begin{aligned}
 & \dots \\
 & \dots \\
 & \dots
 \end{aligned}$$

It is assumed that the perturbation is small and the average is taken over one period of the perturbation. The perturbation is assumed to be small and the average is taken over one period of the perturbation.

The perturbation is assumed to be small and the average is taken over one period of the perturbation. The perturbation is assumed to be small and the average is taken over one period of the perturbation.

$$\begin{aligned}
 & \dots \\
 & \dots \\
 & \dots
 \end{aligned}$$

It is assumed that the perturbation is small and the average is taken over one period of the perturbation. The perturbation is assumed to be small and the average is taken over one period of the perturbation.

Monte Carlo Simulation of Curvature - Elastic Interfaces

In the preceding chapters we have made attempts to model fluctuating membranes by Gaussian random surfaces. Our approximations have so far only allowed us to consider a restricted set of structures, sponge-like and lamellar phases. Although the results for these systems were satisfactory we certainly would like to deal with a more general set of structures covering a wider range of topologies.

In the current absence of generalizations of the mean-spherical model to other surfactant phases we want to discuss in this chapter a numerical scheme which provides – within the limits of a numerical simulation – an ‘exact’ approach to Helfrich’s Hamiltonian.

5.1 Introduction

Simulations of amphiphilic systems have so far been mostly discussed either on a microscopic level to study the process of self-assembly itself, or to investigate a few stacked membrane sheets in the context of steric interaction and the unbinding transition in smectic lamellar phases¹.

Microscopic simulations are often performed on the basis of standard Ising systems

¹We do not discuss here simulations of tethered membranes [114] and crumpling effects [115] which are hardly applicable to fluid membranes.

(*cf.* Chapter 1) where the sample size is necessarily very small. These simulations usually suffer from the absence of long range terms in Ising theories of amphiphilic systems. Their results are most useful for checking predictions of analytic approximations of microscopic lattice models or solving those in case no approximate solutions are available [116].

A truly continuous microscopic description was achieved by Smit *et al.* who simulated freely moving molecules which interact via a Lennard - Jones potential [3]. Their results are pioneering in predicting details of the process of self-assembly as a function of molecular geometry. These simulations have also been successfully used in industrial applications.

Simulations of a few unbinding membranes were mostly performed by the group around Lipowsky [117]. There the amphiphilic sheets were discretized and updated in real space using the harmonic low-temperature bending Hamiltonian in Monge gauge. The results comprise confirmation of analytical results for the unbinding transition. Other simulations in the context of smectic lamellar phases address the strength of the steric repulsion [56] (*cf.* Chapter 2); again the low temperature approximation was applied and the system sizes were very limited and topologically fixed.

Our aim is to provide a simulation of fluctuating membranes which operates with truly continuous, self-avoiding, lattice-independent interfaces of variable topology under the full, non-linear bending Hamiltonian. We proceed very similar to our analytic approximation *not* by coarse graining and manipulating the membranes in real space but by defining them in a continuous way in \vec{k} space.

5.2 Methods

5.2.1 Simulation of Continuous, Self-Avoiding Surfaces

The interfaces used by our Monte Carlo (MC) simulation are given again in implicit representation based on a decomposition into modes in an appropriate base function space, eqn. (1.12)

$$s(\vec{r}) = \sum_m \eta_m \phi_m(\vec{r}) = 0 \quad (5.1)$$

as in the introductory chapter. An elementary MC step is effected by a small change in the amplitudes (or the spectral components) of the base functions, $\eta_m \rightarrow \eta'_m$, and

not by changing configurations in real space. After each change the new state $s'(\vec{r})$ of the interface is therefore again given in analytical form and perfectly continuous and self-avoiding. This property makes the representation eqn. (5.1) ideal for evaluating the surface integrals associated with the bending energy model.

The loci of the interfaces can be determined by dividing the cubic sample volume V into subcubes small enough to allow for linear approximation within each subcube. Starting from the centre of each subcube the field gradient can be followed in several iterations until the surface is reached to a given accuracy. The length $|\vec{r}_{j+1}|$ of the $(j+1)$ th iterative displacement is determined by Taylor expansion

$$s(\vec{r}_{j+1}) = s(\vec{r}_j) + |\vec{\nabla}s(\vec{r})|_{\vec{r}=\vec{r}_j} |\vec{r}_{j+1}| = 0 \quad (5.2)$$

Projection onto the local coordinate system (of the subcube) gives then the shift from the subcube centre in each direction

$$\vec{r}_{j+1} = -\vec{\nabla}s(\vec{r}_j) \frac{s(\vec{r}_j)}{|\vec{\nabla}s(\vec{r}_j)|^2} \quad (5.3)$$

To make sure that the interface finally found after a few iterations is still within the subcube where the iterations started from we can calculate the projection of the final position vector of the surface onto the surface normal. If this is larger than the maximum given by the size of the cube, we have to discard this surface position in order to avoid overcounting. Measurement of two or more interfaces which might occur simultaneously in a subcube is not possible with this method, but can be neglected for all practical purposes. Alternatively to using a cubic lattice for measurements one can also compute the area by distributing small subcubes randomly within V and measuring the surface contained in those. But for convenience we prefer simple subdivision. In principle, however, the method is completely lattice independent *i.e.* a lattice is not needed to define the surface. All information is given by eqn. (5.1). Interference with the lattice is minimal. In order to exploit this fully we will later also chose to create random surface configurations in spherical coordinates rather than by (lattice based) Fourier transform. The approximate surface area $\Delta S(\vec{r}_i)$ on each surface site \vec{r}_i is evaluated by very accurate (*cf.* Appendix) polygon tiling following an algorithm due to Gilat & Raubenheimer [118].

For a numerical estimate of the general curvature energy

$$E = \int_S dS \left[\beta_1 H + \beta_2 H^2 + \beta_3 K + \gamma_1 H K + \gamma_2 H^3 + \dots \right] \quad (5.4)$$

we use the discretized

$$E \approx \sum_{i=1}^N \left[\beta_1 H(\vec{r}_i) + \beta_2 H^2(\vec{r}_i) + \beta_3 K(\vec{r}_i) + \gamma_1 H K(\vec{r}_i) + \gamma_2(\vec{r}_i) H^3 + \dots \right] \Delta S(\vec{r}_i) \quad (5.5)$$

where the surface points \vec{r}_i and surface areas $\Delta S(\vec{r}_i)$ have been determined above. We stress again that the values of the differential curvature operators given in eqn. (5.5) (*cf.* eqn. (3.A1)) can be calculated *analytically* at all the \vec{r}_i from the readily known first and second derivatives of eqn. (5.1) at any time during the MC run. In the Appendix we give an estimate of the numerical accuracy of the surface integrals. Our results for the example of Gaussian random surfaces (GRS) are in excellent agreement with the exact expressions, eqn. (3.A3) - eqn. (3.A8), and resolve the discrepancy between the results for these quantities given by [34] and by [37] in favour of [37].

Next we have to take care of the surface area constraint eqn. (1.3). It is enforced in a natural way with the help of a stretching / compression energy [16]

$$\Delta E_s \sim \frac{1}{2} \kappa_s S \left[\frac{\Delta S}{S_{initial}} \right]^2 \quad (5.6)$$

where S , $S_{initial}$ are the current and initial areas, and ΔS their difference. ΔE_s enters the Boltzmann factor after each MC step. A large value of the stretch modulus κ_s keeps the fluctuation of the surface area negligibly small ($< 0.01\%$ in our computations), *i.e.* κ_s is used here as a simple implementation of the surface area constraint only. Simulation of stretchable surfaces with realistic κ_s is possible, but would break the scale-invariance of the system which we want to avoid. Without constraint the interfacial system is seen to gradually drift into trivial states with different surface area. This behaviour is a useful check and should be characteristic for systems based on an interfacial Hamiltonian when the interfacial area is uncontrolled.

We should also implement a volume conservation constraint

$$\Delta E_V \sim \frac{1}{2} \kappa_V V \left[\frac{\Delta V}{V_{initial}} \right]^2 \quad (5.7)$$

where V refers to, say, V_{oil} . For binary L_3 phases this constraint is not needed. It is particularly important when simulating oil-water systems with non-zero spontaneous curvature.

After having set up and performed the usual set of checks for MC simulations (*cf.* Appendix) we can proceed with the Metropolis MC scheme [119, 23].

5.2.2 Analysis of Bulk and Film Structure Factors

For analysis of the results the structure factors can be gained numerically either by directly computing the correlation function from [24]

$$\langle s(0)s(r) \rangle \sim \frac{\text{number of black pixels at distance } r \text{ from a given black pixel at } \vec{r}_0}{\text{total number of pixels at distance } r \text{ from a given black pixel at } \vec{r}_0}$$

and then taking the spherical Fourier transform.

Alternatively, if one is not interested in the correlation function in real space (which cannot be directly measured) one can apply the standard procedure used in data analysis drawn schematically

$$s(\vec{r}) \xrightarrow{\text{clipping}} s_{bw}(\vec{r}) \xrightarrow{\text{FFT}} s(\vec{k}) \xrightarrow{\text{convolution}} I(\vec{k}) = s(\vec{k})s^*(\vec{k}) \xrightarrow{\text{spherical averaging}} I(k) \quad (5.8)$$

where clipping denotes transform into an appropriate spin system with $s(\vec{r}) = 1$ or 0 ('black' or 'white', cf. eqn. (1.7)). Then one takes the Fast Fourier Transform [120] of the clipped field $s(\vec{r})_{bw}$ sampled at N^3 points,

$$s_{bw}(k_l, k_m, k_n) = \sum_{l', m', n'=0}^{N-1} s_{bw}(r_{l'}, r_{m'}, r_{n'}) e^{-i(r_{l'}k_l + r_{m'}k_m + r_{n'}k_n)},$$

$$k_l = lk_s, \quad k_m = mk_s, \quad k_n = nk_s, \quad k_s = 2\pi/d_s$$

where $d_s = N \cdot T$ is the side length of the sample cube. As only a finite number of points is involved, $s_{bw}(k_l, k_m, k_n)$ corresponds to the Fourier transform of a sum over delta functions located at the subcube centres. This can be improved by applying a standard convolution which corresponds to a homogeneous value $s_{bw}(r_{l'}, r_{m'}, r_{n'})$ over a whole subcube. In \vec{k} -space this corresponds to a multiplication of $s_{bw}(k_l, k_m, k_n)$ with [121, 122]

$$\left[\frac{\sin(\pi l N^{-1})}{\pi l N^{-1}} \right] \left[\frac{\sin(\pi m N^{-1})}{\pi m N^{-1}} \right] \left[\frac{\sin(\pi n N^{-1})}{\pi n N^{-1}} \right]$$

This operation makes sure that we take the genuine Fourier transform of homogeneous 'black' (0) and 'white' (1) subregions in the real space sample. These regions are grained at the boundaries. This should not be a problem when evaluating bulk scattering where black and white regions are assigned the weights 0 or 1 depending to whether $s(\vec{r}) > 0$ or $s(\vec{r}) < 0$. Calculation of the film structure factor is more delicate. Uniformity of the film thickness cannot be properly implemented. We can again chose to either work with films which have non-uniform thickness corresponding to 0 or 1 for $|s(\vec{r})| < r_c$ (we call it again method (a)) or with films which have a linear correction to the fluctuations of

the film thickness so that $|s(\vec{r})| < r_c |\vec{\nabla} s(\vec{r})|$ (method (b)). Note, however, that the linear correction in method (b) does still not assure an ideally uniform film.

We should test the method for film scattering to get an idea of its sensitivity. We chose a rather complicated surface, the approximate Schwarz P-surface represented by [123]²

$$s(\vec{r}) = \cos k_x x + \cos k_y y + \cos k_z z \quad (5.9)$$

which is topologically as complex as the surfaces we are going to deal with. The result is given in fig. (5-1)

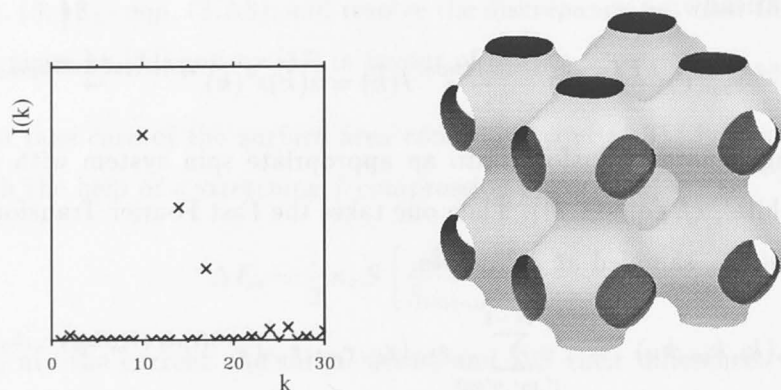


Figure 5-1: (left) Angle-averaged film scattering signal from a Schwarz P-surface, eqn. (5.9). The sample size was 7 structural wavelengths $d_0 = 7\pi k_0^{-1}$ and the FFT grid was 128^3 . The Bragg peaks follow the expected sequence $\sqrt{2}, \sqrt{4}, \sqrt{6}, \sqrt{8}, \sqrt{10}, \sqrt{12}, \sqrt{14}$ times the structural wave vector (here 7). The peak at position $7\sqrt{8} \approx 20$ is barely visible on this scale, but a factor of 4 higher than the neighboring noise. The small peak at position 2 is an artefact. (right) Eight unit cells of the nodal surface eqn. (5.9).

with Bragg reflections as expected for the $Im3m$ space group assigned to the P-surface [125]. However, very small ($k \ll k_0$) and very large ($k \gg k_0$) frequencies should not be taken too seriously because of finite sample size and graining. Uniform and non-uniform films showed little difference in this case because the surfaces eqn. (5.9) are not random and to a good approximation parallel.

We will use throughout this chapter FFT grid sizes of 128^3 and a total sample side length of $7 \cdot 2\pi k_0^{-1}$. The seventh entry $k = 7$ in the structure factor corresponds therefore to the structural wavelength k_0 .

²Many other periodic minimal surfaces *incl.* D, F, Y *etc.* can be approximately described by a Fourier expansion [124].

5.2.3 Topology, Curvature

Comparison of topological properties can be based on the Gauss-Bonnet theorem

$$\int_S K dS = 4\pi (n_c - n_h) = 2\pi \chi_E$$

where n_c , n_h are the numbers of components and handles and χ_E is the Euler characteristic. Resemblance of various structures to the thoroughly studied cubic phases can be measured using the scaled Euler characteristic introduced in various forms and definitions in [126, 108, 127]. As part of the free energy (coupled by $\bar{\kappa}$), the Euler characteristic of a surfactant system is also invariant under a change of scale. Therefore, under dilutions an invariant scaled Euler characteristic is

$$\chi_0 \sim \frac{\chi_E}{V} \left(\frac{S}{V}\right)^{-3}$$

This relates to the definition for the average Gaussian curvature by

$$\chi_0 = -\frac{1}{2\pi} \left\langle \delta(s) |\vec{\nabla}_s \cdot \dot{K}| \right\rangle \left(\frac{S}{V}\right)^{-3} \quad (5.10)$$

where we have left away the subscript $_0$ because the averages are not necessarily Gaussian. Similarly, we can use a scaled mean square curvature

$$\psi_0 = \frac{1}{2\pi} \left\langle \delta(s) |\vec{\nabla}_s | H^2 | \right\rangle \left(\frac{S}{V}\right)^{-3} \quad (5.11)$$

to follow the evolution of the mean square curvature.

5.3 Application to Disordered Surfactant Interfaces

Our aim is twofold. Firstly we want to back up the analytical calculations in the random interface scheme where all interface configurations were assumed perfectly Gaussian without mode - mode coupling. In the numerical scheme there are no such restrictions and during an MC process modes can correlate freely. It is therefore interesting to ask whether we can determine by simulation how well the state space which we used in Chapters 3 and 4 corresponds to reality and where its limits of applicability are.

Secondly, the algorithm allows us nearly unique access to a wide range of topologies. No theory can handle Gaussian curvature (even random interface theory in its current form leaves space for improvement in this respect) in more than a crude way and very little

is known quantitatively about this problem. On the other hand there is a great deal of qualitative discussion surrounding this topic [27, 22, 106] and many authors point to the urgency of more quantitative approaches [4]. Our second aim will therefore be to gain insight into the effects of various saddle-splay moduli on a surface configuration where we restrict ourselves here (mainly for runtime reasons, *cf.* Appendix) to the zero spontaneous curvature Hamiltonian used throughout this thesis, $\mathcal{H} = \int_s dS [2\kappa H^2 + \bar{\kappa}K]$.

We do not in the context of this chapter discuss structural transitions associated with a variation of surfactant concentration. As we have pointed out in previous chapters these are intimately related to invariance breaking due to the microscopic length scale. Simulations in this context are possible, but exceed run-time constraints because the phase space to be covered becomes exceedingly large. If the mode expansion is essentially limited to the physical range of k -values, up to some cut-off value k_c , the number of degrees of freedom in the finite system of volume V under investigation can be roughly estimated by the volume of the corresponding phase space

$$N \approx 4\pi k_0^2 \Delta k \cdot V$$

For the chosen sample size, $V = (7d_0)^3$, and an upper limit in k -space which is a multiple of k_0 of $O(1)$, the number of degrees of freedom is of the order of $\sim 10^6 - 10^7$ and the simulation becomes untractable. Moreover, detailed attention would have to be spent (a) on correctly measuring the curvatures of possibly small structures (small ripples *etc.*) which demands a very fine grid resolution and (b) on a rigorous enforcement of the cut-off wave length. Both tasks are computationally out of reach. Hence we do not investigate here systems which are close to an instability driven by microscopic entropy such as the S/A transition or multiphase coexistence. We rather operate well within the scale invariant region where configurational or topological entropy plays an important role. Examples of such systems would be the bilayer phases investigated by Porte *et al.* which show a S/L transition upon change of the saddle-splay modulus (Chapter 4) or sponges with varying degrees of ordering studied by Chen *et al.* [76]. Scale-invariant description of these systems should be a reasonable approximation. If we describe surfactant interfaces by the standard Fourier expansion of the implicit surface representation $s(\vec{r})$, eqn. (1.13), a good approximation of an initial, disordered isotropic configuration is Berk's original distribution $\nu(k) \sim \delta(k - k_0)$ (*i.e.* large ξ , regime (i) in Chapter 3) [34] with $4 \cdot 10^4$ degrees of freedom ($3 \cdot 10^4$ wave vector components and 10^4 phases)³.

³We should note that the 'ghost waves' of eqn. (1.8) carry very little information of physical relevance.

With a side length $7d_0$, and – by neglecting short-length scale fluctuations – an effective width in k -space of no more than k_0 the number of degrees of freedom of the system should be $\sim 10^5$ so that the states are reasonably described by our basis set. The simulation box size is somewhat above the minimal size required to contain finite size effects (*cf.* Appendix). The grid resolution was 64^3 *i.e.* good enough to follow topological changes, but – as we said above – not sufficient to measure structural details related to fluctuations on a small scale. A real space figure of an initial configuration is given (approximately) in fig. (3-3). Numerically determined structure factors and a probability profile are given in fig. (5-2). Note that the bulk structure factor defined by the procedure eqn. (5.8) is not exactly a delta function because the black - white clipping causes smoothing [34, 128]. The film structure factor is shown for the cases of non-uniform and (approximately) uniform film thicknesses. For the non-uniform case we can compare with the analytical result (eqn. (3.28) in Chapter 3) and agreement is excellent.

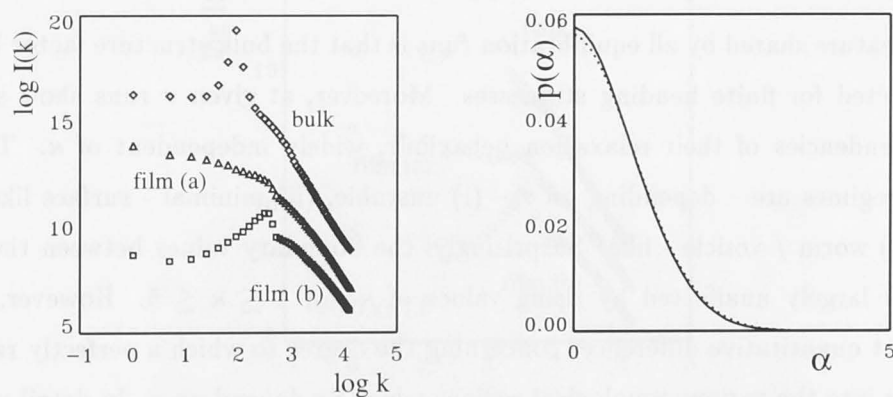


Figure 5-2: (left) Bulk and film structure factors from Gaussian random surfaces. Averages over 5 different random configurations were taken. We see, as expected from the analytical calculation, a peak at k_0 in the bulk structure factor and a shoulder at $2k_0$ in the film structure factor according to method (a), eqn. (3.28). If we use method (b) for the film structure factor we see – as indicated by our analytical calculation in Chapter 3 – that a peak rather than a simple shoulder appears at $2k_0$ in the film structure. All structure factors converge asymptotically towards Porod's k^{-4} law as they should. (right) $p(\alpha) = 1/\sqrt{(2\pi)} \int_{\alpha}^{\alpha+\Delta\alpha} dt \exp[-\frac{1}{2}t^2]$ with $\Delta\alpha \approx 0.14$. The full line is from a histogram averaged over 5 configurations. The dotted line compares with the analytical expression.

This random configuration was taken as the initial state of most runs (although some test runs were started with cubic and lamellar configurations, *cf.* Appendix). Its characteristic

For example, pairs of waves can interfere destructively and therefore contribute nothing to a configuration. Therefore we do not need to pay attention to the distribution of wave vectors and phases.

curvature values are

$$\chi_0 = \chi_0^{GRS} \approx 0.2, \quad \psi_0 = \psi_0^{GRS} \approx 0.045.$$

The final equilibrium structure depends on both elastic moduli, κ and $\bar{\kappa}$. It is convenient to discuss the results separately in terms of their dependence on the absolute value of κ , and on the temperature independent, dimensionless topological ratio which we denote

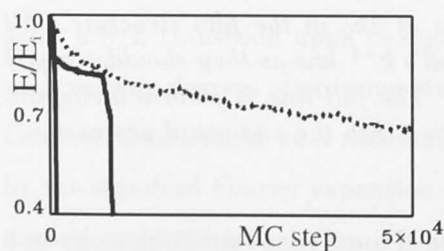
$$\tau = -\frac{\bar{\kappa}}{\kappa} \quad (5.12)$$

As outlined above, it is natural to assume that Gaussian states are stable for low values of the bending rigidity. A typical experimental value for the stiffness of disordered systems is κ of the order of 1. We therefore performed a sequence of runs for different values of τ and $\kappa = 1$. On the other hand we are also interested in the question of topological transitions. In order to get more information about these phenomena we undertook simulations of a few selected samples at κ considerably larger than 1.

A common feature shared by all equilibration runs is that the bulk structure factor broadens, as expected for finite bending stiffnesses. Moreover, at given τ runs show similar *qualitative* tendencies of their relaxation behaviour, widely independent of κ . Typical topological regimes are – depending on τ – (i) unstable, (ii) minimal - surface like, (iii) lamellar, (iv) worm / vesicle - like. Surprisingly, the boundary values between these regions appear largely unaffected by rising values of κ , for $1 \lesssim \kappa \lesssim 5$. However, there are significant quantitative differences concerning the degree to which a perfectly random sponge drifts into the various topological regions which do depend on κ . In detail we find

(i) **Unstable:** $\tau < 0$ and $\tau > 2$

No stable runs were found in this region. This is easily understood from the well-known



local stability criterion for the bending energy $-2\kappa \leq \bar{\kappa} \leq 0$ and is a very good check of the numerical algorithm. We show in the inset a typical evolution of the internal energy which demonstrates instability: solid lines depict unstable runs, in comparison to a typical stable run (dotted line).

However, the stability limits may change when higher order curvature terms are included. Because we do not consider higher order terms which would lead to physically reasonable

states of small vesicles or saddles (but would break the scale-invariance), we did not follow the evolution in the unstable regime.

(ii) **Minimal Surface - Like:** $0 \leq \tau \lesssim 0.3$

The final state has a lower mean square curvature $\psi_0 < \psi_0^{GRS}$ and lower mean saddle-splay curvature $\chi_0 < \chi_0^{GRS}$ than the initial state, for the investigated range of $0.25 \lesssim \kappa \lesssim 10$.

For a system, $\kappa = 1$, we found that equilibration was swift and the final state differed clearly from the initial Gaussian. All indicators, such as curvatures, probability distribution and structure factors show characteristic deviations from randomness. In fig. (5-3) we show the film and bulk structure factors from an equilibrated sample⁴.

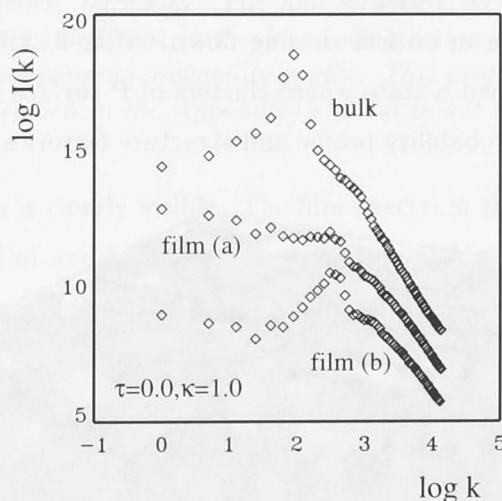


Figure 5-3: Film and bulk structure factors from a sample equilibrated with $\kappa = 1$, $\tau = 0$. Final curvatures were $\psi_0/\psi_0^{GRS} \approx 0.64$ and $\chi_0/\chi_0^{GRS} \approx 1.17$.

The bulk structure factor has undergone little change. We notice a slight shift towards lower frequencies. For the film structure factor, however, both methods (a) and (b) show now clearly that relative to the initial state a peak pattern at $2k_0$ has either evolved or become more pronounced. This indicates an increase in correlation which – due to the changes in the curvatures – can only be of local minimal surface-like nature. We may therefore conclude that we even expect rather soft sponges (with saddle-splay modulus

⁴This equilibration was used as the *drosophila* in this simulation. Runs were started from GRS, cubic and lamellar structures and were equilibrated over long run times, cf. Appendix. The results can be viewed with a high degree of confidence.

close to zero) to depart from randomness into a weak locally minimal surface-like organization, consistent with the picture of the sponge as a molten cubic phase proposed by [129, 22, 5]. In the Appendix we will also show that the same equilibrium structure can be reached after very short equilibration time when we start the simulation with a cubic phase and literally melt it. For increasing κ the trend to higher connectivity rises. The film scattering peak at $2k_0$ becomes successively more sharp for $\tau = 0$ and higher values of $\kappa > 1$ (*cf.* fig. (5-5)).

This tendency even prevails for non-zero τ *e.g.* for $\kappa = 5.0$, $\tau = 0.2$. Although there is now an energetic penalty for saddles we find equilibrium values of $\psi_0/\psi_0^{GRS} \approx 0.35$ and $\chi_0/\chi_0^{GRS} \approx 1.09$. The spectra are similar to the ones for $\kappa = 1$, $\tau = 0$, but with a sharper peak in the film scattering structure factor.

Finally, we tried to probe into the region of high κ , $\tau = 0$ and found that the equilibration time became untractable due to critical slowing down. After $2 \cdot 10^6$ MC steps a system with $\kappa = 10$, $\tau = 0$ has reached a state where clusters of P-surface like shape are clearly discernible, fig. (5-4). The probability profile and structure factors are shown in fig. (5-5).

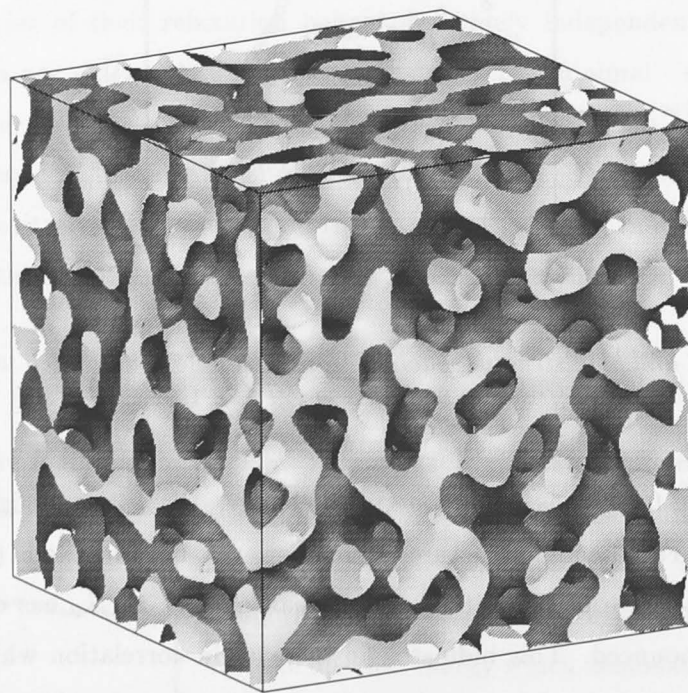


Figure 5-4: Three dimensional image of the interfacial structure, $\kappa = 10.0$, $\tau = 0.0$ after $2 \cdot 10^6$ MC updates. It has ratios of final and initial curvatures of $\psi_0/\psi_0^{GRS} \approx 0.14$ and $\chi_0/\chi_0^{GRS} \approx 1.29$, with an absolute $\chi_0 \approx 0.27$ just below that of a periodic minimal D-surface.

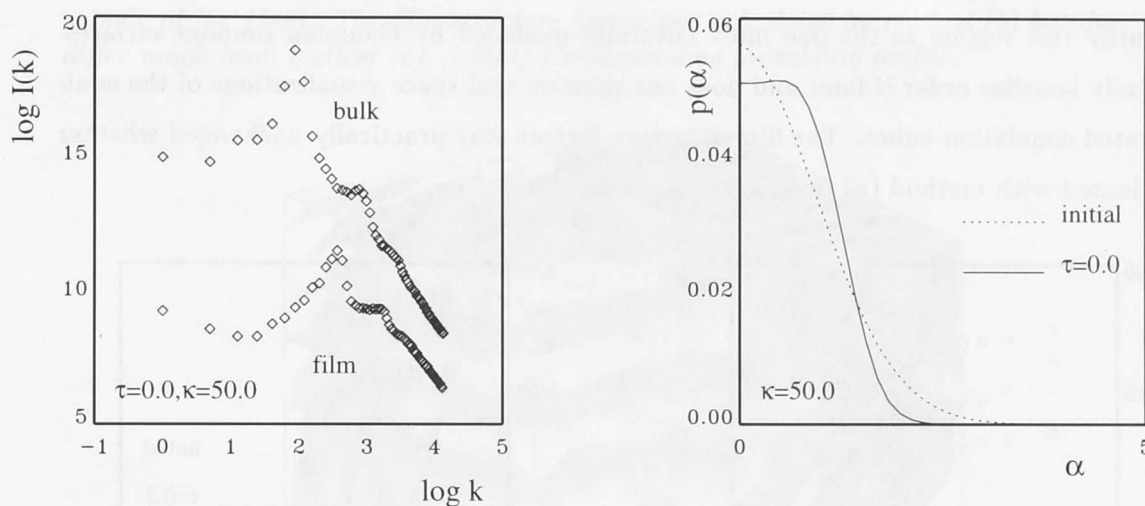


Figure 5-5: (left) Film and bulk structure factors from the strongly locally minimal surface-like sample above, fig. (5-4). The film structure factors calculated from methods (a) and (b) are not very different in the interesting region so that we only show method (b) here. (right) Corresponding probability profile. This profile can be compared to that of a genuine P-surface (given in the Appendix) and turns out to have quite similar shape.

The onset of ordering is clearly visible. The film spectrum shows now a sharp correlation peak at $2k_0$. Both film and bulk spectra show several higher order peaks indicative of a strong tendency to build up a more ordered structure. At the same time there is no indication that the overall isotropy has been broken. It is worthwhile mentioning that the existence of non-periodic, isotropic yet truly minimal surfaces is an unresolved problem [130]. Structures of the kind fig. (5-5) could be candidates. For periodic minimal surfaces we know that

$$0.28 < \chi_0 < 0.37, \quad \psi_0 = 0 \quad (5.13)$$

so that the above case of $\kappa = 10.0, \tau = 0.0$ with $\chi_0 \approx 0.27$ and a drop of the mean square curvature to 10% of its initial GRS value are converging towards a state structurally similar to periodic minimal surfaces.

(iii) Lamellar: $0.3 \lesssim \tau \lesssim 1.0$

In this region all samples drifted towards a more or less lamellar structure compared to ideal randomness. For soft membranes, $\kappa = 1$, this tendency was very weak and we found that equilibrated structures in the entire regime were practically indistinguishable from the initial Gaussian configuration in terms of all probed quantities: internal energy,

curvatures, one point distribution and structure factors (*cf.* fig. (5-6)). We may therefore identify this regime as the one most faithfully modelled by Gaussian random surfaces. Locally lamellar order is faint and does not show on real-space visualizations of the equilibrated simulation cubes. The film structure factors stay practically unchanged whether evaluated with method (a) or (b).

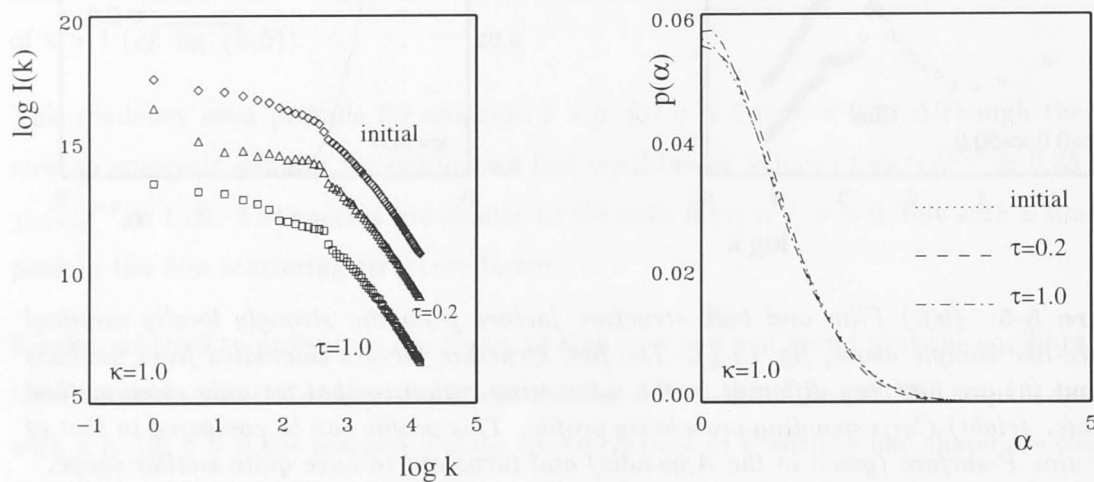


Figure 5-6: (left) Equilibrated film structure factors, gained from method (a), compared to the initial shape. (right) Corresponding probability profiles.

For rising κ , however, the picture changes dramatically. For $\kappa = 5.0$, $\tau = 0.4$ the system gets caught in successive metastable states and the equilibration does not appear complete even after $6 \cdot 10^6$ MC steps indicative of the approach to a phase transition. The state of the system changes strongly in comparison to the initial random configuration. In fig. (5-8) we show the real-space image of the simulation cube. In fig. (5-7) the structure factors and probability profile corresponding to fig. (5-8) are presented.

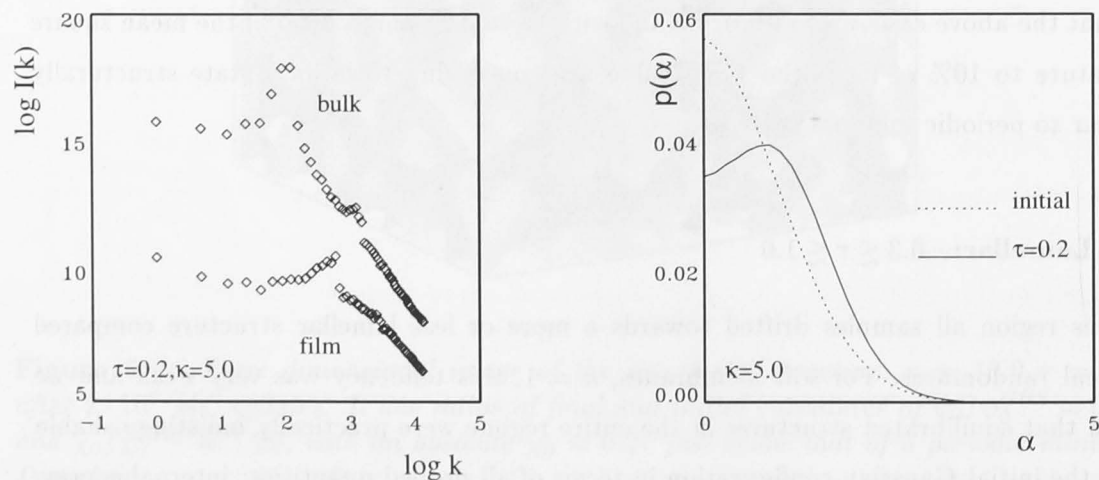


Figure 5-7: (left) Film and bulk structure factors from the locally lamellar, metastable sample of fig. (5-8). The film structure factor was calculated by method (b) but does not differ much from method (a). (right) Corresponding probability profile.

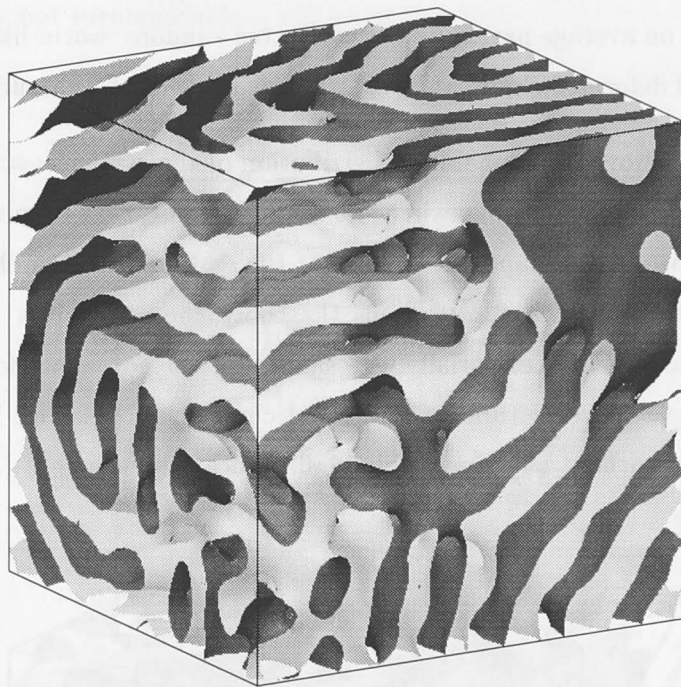


Figure 5-8: Three dimensional image of the interfacial structure, $\kappa = 5.0, \tau = 0.4$ after $6 \cdot 10^6$ MC updates. It has ratios of final and initial curvatures of $\chi_0/\chi_0^{GRS} \approx 0.37$ and $\psi_0/\psi_0^{GRS} \approx 0.4$. The undulations of the stacked layers in the lamellar regions are very smooth, as expected from a system driven by curvature elasticity.

While in fig. (5-8) large regions show lamellar order, some regions still retain disordered character typical for metastability. Overall, the system appears to be still isotropic [131]. In any way, there can be little doubt that at $\kappa = 5$ the S/L transition is imminent. The most notable feature in the 'lamellar' bulk structure factor is the shift of the peak to a higher wave vector, as expected for lamellar ordering where the swelling law, eqn. (3.49), is $\beta \approx 1$ in contrast to the swelling of a sponge, $\beta > 1$. We also see higher order peaks at odd multiples of k_0 which are characteristic of a lamellar square wave and which stress the tendency of the system to converge towards an ordered state. Similarly, the film structure factor also reveals a strong correlation peak at $\approx 2k_0$ which has clearly moved towards higher k as well as higher reflections at even multiples of $2k_0$. Finally the probability profile shows a characteristic double peaked shape ($\alpha < 0$ is symmetric) in agreement with what is termed order parameter distribution in the lamellar region of a Ginzburg-Landau MC due to Gompper & Kraus [127].

(iv) Worm / Vesicle - Like: $1.0 \lesssim \tau \leq 2.0$

In this regime the final state of the system has less connectivity χ_0 and higher mean square curvature ψ_0 than the initial state. Our results support the idea of an equilibrium structure which is on average parabolic *i.e.* connected random 'worm-like' shapes [132] or random clusters of deformed closed objects (lamellar phase with spherulite texture [110]).

Neither structure factors nor probability distribution of the system $\kappa = 1.0, \tau = 2.0$ after $6 \cdot 10^6$ MC steps show much change where we note, however, that despite the substantial runtime critical slowing down appears to prevent the system from complete equilibration. In any way, we observed after $6 \cdot 10^6$ steps that both the probability distribution, and the structure factors stayed essentially the same and do not allow for any particular conclusion. The real-space picture fig. (5-9) and curvatures, however, indicate a strong loss of connectivity without any discernible kind of local ordering.

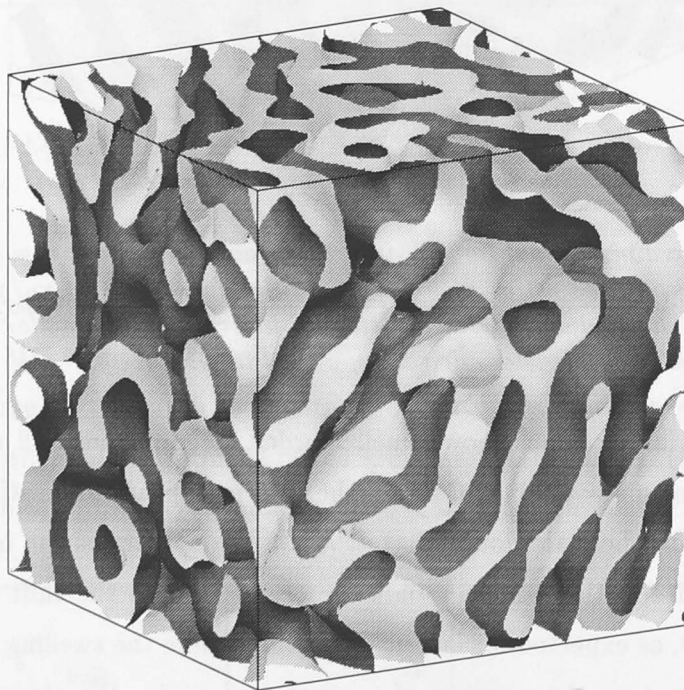


Figure 5-9: Three dimensional image of the interfacial structure, $\kappa = 1.0, \tau = 2.0$ after $6 \cdot 10^6$ MC updates. It has ratios of final and initial curvatures of $\chi_0/\chi_0^{GRS} \approx 0.15$ and $\psi_0^{GRS}/\psi_0 \approx 1.4$. Note the parabolic endcap in the centre of the righthand face.

From the extremely low Euler characteristic, $\chi_0 \approx 0.03$, we can conclude that the genuine end state will not or hardly be on average hyperbolic. Whether the final state will be worm-like or vesicular, however, cannot be decided here. In any way, it is remarkable that

even in the absence of spontaneous curvature the formation of parabolic structures can be approached by variation of the Gaussian modulus only. Although the technological importance of bilayer vesicles would make runs for higher values of κ desirable, the runtime effort is currently not surmountable.

In figs. (5-10,5-11) we summarize the results in the four regimes.

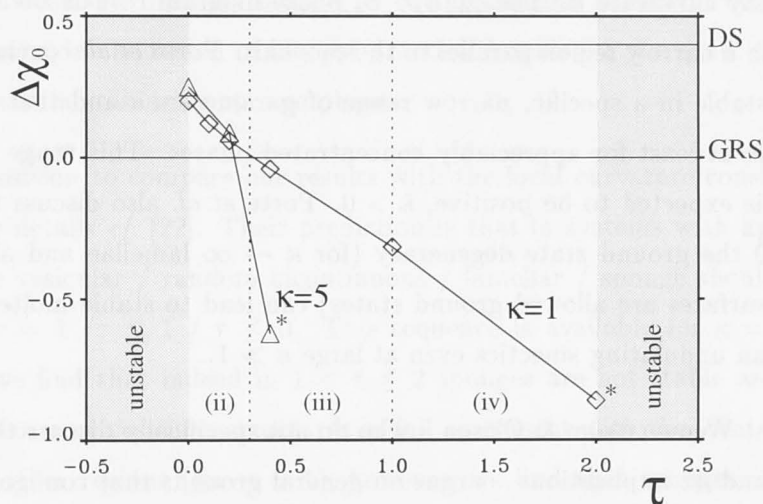


Figure 5-10: Deviation of the scaled Euler characteristic from the Gaussian values, $\Delta\chi_0 = (\chi_0 - \chi_0^{GRS})/\chi_0^{GRS}$ for samples equilibrated under various values of τ and κ (samples labelled \star are after a large number of MC steps still drifting downwards). The horizontal line marked 'DS' gives the value of $\Delta\chi_0$ for the minimal D-surface.

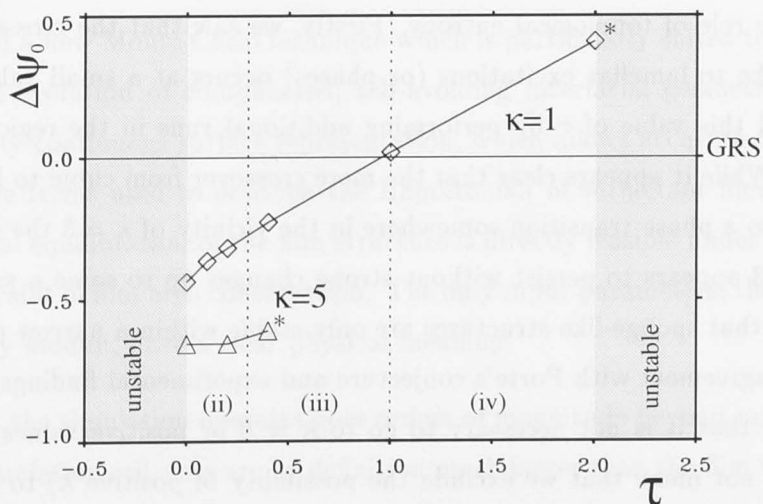


Figure 5-11: Same as fig. (5-10) for $\Delta\psi_0$. Samples labelled by \star are again still drifting, downwards in the case $\kappa = 5$ and upwards for $\kappa = 1$. From comparison with fig. (5-10) we see that for $\kappa = 5$ similar values of the mean square curvature can be associated with vastly different topologies.

Discussion Previous work concerned with similar aspects of the stability of sponge phases is mainly that of Porte *et al.* and Anderson *et al.* These authors investigate and discuss the well-known experimental fact that sponges at not too low concentration (*i.e.* in the scaling regime) appear to exist in a narrow range of the parameters ϕ_a/ϕ_s where ϕ_a is the concentration of alcohol in pseudoternary surfactant - alcohol - brine mixtures. This ratio is related by Porte *et al.* – using a model by Petrov *et al.* [133] – to the value of the saddle-splay curvature $\bar{\kappa}$. The $\phi_a/\phi_s - \phi_s$ phase diagram reveals then that the L_3 phase is stable in a narrow region parallel to the ϕ_s - axis. Porte *et al.* conclude that the sponge phase is stable in a specific, narrow range of parameters $\bar{\kappa}$ and that ϕ_s does not play a strong role at least for appreciably concentrated phases. This range of the saddle-splay modulus is expected to be positive, $\bar{\kappa} > 0$. Porte *et al.* also discuss the possibility that for $\bar{\kappa} = 0$ the ground state degeneracy (for $\kappa \rightarrow \infty$ lamellae and all possible periodic minimal surfaces are allowed ground states) can lead to stable molten minimal surfaces rather than undulating smectics even at large $\kappa \gg 1$.

In contrast Wennerström & Olsson – who do not specifically discuss the $\phi_a/\phi_s - \phi_s$ phase diagram and its implications – argue on general grounds that configurational ('topological') entropy from the formation of saddle-like connections could possibly offset the energy loss due to negative $\bar{\kappa}$ and that sponges can therefore be in principle stable at $\bar{\kappa} < 0$.

Our findings support, in part, both views. The main contribution of our simulation to this discussion is that we can actually make quantitative statements on the issue at stake, the role of topological entropy. Firstly, we saw that the crossover from minimal-surface like to lamellar excitations (or phases) occurs at a small value of $\tau \sim 0.3$. We confirmed this value of τ by performing additional runs in the region up to a value of $\kappa = 10$. While it appears clear that the mere crossover from cubic to lamellar excitations changes to a phase transition somewhere in the vicinity of $\kappa = 5$ the characteristic value of $\tau \sim 0.3$ appears to persist without strong changes up to some $\kappa \approx 10$ so that we can conclude that sponge-like structures are only stable within a narrow region in parameter space in agreement with Porte's conjecture and experimental findings. At the same time we found that it is not necessary to go to $\bar{\kappa} = 0$ or positive values, $\bar{\kappa} > 0$, (although this does not mean that we exclude the possibility of positive $\bar{\kappa}$) to overcome energetic constraints in agreement with Wennerström & Olsson's suggestion. On the other hand, we cannot confirm Wennerström & Olsson's claim that the Hamiltonian eqn. (1.2) leads to a thermodynamic instability and requires to be stabilized by higher order curvature

terms. There is no such indication in our data. Furthermore we cannot confirm that $\bar{\kappa}$ plays a much more important role than κ in stabilizing the sponge phase. While $\bar{\kappa}$ seems to assure stability of the sponge phase over a surprisingly large (though narrow in $\bar{\kappa}$) range of κ we also saw that the absolute value of κ is important. At small κ the range of sponge stability extends far beyond the minimum assured by topological entropy. For $\kappa = 1$ a sponge best described as a molten lamellar phase is stable for $0 < \tau < 1.0$. At the same time it is clear that for very large $\kappa \rightarrow \infty$ the lamellar state will be dominant for all $\bar{\kappa} < 0$. However, in the region of highest practical interest, $1 \lesssim \kappa \lesssim 10$, the role of $\bar{\kappa}$ is indeed prominent in stabilizing sponge phases.

We are also in a position to compare our results with the local curvature considerations by Porte *et al.*, for details *cf.* [22]. Their prediction is that in systems with appreciable entropy a sequence vesicular / random bicontinuous / lamellar / sponge should be seen for $1 < \tau \leq 2$ / $\tau = 1$ / $\tau \leq 1$ / $\tau \leq 0$. This sequence is available for $\kappa = 1$ in our simulation where we find that indeed in $1 < \tau \leq 2$ sponges are not stable and at best loosely connected worm or vesicular structures in full agreement with the local curvature argument. In the other regions (for $\kappa = 1$), however, we find that sponges are always stable although they are not necessarily Gaussian.

5.4 Summary and Outlook

We have introduced a new Monte Carlo technique which is particularly suited to simulate the configurational evolution of complicated, self-avoiding interfacial geometries. It is based on a genuinely continuous surface representation, which allows accurate evaluation of surface curvature terms used to describe the Hamiltonian of surfactant film systems. Thus configurational equilibration of the film structure is directly feasible under the physically crucial constraint of film area conservation. The only input parameters, the bending and the saddle-splay moduli, have a clear physical meaning.

The scale on which the simulation operates goes orders of magnitude beyond microscopic simulations. All simulation cell sizes are by definition much larger than the film thickness, $d_0 \gg r_c$, setting the scale of our simulation sample between hundreds and thousands of Ångstroms. The only simulation comparable in these scales is the one of Gompper & Kraus [127]. However, we have to note that the simulation presented here and in [127] are practically not comparable. In [127] an effective GL free energy is assumed with five

adjustable parameters which are preset in a way so that only sponges and lamellae are possible. The only area where the two simulations seem to overlap is the probability distribution in lamellar phases. Comparison with respect to most other aspects is not possible because the mapping of the parameter spaces is unclear and can be only done when Gompper & Kraus use concepts of effective interface theory such as the connectivity of interfaces. There the GL sponges have $\chi_0 \approx 0.17$ compared to a typical $\chi_0 \approx 0.25$ for sponges in our simulation.

The insights gained from our simulation encourage its more general application. New areas of investigation should include

1. spontaneous curvature, $H_0 \neq 0$,
2. higher order bending terms,
3. stacks of layers beyond the harmonic approximation of the Hamiltonian,
4. single vesicles, where the base functions in eqn. (1.12) should be chosen *e.g.* as spherical Bessel functions.

All of these require only marginal changes to the existing algorithm.

5.A Appendix

The Appendix contains some of the necessary precautions and checks done in MC simulations [134]: checking of the algorithms, equilibration, sensitivity to initial conditions, error estimates. Particularly for a practically unknown simulation technique as introduced in this chapter this discussion is relevant.

Surface Integrals To gain an estimate of the accuracy of the algorithm we compare with known results for the periodic Schwarz P-surface, eqn. (5.9), and the aperiodic Gaussian random surface for a spectrum $\nu(k) \sim \delta(k - k_0)$. For a fine grid size of 32 per unit cell we found errors of only $\approx 0.16\%$, $\approx 0.26\%$, for surface area and average Gaussian curvature of the P-surface.

In the case of random interfaces we have to average over several independent configurations and the sample size has to be large enough to assure good statistics. We list results for various asymmetries α in the following table. We used 6 unit cells side length for a cubic sample, a grid density of 128 and averaged over 50 independent configurations

	ex.	num.	ex.	num.	ex.	num.	ex.	num.
	$\alpha = 0$		$\alpha = 0.1$		$\alpha = 0.2$		$\alpha = 0.5$	
S/V	0.367	0.368	0.365	0.366	0.360	0.360	0.323	0.324
$(S/V)^{-1} \langle \delta(s) \vec{\nabla}s H \rangle_0$	0	10^{-3}	0.0362	0.0380	0.0724	0.0723	0.181	0.183
$-(S/V)^{-1} \langle \delta(s) \vec{\nabla}s K \rangle_0$	0.167	0.168	0.165	0.167	0.16	0.162	0.125	0.121
$(S/V)^{-1} \langle \delta(s) \vec{\nabla}s H^2 \rangle_0$	0.0333	0.0345	0.0350	0.0363	0.0400	0.0413	0.0750	0.0773
$(S/V)^{-1} \langle \delta(s) \vec{\nabla}s HK \rangle_0$	0	10^{-4}	0.0106	0.00905	0.0218	0.0186	0.0642	0.0641

(values for $(S/V)^{-1} \langle \delta(s) |\vec{\nabla}s| H^3 \rangle_0$ are too small to allow for sensible comparison). All numerical results (denoted 'num.>') compare well with the exact ones (denoted 'ex.>') gained from eqn. (3.A3) - eqn. (3.A7).

Finite Size Effects Finite size effects were checked by re-running samples of twice the side length ($14d_0$) and a grid density of 128, for the case $\kappa = 1$, $\tau = 0$ without visible effect on the results. Finite-size effects were observed for side lengths smaller than $\approx 4d_0$.

Equilibration, Initial Conditions We checked equilibration for several cases and under various circumstances. Firstly, we did very long runs (starting from a GRS) for two cases, $\kappa = 1$, $\tau = 0$, and $\kappa = 5$, $\tau = 0.2$. Equilibration of the internal energy is shown in fig. (5-12)

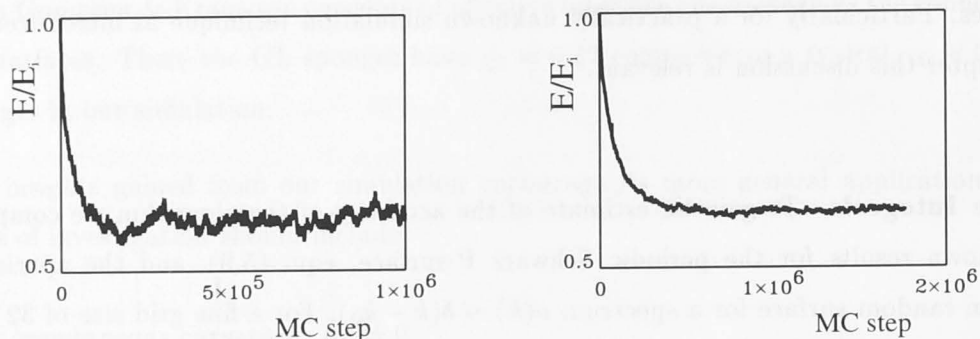


Figure 5-12: *Equilibration of the internal energy for $\kappa = 1$, $\tau = 0$, (left) and $\kappa = 5$, $\tau = 0.2$, (right) for initial random surface states.*

For the swiftly equilibrating system $\kappa = 1$, $\tau = 0$, 10^6 MC steps are enough to achieve an averaging time roughly a factor of 10 larger than the relaxation time. For $\kappa = 5$, $\tau = 0.2$, $1.75 \cdot 10^6$ suffice only to achieve an averaging time about three times larger than the relaxation time. Equilibration of the topology and mean square curvature follows the same pattern. We also checked the equilibration of probability profiles, with similar results.

Next, we check the sensitivity to the initial state. To make sure that results from very different initial states are compared we performed two very long runs for $\kappa = 1$, $\tau = 0$ which started from a P-surface and the locally lamellar surface fig. (5-8). Fig. (5-13) shows the result for the scaled topologies

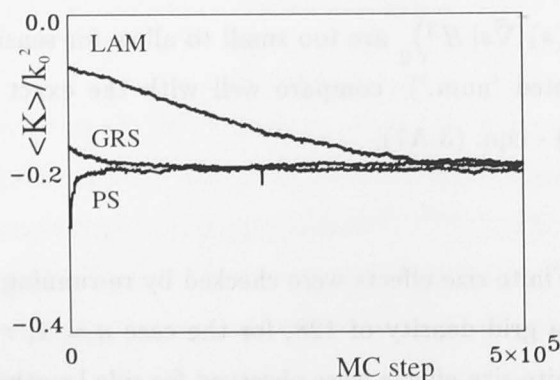


Figure 5-13: *Equilibration of the scaled Euler characteristic for $\kappa = 1$, $\tau = 0$ starting from initially Gaussian random, cubic and strongly lamellar interfaces labelled (GRS), (PS), (LAM), respectively. Internal energies and mean square energies follow similar patterns.*

where we note the very quick equilibration when the initial state is a cubic phase. On the other hand, equilibration starting from a strongly lamellar geometry is slow. In fig. (5-13) all runs were performed over 10^6 steps; only the first $5 \cdot 10^5$ are shown in order to make the equilibration from the random and the cubic phase visible. We verify the similarity of the final states also in their film scattering curves and probability profiles

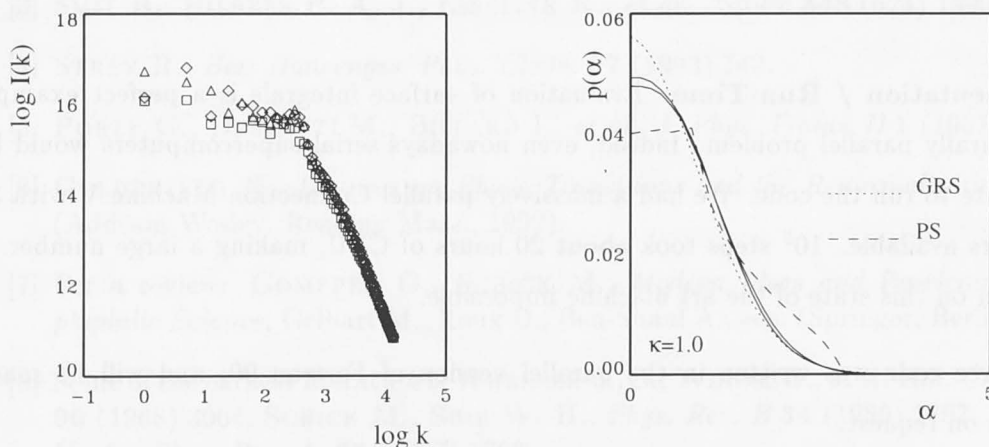


Figure 5-14: (left) *Film scattering (computed by method (a)) for $\kappa = 1$, $\tau = 0$ after 10^6 MC steps where initial states were random (\diamond), cubic (\triangle) and lamellar (\square). (right) *Field distributions for the same cases where PS denotes P-surface.**

The film spectra which started from random and cubic phases are practically indistinguishable, while the one which started from a locally lamellar structure appears a little off; we attribute this to the very long equilibration time so that the final state is expected to have a larger error.

We also cross-checked the final state of the run $\kappa = 5$, $\tau = 0.2$ by using an initial state biased towards a lamellar structure with initial $\chi_0 \approx 0.13$, $\psi_0 \approx 0.016$. Although the long equilibration time goes beyond our possibilities (the lamellar state is very far away from the final state) we can confirm that within the $5 \cdot 10^5$ steps we monitored the structure drifts systematically towards higher connectivity. We can therefore practically exclude the possibility that a lamellar state would be stable for these parameters.

Statistical Error The error estimate can be calculated by usual statistical analysis [135, 23]. The sampling points were taken well after the relaxation time and at distances of 10^3 MC steps to avoid correlation. This results in an error estimate of between 5% and 10% depending on the length of the run.

A better way of estimating the error would be by running several simulations for the same parameters [135] (we did this to some extent above to assure that metastability is not affecting the results) and comparing the final results. To do this we had to avoid the most studied parameter region which is too costly in run time and we only tested systems for parameters bound to equilibrate faster. For $\kappa = 0.25$, $\tau = 0$, 10^5 MC steps are sufficient to reach equilibrium. The final energies of 10 runs which started from different GRS configurations did not differ by more than 10%.

Implementation / Run-Time Evaluation of surface integrals is a perfect example of a naturally parallel problem. Indeed, even nowadays serial supercomputers would be inadequate to run the code. We had a massively parallel Connection Machine V with 32 processors available. 10^5 steps took about 20 hours of CPU, making a large number of runs even on this state of the art machine impossible.

The source code was written in the parallel version of Fortran 90, and will be made available on request.

Bibliography

- [1] For reviews, *e.g.*, *Physics of Amphiphilic Layers*, Meunier J., Langevin D., Boccara N., eds. (Springer, Berlin, 1987), *Statistical Mechanics of Membranes and Surfaces*, Nelson D., Weinberg S., eds. (World Scientific, Singapore, 1989), *Structure and Dynamics of Strongly Interacting Colloids and Supramolecular Aggregates in Solution*, Chen S. H., Huang J. S., Tartaglia, P., eds. (Kluwer, Boston, 1992), *Modern Ideas and Problems in Amphiphilic Science*, Gelbart W. M., Roux D., Ben - Shaul A., eds. (Springer, Berlin, 1994), *Phase Transitions and Critical Phenomena*, Vol. 16, Domb C., Lebovitz J., eds. (Academic Press, London, 1994).
- [2] SAFRAN S. A., *Statistical Thermodynamics of Surfaces, Interfaces, and Membranes* (Addison Wesley, Reading Mass., 1994).
- [3] SMIT B., HILBERS P. A. J., ESSELINK K., *et al.*, *Nature* **348** (624) 1990.
- [4] STREY R., *Ber. Bunsenges. Phys. Chem.* **97** (1993) 742.
- [5] PORTE G., DELSANTI M., BILLARD I., *et al.*, *J. Phys. France II* **1** (1991) 1101.
- [6] GOLDENFELD N., *Lectures on Phase Transitions and the Renormalization Group* (Addison Wesley, Reading Mass., 1992).
- [7] For a review: GOMPPER G., SCHICK M., *Modern Ideas and Problems in Amphiphilic Science*, Gelbart M., Roux D., Ben-Shaul A., eds. (Springer, Berlin, 1994).
- [8] Some of the earliest literature is WHEELER J. C., WIDOM B., *J. A. Am. Chem. Soc.* **90** (1968) 3064, SCHICK M., SHIH W. H., *Phys. Rev. B* **34** (1986) 1797, DAWSON K. A., *Phys. Rev. A* **35** (1987) 1766.
- [9] LARSON R. G., SCRIVEN L. E., DAVIS H. T., *J. Chem. Phys.* **83** (2411) 1985.
- [10] LARCHE F. C., APPELL J., PORTE G., *et al.*, *Phys. Rev. Lett.* **56** (1986) 1700.
- [11] TEUBNER M., STREY R., *J. Chem. Phys.* **87** (1987) 3195.
- [12] ROUX D., CATES M. E., OLSSON U. *et al.*, *Europhys. Lett.* **11** (1990) 229, COULON C., ROUX D., BELLOCQ A. M., *Phys. Rev. Lett.* **66** (1991) 1709, COULON C., ROUX D., CATES M. E., *Phys. Rev. Lett.* **67** (1991) 3194, GRANEK, R. AND CATES M. E., *Phys. Rev. A* **46** (1992) 3319, ROUX D., COULON C., CATES M. E., *J. Phys. Chem.* **96** (1992) 4174.
- [13] GOMPPER, G., SCHICK M., *Phys. Rev. B.* **41** (1990) 9148 and references therein.
- [14] BROCHARD F., DE GENNES P. -G., PFEUTY P., *J. Phys. France* **37** (1976) 1099.
- [15] LEIBLER S., LIPOWSKY R., PELITI L., in *Physics of Amphiphilic Layers*, Meunier J., Langevin D., Boccara N., eds. (Springer, Berlin, 1987).
- [16] CANHAM P. B., *J. Theor. Biol.* **26** (1970) 61, HELFRICH W., *Z. Naturforsch.* **28c** (1973) 693.

- [17] For example: FRÖHLICH J., in *Progress in Gauge Field Theory*, 't Hooft G., ed. (Plenum, New York, 1984), KAROWSKI M., THUN H. J., *Phys. Rev. Lett.* **54** (1985) 2556, DAVID F., *Europhys. Lett.* **9** (575) 1989.
- [18] BINKS B. P., KELLAY H., MEUNIER J., *Europhys. Lett.* **16** (1991) 53 and references therein.
- [19] BEN - SHAUL A., SZLEIFER L., GELBART W. M., in *Physics of Amphiphilic Layers*, Meunier J., Langevin D., Boccara N., eds. (Springer, Berlin, 1987) and references therein.
- [20] KELLAY H., MEUNIER J., BINKS B. P., *Phys. Rev. Lett.* **70** (1993) 1485 and references therein.
- [21] STREY R., WINKLER J., MAGID L., *J. Phys. Chem.* **95** (1991) 7502.
- [22] PORTE G., APPELL J., BASSEREAU P., *et al.*, *J. Phys. France* **50** (1989) 1335.
- [23] YEOMANS J. M., *Statistical Mechanics of Phase Transitions* (Clarendon Press, Oxford, 1992).
- [24] CHEN S.-H., CHANG S.-L., STREY R., *J. Appl. Cryst.* **24** (1991) 721.
- [25] SAFRAN S. A., *Langmuir* **7** (1991) 1864.
- [26] HELFRICH W., *Z. Naturforsch.* **33a** (1978) 305.
- [27] WENNERSTRÖM, H., OLSSON, U., *Langmuir* **9** (1993) 365.
- [28] TALMON Y., PRAGER S., *J. Chem. Phys.* **69** (1978) 2984.
- [29] DE GENNES P. G., TAUPIN C., *J. Phys. Chem.* **86** (1982) 2294.
- [30] WIDOM B., *J. Chem. Phys.* **81** (1984) 1030.
- [31] SAFRAN S. A., ROUX D., CATES M. E. *et al.*, *Phys. Rev. Lett.* **57** (1986) 2718, MILNER S. T., SAFRAN S. A., ANDELMAN D. *et al.*, *J. Phys. France* **49** (1988) 1065, ANDELMAN D., CATES M. E., ROUX D. *et al.*, *J. Chem. Phys.* **87** (1987) 7229, CATES M. E., ROUX D., ANDELMAN D. *et al.*, *Europhys. Lett.* **5** (1988) 733, CHANDRA P., SAFRAN S. A., *Europhys. Lett.* **17** (1992) 691.
- [32] GOLUBOVIĆ L., LUBENSKY T. C., *Europhys. Lett.* **10** (1989) 513, GOLUBOVIĆ L., LUBENSKY T. C., *Phys. Rev. A* **41** (1990) 4343.
- [33] HUSE D. A., LEIBLER S., *J. Phys. France* **49** (1988) 605; HUSE D. A., LEIBLER S., *Phys. Rev. Lett.* **66** (1991) 437.
- [34] BERK, N. F., *Phys. Rev. Lett.* **58** (1987) 2718.
- [35] CAHN J. W., *J. Chem. Phys.* **42** (1965) 93.
- [36] ADLER R. J., *The Geometry of Random Fields* (John Wiley, New York, 1981).
- [37] TEUBNER, M., *Europhys. Lett.* **14** (1991) 403.
- [38] MARČELJA S., *J. Phys. Chem.* **94** (1990) 7259.

- [39] AUVRAY L., COTTON J.-P., OBER R., TAUPIN C., *J. Phys. Chem.* **88** (1984) 4586, AUVRAY L., COTTON J.-P., OBER R., TAUPIN C., *J. Phys. France* **45** (1984) 913.
- [40] DEBYE P., ANDERSON H. R., BRUMBERGER H., *J. Appl. Phys.* **20** (1949) 518, DEBYE P., ANDERSON H. R., BRUMBERGER H., *J. Appl. Phys.* **28** (1957) 679.
- [41] WANG M. C., UHLENBECK G. E., *Rev. Mod. Phys.* **17** (1945) 323.
- [42] PIERUSCHKA P., MARČELJA S., *J. Phys. II France* **2** (1992) 235.
- [43] FEYNMAN R. P., *Statistical Mechanics* (Addison Wesley, Reading Mass., 1972).
- [44] SHANNON C. E., WEAVER W., *The Mathematical Theory of Communication* (Univ. of Illinois Press, Urbana, Ill., 1949).
- [45] MIDDLETON D., *An Introduction to Statistical Communication Theory* (McGraw Hill, New York, 1960).
- [46] DE GENNES P. G., *The Physics of Liquid Crystals* (Clarendon Press, Oxford, 1974).
- [47] SAFINYA C. R., ROUX D., SMITH G. S., *et al.*, *Phys. Rev. Lett.* **57** (1986) 2718, ROUX D., SAFINYA C. R., *J. Phys. France* **49** (1988) 307.
- [48] CAILLE A., *C. R. Acad. Sc. Paris* **274** (1972) 891.
- [49] BASSEREAU P., MARIGNAN J., PORTE G., *J. Phys. France* **48** (1987) 673.
- [50] PORTE G., MARIGNAN J., BASSEREAU P. *et al.*, *Europhys. Lett.* **7** (1988) 713.
- [51] GOLUBOVIĆ L., LUBENSKY T. C., *Phys. Rev. B* **39** (1989) 12110.
- [52] For a detailed review of Helfrich's and subsequent work: SORNETTE D., OSTROWSKY N. in *Micelles, Membranes, Microemulsions and Monolayers*; Gelbart W. M., Ben - Shaul A., Roux D., eds., (Springer, New York, 1993).
- [53] DAVID F., LEIBLER S., *J. Phys. France III* **1** (1991) 959; the authors discuss in detail the extensive variables (real and projected film area) and their conjugate surface tension terms.
- [54] FOGDEN A., MITCHELL D. J., NINHAM B. W., *Langmuir* **6** (1990) 159.
- [55] PORTE G., BASSEREAU P., MARIGNAN J. *et al.*, in *Physics of Amphiphilic Layers*, Meunier J., Langevin D., Boccara N., eds. (Springer, Berlin, 1987).
- [56] JANKE W., KLEINERT H., *Phys. Lett. A* **117** (1986) 353, JANKE W., KLEINERT H., *Phys. Rev. Lett.* **58** (1987) 144, GOMPPER G., KROLL D. M., *Europhys. Lett.* **9** (1989) 59.
- [57] ROUX D., NALLET F., FREYSSINGEAS E., *et al.*, *Europhys. Lett.* **17** (1992) 575.
- [58] HELFRICH W., *J. Phys. France* **46** (1985) 1263.
- [59] KLEINERT, H., *Phys. Lett.* **114A** (1986) 263.
- [60] PELITI L., LEIBLER S., *Phys. Rev. Lett.* **54** (1985) 1690.

- [61] SMIRNOW W. I., *Lehrgang der Höheren Mathematik*, Vol. 4 (VEB Deutscher Verlag der Wissenschaften, Berlin, 1982).
- [62] MITCHELL D. J., NINHAM B., PIERUSCHKA P., to appear.
- [63] ROUX D., private communication.
- [64] CAI W., LUBENSKY T. C., POWERS T., *et al.*, *J. Phys. II France* **4** (1994) 931.
- [65] AMIT D. J., *Field Theory, the Renormalization Group, and Critical Phenomena* (World Scientific, Singapore, 1989).
- [66] BERLIN, T. H., KAC, M., *Phys. Rev.* **86** (1952) 821.
- [67] GOMPPER G., SCHICK M., *Phys. Rev. E* **49** (1994) 1478 and references therein.
- [68] GOMPPER G., ZSCHOCKE S., *Europhys. Lett.* **16** (1991) 731, GOMPPER G., ZSCHOCKE S., *Phys. Rev. A* **46** (1992) 4836.
- [69] LERCZAK J., SCHICK M., GOMPPER G., *Phys. Rev. A* **45** (1992) 7309.
- [70] ENNIS J., *J. Chem. Phys.* **97** (1992) 663.
- [71] KELLAY H., HENDRIKX Y., MEUNIER J., *et al.*, *J. Phys. II France* **3** (1993) 1747.
- [72] CHEN S. H., private communication.
- [73] CURTIS S. R., OPPENHEIM A. V., *J. Opt. Soc. Am. A* **4** (1987) 221.
- [74] JAYNES E. T., *Papers on Probability, Statistics, and Statistical Physics*, Rosenkrantz R. D., ed. (D. Reidel, Dordrecht, 1983).
- [75] BERK N. F., *Phys. Rev. A* **44** (1991) 5069.
- [76] CHEN S.-H., LEE D., CHANG S.-L., *J. Mol. Struct.* **296** (1993) 259.
- [77] VINCHES C., COULON C., ROUX D., *J. Phys. II France* **4** (1994) 1165.
- [78] ZEMB T., private communication.
- [79] FILALI M., PORTE G., APPELL J., PFEUTY P., *J. Phys. France II* **4** (1994) 349.
- [80] HUSE D., LEIBLER S., *Phys. Rev. Lett.* **66** (1991) 1709.
- [81] TEUBNER M., private communication.
- [82] GOMPPER G., HENNES M., *J. Phys. France II* **4** (1994) 1375.
- [83] GOMPPER G., GOOS J., *Phys. Rev. E* **50** (1994) 1325.
- [84] MARČELJA S., PIERUSCHKA P., SAFRAN S. A., submitted to *Phys. Rev. E*.
- [85] STREY R., SCHOMÄCKER R., ROUX D. *et al.*, *J. Chem. Soc. Faraday Trans.* **86** (1990) 2253.
- [86] PORTE G., MARIGNAN J., BASSEREAU P. *et al.*, *J. Phys. France* **49** (1988) 511.

- [87] SCHUBERT K. V., STREY R., *J. Chem. Phys.* **95** (1991) 8532.
- [88] JAHN W., STREY R., *J. Phys. Chem.* **92** (1988) 2294.
- [89] SAFRAN S. A., in *Modern Ideas and Problems in Amphiphilic Science*, Gelbart W. M., Roux D., Ben - Shaul A., eds. (Springer, Berlin, 1994).
- [90] DE GEYER A., TABONY J., *Chem. Phys. Lett.* **124** (1986) 357.
- [91] SKOURI M., MARIGNAN J., APPELL J., PORTE G., *J. Phys. France II* **1** (1991) 1121.
- [92] GAZEAU D., BELLOCQ A. M., ROUX D., *et al.*, *Europhys. Lett.* **9** (1989) 447.
- [93] GAZEAU D., PhD Thesis (Bordeaux, 1989).
- [94] KABALNOV A., OLSSON U., WENNERSTRÖM H., *Langmuir* to appear.
- [95] MORSE, MILNER, *Europhys. Lett* **26** (565) 1994.
- [96] PLISCHKE M., BERGERSEN B., *Equilibrium Statistical Physics* (Prentice - Hall, New Jersey, 1989).
- [97] BLUME M., EMERY V., GRIFFITHS R. B., *Phys. Rev. A.* **4** (1971) 1071.
- [98] STURGEON K. S., REISS H., *J. Chem. Phys.* **98** (1993) 1493.
- [99] MENES R., SAFRAN S. A., Reentrant Phase Separation in Microemulsions, submitted to *Phys. Rev. Lett.*
- [100] WEATHERBURN, C. E., *Differential Geometry of Three Dimensions* (Cambridge University Press, Cambridge, 1955).
- [101] SHVARTSMAN N, FREUND I., *Phys. Rev. Lett.* **72** (1994) 1008, BERRY M. V., ROBNIK M., *J. Phys. A: Math. Gen.* **19** (1986) 1365, BERRY M. V., *J. Phys. A: Math. Gen.* **11** (1977) 27.
- [102] GRADSHTEYN I. S., RYZHIK J. M., *Table of Integrals, Series, and Products* (Academic Press, San Diego, 1993).
- [103] BRAZOVSKII S. A., *Sov. Phys.-JETP* **41** (1975) 85.
- [104] CATES M. E., *Physica A* **176** (1991) 187.
- [105] MORSE D. C., MILNER S. T., *Phys. Rev. E* **47** (1993) 1119.
- [106] CATES M. E., *Colloque de Physique* **51** (1990) C7-73.
- [107] STREY R., JAHN W., PORTE G. *et al.*, *Langmuir* **6** (1990) 1635.
- [108] ANDERSON, D., WENNERSTRÖM, H., OLSSON, U., *J. Phys. Chem.* **50** (1989) 1335.
- [109] PORTE G., private communication.
- [110] BOLTENHAGEN P., KLÉMAN M., LAVRENTOVICH O. D., *J. Phys. II France* **4** (1994) 1439.

- [111] MONASTYRSKY M., *Topology of Gauge Fields and Condensed Matter* (Plenum, New York, 1993).
- [112] MAIER W., SAUPE A., *Z. Naturforsch.* **A14** (882) 1959, MAIER W., SAUPE A., *Z. Naturforsch.* **A15** (287) 1960.
- [113] KNACKSTEDT M. A., private communication.
- [114] KANTOR Y., NELSON D. R., *Phys. Rev. Lett.* **58** (1987) 2774.
- [115] BAUMGÄRTNER A., HO J.-S., *Phys. Rev. A* **41** (1990) 5747, HO J.-S., BAUMGÄRTNER A., *Europhys. Lett.* **12** (1990) 295.
- [116] For a review which stresses the computational aspects of lattice descriptions: CARE C. M., DESPLAT J. C., BRINDLE D., *Tenside Surf. Det.* **30** (1993) 281.
- [117] LIPOWSKY R., ZIELINSKA B., *Phys. Rev. Lett.* **62** (1989) 1572, COOK - RÖDER J., LIPOWSKY R., *Europhys. Lett.* **18** (1992) 433.
- [118] GILAT, G., RAUBENHEIMER, L. J., *Phys. Rev.* **144** (1966) 390, RAUBENHEIMER, L. J., GILAT, G., *Phys. Rev.* **157** (1967) 586.
- [119] METROPOLIS N., ROSENBLUTH A. W., ROSENBLUTH M. N. *et al.*, *J. Chem. Phys.* **21** (1953) 1087.
- [120] *CMSSL for CM Fortran, CM-5 Edition, Vol. 2*, Thinking Machines Corporation, Cambridge, Mass., 1993.
- [121] BARNES I. S., *PhD Thesis* (Australian National University, Canberra, 1990).
- [122] BELLONI L., *Chemical Physics* **99** (1985) 52, BRIGHAM E. O., *The Fast Fourier Transform* (Prentice Hall, Englewood Cliffs, N. J., 1974).
- [123] MACKAY A. L., *Ang. Chemie* **27** (1988) 849.
- [124] VON SCHNERING H. G., NESPER R., *Z. Physik* in press.
- [125] MADDAFORD P. J., TOPRAKCIOGLU C., *Langmuir* **9** (1993) 2868.
- [126] HYDE, S. T., *Colloque de Physique* **C7** (1990) 209.
- [127] GOMPPER G., KRAUS M., *Phys. Rev. E* **47** (1993) 4301.
- [128] VAN VLECK J. H., MIDDLETON D., *Proc. IEEE* **54** (1966) 2
- [129] SCRIVEN L. E., *Nature* **263** (1976) 123, and in *Micellization, Solubilization and Microemulsions*, Vol. 2, Mittal K. L., ed. (Plenum, New York, 1977).
- [130] HOFFMAN, D. A., *Colloque de Physique* **C7** (1990) 197.
- [131] VONK C. G., BILLMANN J. F., KALER E. W., *J. Chem. Phys.* **88** (1988) 3970.
- [132] SAFRAN S. A., TURKEVICH L. A., PINCUS, P., *J. Phys. France Lett.* **45** (1984) 69
- [133] PETROV A. G., MITOV M. D., DERZHANSKI A., *Phys. Lett.* **65A** (1978) 374.

- [134] BINDER K., *Monte Carlo Methods in Statistical Physics*, Binder K., ed. (Springer, Berlin, 1979).
- [135] BINDER K., STAUFFER D., *Applications of the Monte Carlo Method in Statistical Physics*, Binder K., ed. (Springer, Berlin, 1987).